Office of Naval Research

Award Number: G N00014-01-1-0872

Compact Transducers and Arrays

Final Report

May 2005

Contacts:

Dr. Robert E. Newnham
The Pennsylvania State University, 251 MRL, University Park, PA 16802
phone: (814) 865-1612 fax: (814) 865-2326 email: bobnewnham@psu.edu

Dr. Richard J. Meyer, Jr.
Systems Engineering (Transducers), ARL, PO Box 30, State College, PA 16804-0030
phone: (814) 865-9607 fax: (814) 863-7270 email: rmeyer@psu.edu

REPORT DOCUMENTATION PAGE

Form Approved
OMB NO. 0704-0188

1. AGENCY USE ONLY (Leave Blank)	2. REPORT DATE	3. REPORT TYPE AND DATES COVERED
	05/28/2005	06/01/2001-05/31/2005

4. TITLE AND SUBTITLE
Compact Transducers and Arrays

5. FUNDING NUMBERS
G
N00014-01-1-0872

6. AUTHOR(S)
(1)Dr. Robert E. Newnham
(2)Dr. Richard J. Meyer, Jr.

7. PERFORMING ORGANIZATION NAME(S) AND ADDRESS(ES)
(1)The Pennsylvania State University, 251 MRL, University Park, PA 16802
(2)Systems Engineering (Transducers), ARL, PO Box 30, State College, PA 16804-0030

8. PERFORMING ORGANIZATION REPORT NUMBER

9. SPONSORING / MONITORING AGENCY NAME(S) AND ADDRESS(ES)
Program Officer
Yolanda Williams-Tabo ONR 245
Office of Naval Research Regional Office Chicago
230 South Dearborn, Room 380
Chicago/IL 60604-1595

10. SPONSORING / MONITORING AGENCY REPORT NUMBER

11. SUPPLEMENTARY NOTES
The views, opinions and/or findings contained in this report are those of the author(s) and should not be construed as an official Department of the Army position, policy or decision, unless so designated by other documentation.

12 a. DISTRIBUTION / AVAILABILITY STATEMENT
APPROVED for PUBLIC RELEASE, DISTRIBUTION UNLIMITED

12 b. DISTRIBUTION CODE

13. ABSTRACT (Maximum 200 words)

The main objective of this work is to take traditional high-power, low frequency transducers and miniaturize them to expand the operating range, reduce fabrication costs, and improve performance. This effort began with the development of the "cymbal" and "moonie" miniature flextensional transducers. This project improved upon the cymbal design, explored modifications and developed new designs based on other low-frequency technology, such as the hollow sphere and more complex flextensionals miniaturized through extrusion and Fused Deposition of Ceramics (FDC) technology. Transducer development has been supported heavily by finite element analysis. Applications for cymbals, cymbal modifications, BB miniature hollow spheres, and monolithic multimode transducers has been explored. Emphasis is placed on Navy needs and biomedical applications.

14. SUBJECT TERMS
underwater transducers: cymbal, multimode, hollow sphere, miniaturization, finite element analysis, biomedical transducers

15. NUMBER OF PAGES
19

16. PRICE CODE

17. SECURITY CLASSIFICATION OR REPORT	18. SECURITY CLASSIFICATION ON THIS PAGE	19. SECURITY CLASSIFICATION OF ABSTRACT	20. LIMITATION OF ABSTRACT
UNCLASSIFIED	UNCLASSIFIED	UNCLASSIFIED	UL

Compact Transducers and Arrays

Dr. Robert E. Newnham
The Pennsylvania State University, 251 MRL, University Park, PA 16802
phone: (814) 865-1612 fax: (814) 865-2326 email: bobnewnham@psu.edu

Dr. Richard J. Meyer, Jr.
Systems Engineering (Transducers), ARL, PO Box 30, State College, PA 16804-0030
phone: (814) 865-9607 fax: (814) 863-7270 email: rmeyer@psu.edu

Award Number: N00014-01-1-0872

LONG-TERM GOALS

To develop a family of compact transducers and arrays based on well-known high-power, low frequency devices. Primary focus includes the advancement of the "cymbal" miniature Class V flextensional transducer and its modifications. Modifications of the cymbal address deep-water survivability [double dipper], signal directionality [double driver], and multimode bandwidth enhancement [rectangular]. Creative exploitation of other transducer geometries, such as miniaturized "BB" hollow spheres and development of monolithic multimode transducers for expanded bandwidth and directionality were also studied.

OBJECTIVES

The main objective of this work is to take traditional high-power, low frequency transducers and miniaturize them to expand the operating range, reduce fabrication costs, and improve performance. This effort began with the development of the "cymbal" and "moonie" miniature flextensional transducers. This project improved upon the cymbal design, explored modifications and developed new designs based on other low-frequency technology, such as the hollow sphere and more complex flextensionals miniaturized through extrusion and Fused Deposition of Ceramics (FDC) technology. Transducer development has been supported heavily by finite element analysis. Applications for cymbals, cymbal modifications, BB miniature hollow spheres, and monolithic multimode transducers has been explored. Emphasis is placed on Navy needs and biomedical applications.

APPROACH

Our work concentrated on a two-track function in that we studied on development of a family of miniature flextensional transducers with broadband response characteristics, directionality, and depth resistance, while at the same time supporting other research efforts investigating these transducer systems by providing modeling studies and fabrication of transducers for testing. Modeling and testing of advanced forms of flextensional transducers were conducted by Mr. Douglas Markley, Mrs. Anne-Christine Hladky and Mr. Erman Uzgur under the direction of Dr. Robert Newnham at the Material

Research Laboratory. Underwater evaluation of advanced transducers and arrays was carried out by Dr. Richard Meyer, Jr., Dr. Jack Hughes, and Mr. Douglas Markley at ARL. Extruded prototype materials are being provided by Dr. Joseph Cochran at Georgia Tech, and Dr. Ahmad Safari at Rutgers is providing FDC prototypes.

Transducer design improvements were based on extensive finite element analyses. These studies yield design guidance for existing devices and new directions for profitable exploration. Improvements and further modifications can be rapidly studied using this computer-aided approach. Interesting designs can then be prototyped and tested.

In-water characterization of single elements and arrays by Dr. Meyer at ARL includes input power to output power analysis, mutual interaction effects, radiation impedance studies and beam forming capabilities tested in the free-field as well as conformably mounted with different types of backing materials. Fabrication issues were examined as production is increased. Reliability, longevity, and linearity were tested for designs.

WORK COMPLETED

Cymbal Design Guide - A comprehensive design guide for cymbal performance versus parametric variations was completed. Beginning with a discussion of cymbal acoustic amplification and vibration modes, and the subtleties of finite element analysis for flextensional transducers, this guide uses a combination of experimental and FEA results to describe the effects of nine different cymbal design parameters, including overall size (scaling), bonding layer thickness, ceramic disk and endcap material selection, ceramic disk and endcap thickness, cavity depth, cavity diameter, and apex diameter. Output parameters that are reported in the guide include resonance frequencies, transmit voltage response, free-field voltage sensitivity, directivity beam patterns, hydrostatic pressure dependence, actuator displacement, and generative force. The final chapter summarizes measured array performance and the reliability of cymbal arrays in regard to pressure and electric field fatigue testing and performance under high drive levels. This guide should serve as a valuable reference in designing customized cymbals tailored to meet the demands of specific applications. Cymbal design guide was submitted with this report as Appendix 1.

Pressure Dependence of Cymbal Transducer - Two methods were used and compared: a simple hydrostatic piezoelectric constant (d_h) single element measurement, and a 9-element array performance test conducted in the ARL high pressure facility. The results show improved pressure tolerance for cymbals with deeper cavities (up to 1600 ft in water) and reasonable correlation between the measurement techniques. Single elements of each basic design being used for current studies were tested for maximum use pressure. Pressure was gradually increased until permanent plastic deformation caused an irreversible change in sensitivity (Fig.1-2). With the ANSYS FEA code stress analysis of transducer was carried out (Fig 3). A paper detailing the accumulated results and associated ANSYS stress analyses was reviewed and accepted for publication in the IEEE Journal of Oceanic Engineering.

Fabrication/Yield Improvement – It has been shown that cymbals intended for use as acoustic transmitters must produce a single flextensional resonance peak. Samples with multiple or split resonance peaks are considered unacceptable for transmitter applications (though they retain usefulness as receivers below resonance). Subtle variations in the resonance frequency of the individual caps have limited yields of single peak samples to approximately 35%. Efforts to improve yield have included using machine made vs. hand-made caps and the introduction of holes in the ceramic disks. This later effort was triggered by an observation that Double-Dippers (inverted cap cymbals) made with rings, produced 100% yields of single peaks. In part of her master's thesis project Susan Danley has quantified this phenomenon.

Life Tests – Reliability – A three-by-three element array using PZT 4 ceramic was evaluated for survivability under high power driving conditions for extended periods of time. No change in resonance frequency, and less than 3% change in impedance was observed up to 53 dBV (11V/mil). The measurement time was approximately 30 minutes with a 7.5% duty cycl (Fig. 4).

Large Area Cymbal Array - Underwater calibration of the 6x34 cymbal array was carried out (Figure 5). Characterization included free-field and on-the-shell transmit/receive performance (Figure 6). These tests were conducted with all the elements connected in parallel. Sub-apertures were tested to verify scaling conditions and array uniformity. The array will be re-wired to demonstrate 1-D and doily beam steering capabilities. Mutual interaction effects and array/shell interactions will also be determined.

After calibration of large arrays, a 204 element array was mounted on the surface of a 21 inch vehicle shell section to study mutual impedance, beam forming, and channel-to-channel uniformity. In this set of tests, the elements of the 6 x 34 element array were re-wired into both a linear array arrangement containing 34 rows of six elements each and a four channel random "doily" or diffraction grating scheme. Receive patterns were measured on each channel or stave simultaneously using a new multi-channel data acquisition system. Steered beam patterns were reconstructed analytically using post-processing software. Taylor and Tschebyscheff shading coefficients were applied to reduce the side lobe levels. The results are shown in Figure 7. These results and a plot of the amplitude and phase variance across the array indicate strong element-to-element interaction or array shell interactions are present. Additional experiments were outlined to further study these effects.

Low Frequency Rectangular Cymbals – In order to bring a solution to narrow bandwidth of the cymbal transducer, rectangular caps were used for combining resonances. FEA parametric analysis was used to modify the rectangular shaped cymbals to lower the frequency range by a factor of two. The rectangular shape allows the powerful ceramic length mode to fall near the cap flextensional resonance frequency. The resulting combined resonance produces greatly increased bandwidth. To combine the resonances, the length of the active material has to increase. Simply increasing the length scale of the cap drops the cap resonance. Therefore the cap has to be stiffened. After FEA

studies, prototypes were fabricated based on these promising modeling results (Figure 8). Testing of single elements and a 3x1 array in-water confirm the modeling results (Figure 9)

Initial studies uncovered an undesirable higher order mode along the cap length. Several methods were examined to stiffen the cap. Dividing the cap into two twin cavities pushed the spurious mode beyond the frequency range of interest. However, potted in-water results show a damping of the ceramic length mode, probably caused by the stiff urethane encapsulant (Fig. 10).

Multimode Monolithics - With the aid of ATILA FEA analysis by Dr. Anne-Christine Hladky-Hennion several designs were developed for monolithic versions of classic flextensional transducers..These new designs, however, utilize extrusion or injection molding technology to produce devices whose flextensional components are made of *active* piezoelectric materials (Figure 11). Through collaboration with Dr. Ahmad Safari at Rutgers University, prototypes of these designs were made using Fused Deposition of Ceramics (FDC). Extruded monolithics were prepared by Prof. Joseph K. Cochran, Jr. at the Georgia Institute of Technology

Samples made by extrusion and FDC were tested in-water. The purpose of these tests was to validate modeling techniques and the fabrication methods. Samples of extruded wagon-wheels and an FDC convex wagon-wheel, and Class IV type device were tested for TVR and beam patterns and for use as directional vector sensors. The extruded wagon-wheel vector sensor yielded voltage level vs. angle plots that matched the theoretical plots very well, in spite of a slight asymmetry in the sample (Figs. 12 & 13). The convex wagon-wheel and Class IV type specimens show TVR curves that closely follow the ATILA model predictions, but at a reduced TVR level (Figure 14). The original models were 2-D for simplicity and assumed an infinitely long specimen.

3-D models were developed to predict more accurately the actual sample performance. These 3-D models gave closer results to the experimental TVR levels (Figure 15). Extrusion techniques, and especially green-handling and binder burnout practices, need to be refined to maintain the desired geometries and densities. Convex and concave Class I shapes have also been made by FDC. The FDC procedure yields good quality prototypes for shapes that can not be extruded; but, for larger quantity orders in which tooling costs can be offset, injection molding methods may reduce costs.

BB Miniature Hollow Sphere Transducers – BB samples were provided to Dr. Gerald Lauchle, Professor of Acoustics, and Dave Van Tol at ARL to be installed as a flow-noise monitoring sensor. The BBs provided sensors with small size, excellent sensitivity and high capacitance (≈1 nF), enabling them be used without disrupting flow or the need for preamplifiers. As shown in Figure 16, it had nearly perfect omnidirectional receive response up to about 100 kHz (and probably higher). The resulting sensitivity (-220 to -223 dB from 5 to 500 kHz with no preamplifier) is very flat and quite high for such a small device.

The size range of fabricated BBs was extended to 0.7mm – 5.9mm (2.8MHz – 280kHz f_r). Internal electrode adhesion was improved by a study of the thickness of the applied Pt layer. Processing refinements continue, including collaboration with the MRI Particulate Materials Center to adjust the ceramic particle surface charges for greater affinity with the internal electrode

We gained experience in BB fabrication. In a recent fabrication run done for a Transition project with Dr. Gerald Lauchle and Mr. Nathan Naluai at ARL, we achieved a yield of 70% of the samples that were suitable for poling. Hydrostatic coefficient measurements were used to match samples for this vector sensor application trial. Four BBs were arranged in each sensor in a tetrahedral pattern (Fig. 17).

Double-Dipper (Deep-Water Cymbal) and Double Driver (Directional Cymbal) - An FEA parametric study was carried out to determine the parameters important for resonance frequency control in double-dipper (concave) cymbals and the parameters important for generating directional beams and frequency dependence in the double-driver type transducers (Figure 18). Double-Dipper prototypes in a range of cavity depths were fabricated and their resonance frequencies matched ATILA calculated values. (Figure 19).

Results

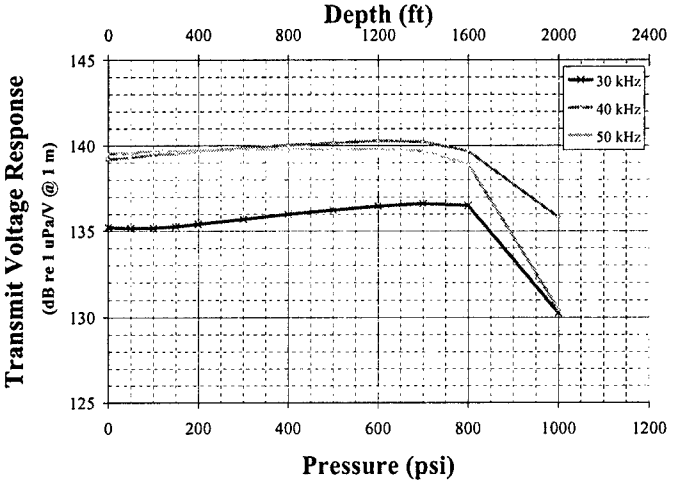

Fig. 1: Cymbal array high-pressure testing a) TVR of a 600 μm cavity depth cymbal array plotted as a function of applied pressure for frequencies below, at and above resonance. Less than 3% change in impedance and output level was observed out to 800 psi (1600 ft of depth).

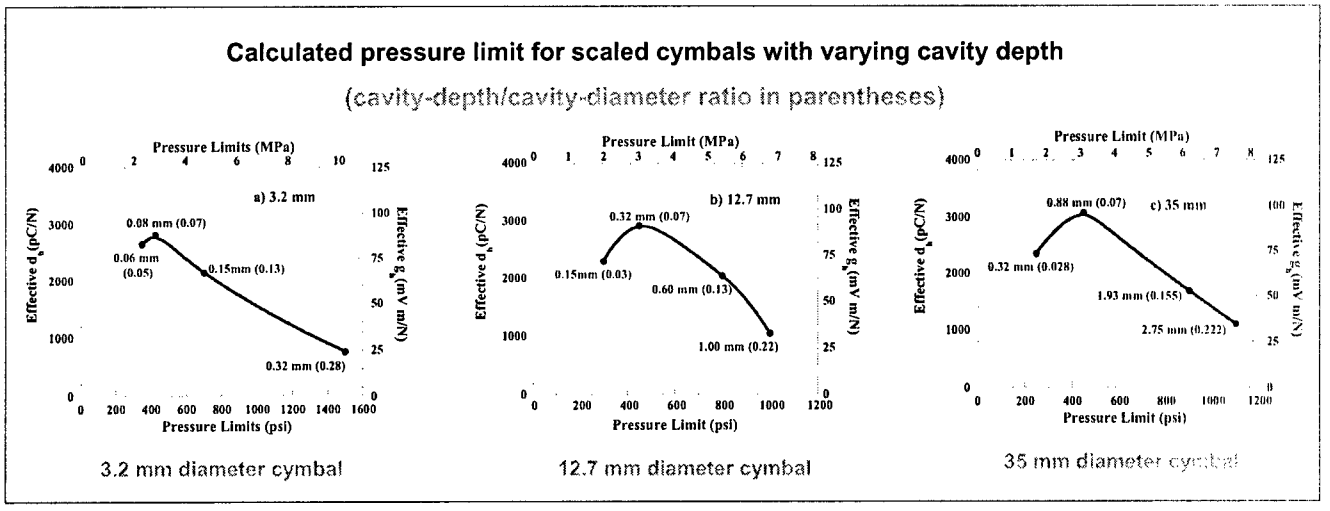

Figure 2. Calculated d_h-pressure limits for scaled cymbals with varying cavity depths in titanium caps: transducer diameters a) 3.2 mm, b) 12.7 mm, c) 35 mm, (cavity-depth/cavity-radius ratio in parentheses). Sensitivity maximums occur at 0.07 cavity-depth/cavity-diameter ratio. Higher ratios can tolerate higher pressure.

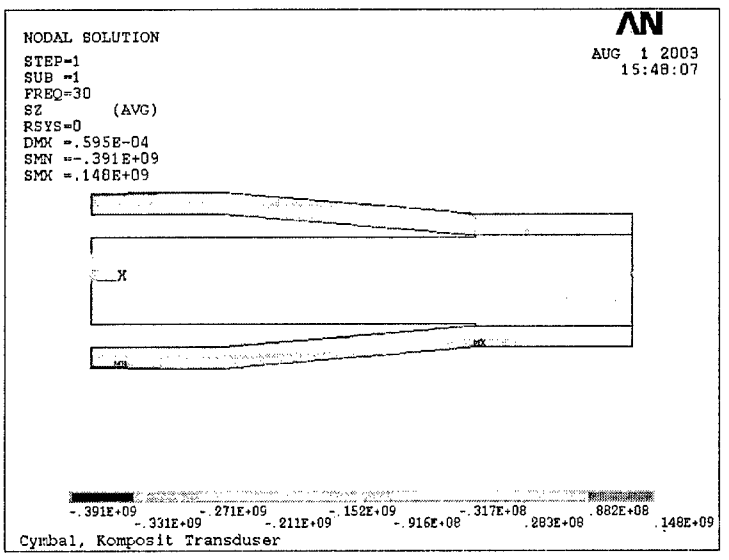

Figure 3. ANSYS output showing z-axis stress induced on a standard cymbal by hydrostatic pressure of 450 psi. The surface of the caps are in compression and the undersides of the caps are in tension. Outputs like this are being used compared to measured failure pressures to identify stress concentrations and failure modes.

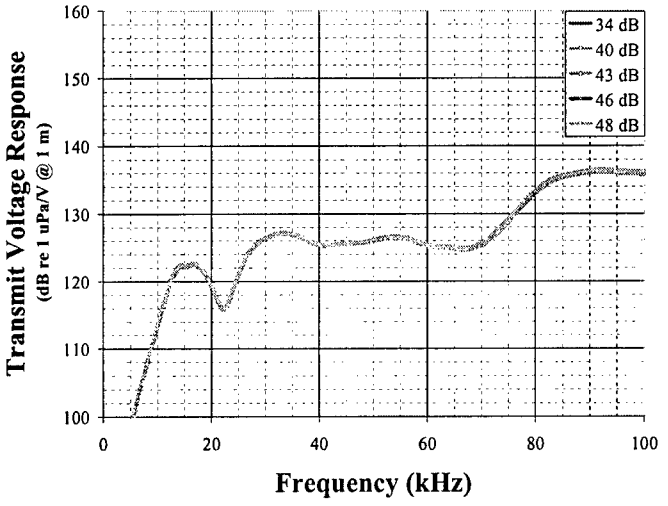

Fig. 4 Transmit voltage response (TVR) plotted as a function of frequency for increasing drive level for a nine-element cymbal array. Legend denotes drive levels in dB.

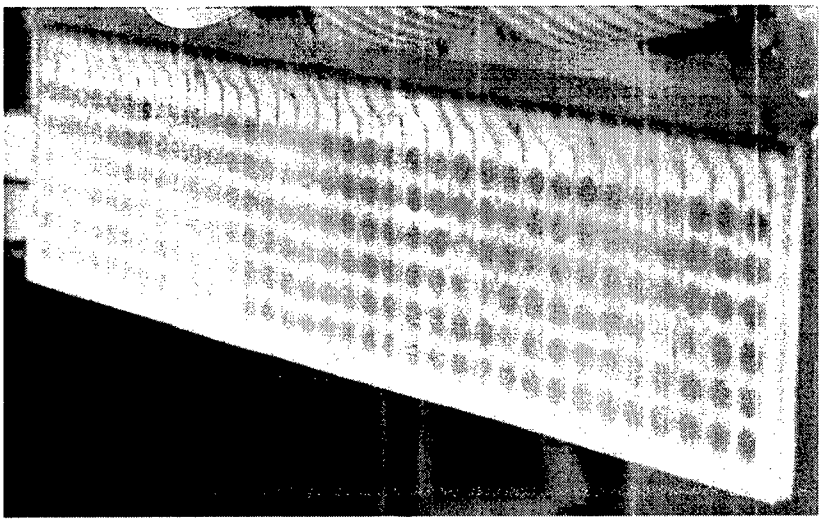

Fig 5 Photograph of the 200-element array with each element wired individually

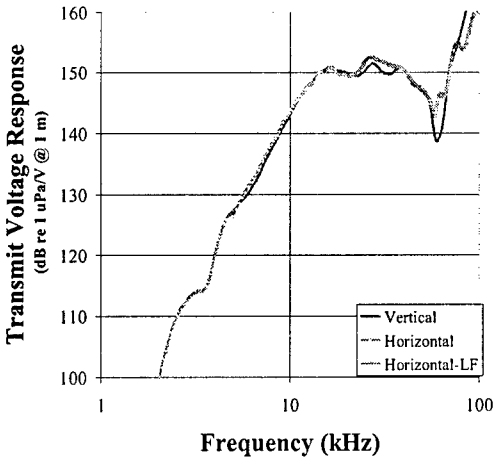

Fig 6 TVR of the array conformally mounted to a 21-inch diameter vehicle shell.

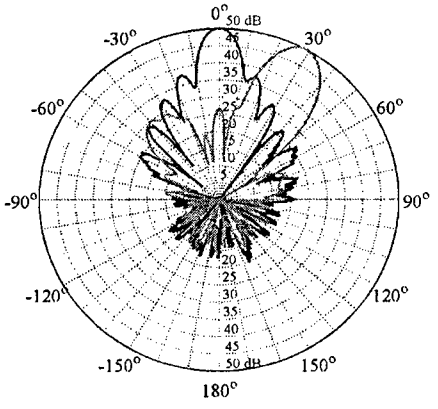

15 kHz Un-shaded (Blue) and Shaded + Steered (Red) Patterns 30 dB Tschebyscheff Shading Coefficients

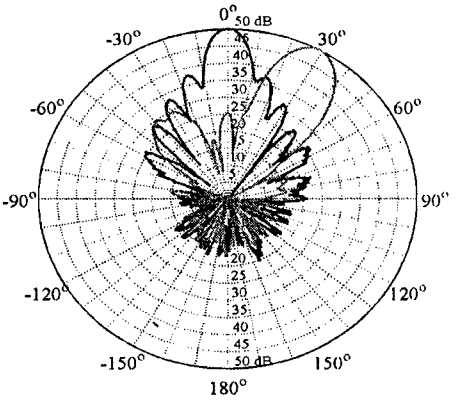

15 kHz Un-shaded (Blue) and Shaded + Steered (Red) Patterns 30 dB Taylor Shading Coefficients

Figure 7. Beam patterns for the 204 element array wired in 34 staves comparing the unshaded patterns to patterns which were both steered and shaded using two different amplitude weighting schemes. In both cases, 30dB coefficients only reduced the side lobe levels by 20dB indicating mutual interaction effects, array-shell interactions, or element-to-element variation.

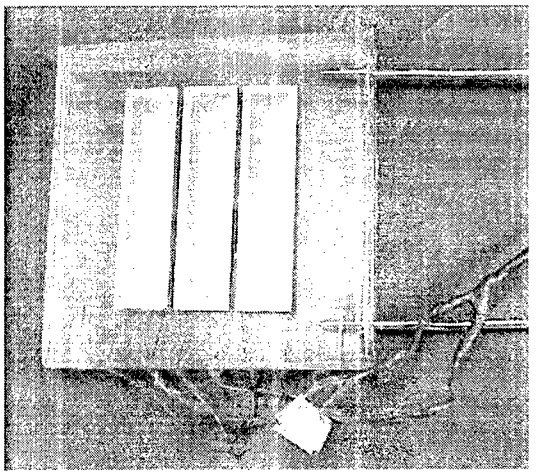

Figure 8. 3x1 potted array of rectangular cymbals, wired and mounted for testing

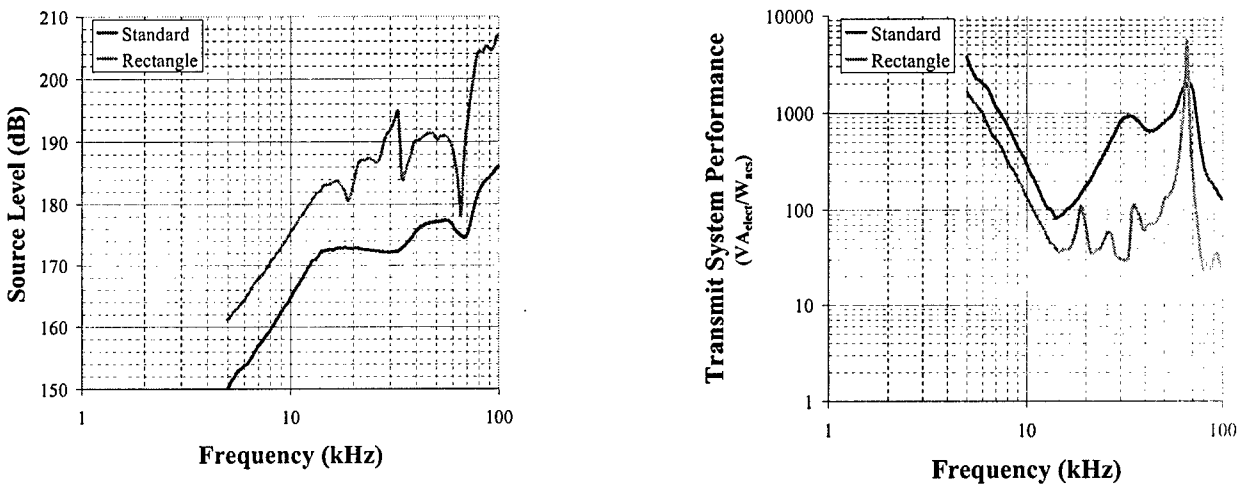

Figure 9. Source level and un- tuned $VA_{elec}/Watt_{acs}$ for a three element array of rectangular cymbals as compared to a nine element array of standard cymbals. SL was derived from in-water measurements of the transmit voltage response at low drive levels and then linearly scaled assuming a drive field of 7 V/milli-inch. The area of the arrays are comparable

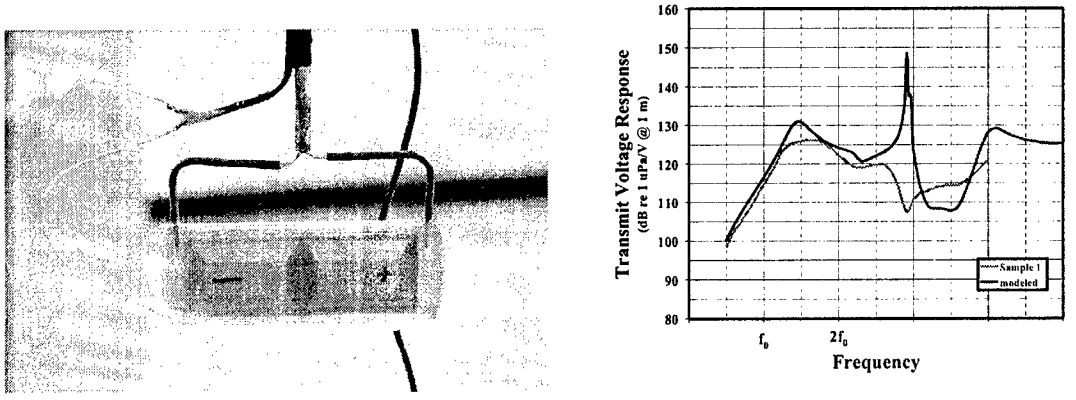

Figure 10. Measured vs. modeled Transmit Voltage response of a Dual-Cavity Rectangular Cymbal. Stiff potting material is believed to have dampened the length-mode resonance relative to the predicted response.

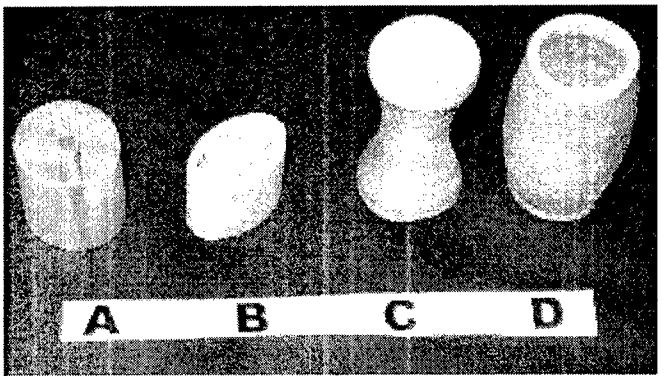

Figure 11. Photograph of four types of monolithic flextensionals; A. wagon-wheel with four electroded quadrants, B. Class IV, C. Class II concave cylinder D. Class I convex cylinder

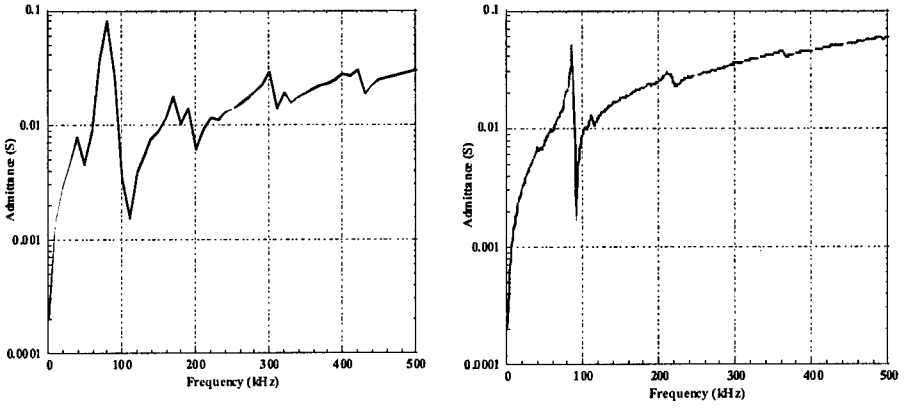

Fig. 12 Comparison of Calculated and Measured Admittance Spectra for Extruded Transducer

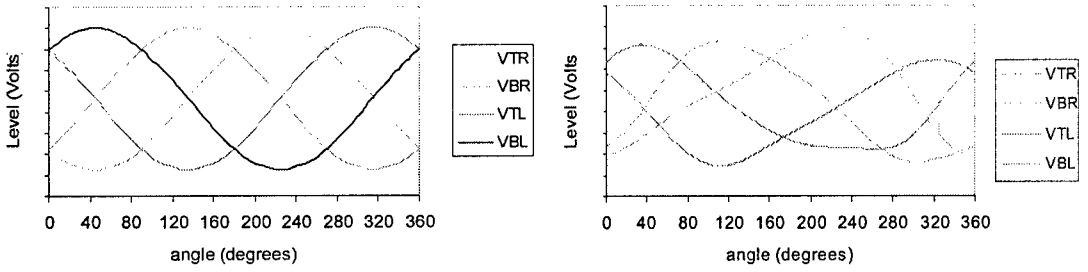

Figure 13. Voltage level vs. incident angle of sound source for each quadrant of a four quadrant wagon-wheel extruded transducer. The graph on the left is the theoretically predicted pattern; the figure on the right is the measured response, showing similar pattern structure with slight asymmetry.

$$V_{TR} = A + B\cos(\theta - 225)$$
$$V_{BR} = A + B\cos(\theta - 135)$$
$$V_{TL} = A + B\cos(\theta + 45)$$
$$V_{BL} = A + B\cos(\theta - 45)$$

$$\theta = Arctg\left(\frac{-V_{TR} + V_{BR} - V_{TL} + V_{BL}}{-V_{TR} - V_{BR} + V_{TL} + V_{BL}}\right)$$

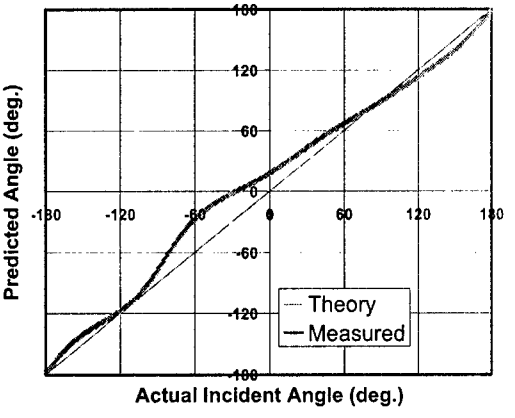

Figure 14. The calculation formula using voltage data from each quadrant to convert to a plot of predicted vs. actual sound source incident angle.

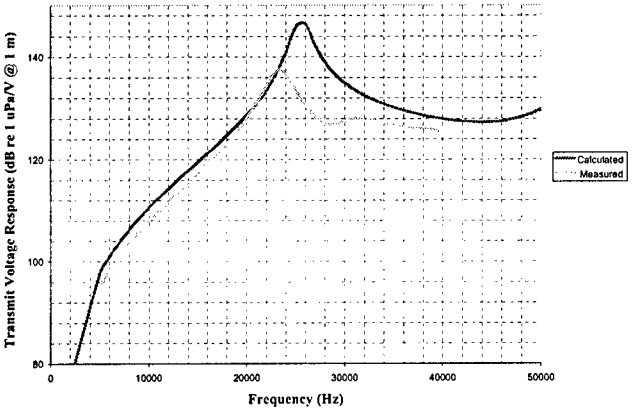

Figure 15. Measured vs. modeled Transmit Voltage response of a monolithitic class IV transducers. 3D model were used for calculations.

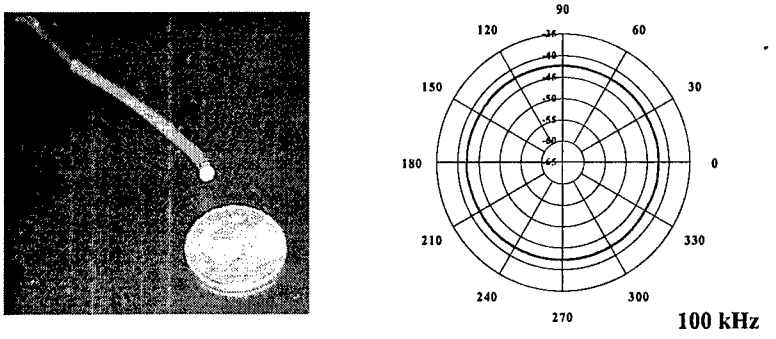

Fig. 16 (a) spherical hydrophone probe on coaxial wire [2.5 mm diameter sphere], and (b) omnidirectional receive pattern

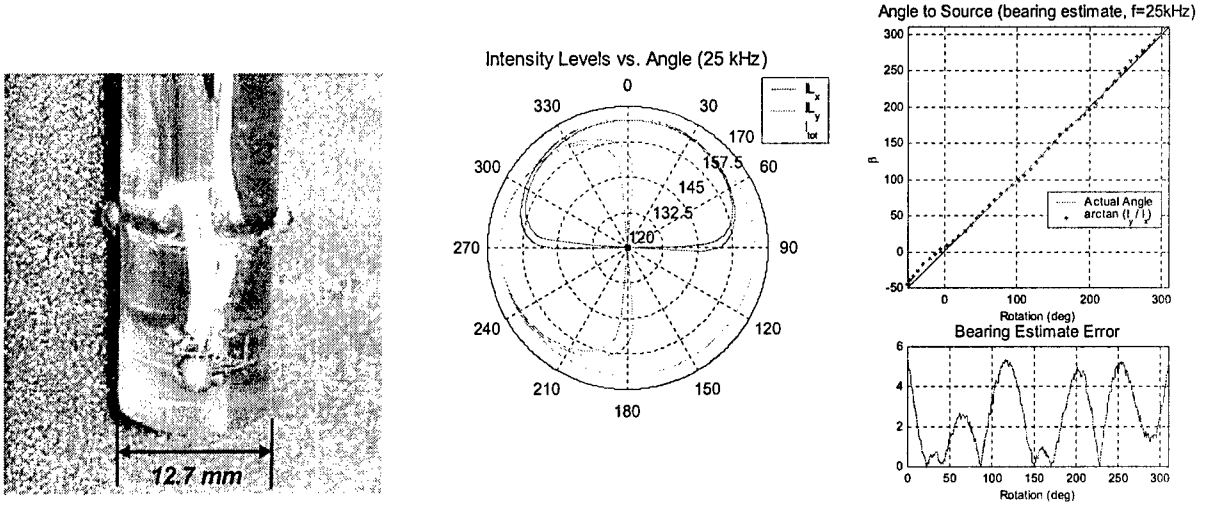

Figure 17. BB Tetrahedral Vector Sensor a) Prototype probe, b) Measured intensity in x- and y-axial directions as a function of bearing angle; b) Computed bearing estimates and errors relative to actual bearing to acoustic source. (Air bubbles in the polyurethane and alteration of the sound field by the intervening polyurethane may be responsible for the <5% error).

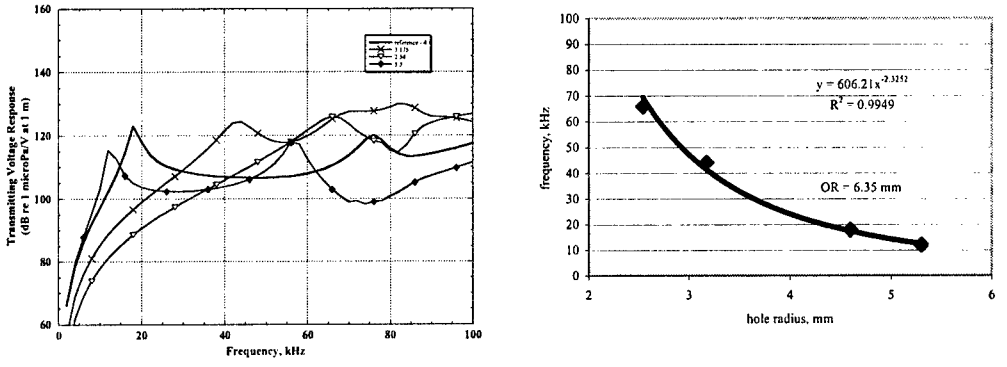

(a) (b)

Fig. 18 Double-Dipper Inner Radius vs. Resonance Frequency, [reducing hole size increases frequency

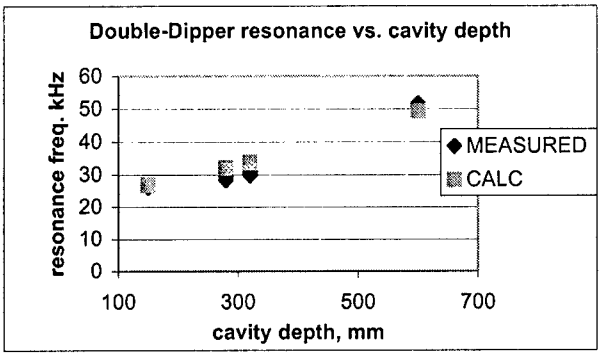

Fig. 19 Measured and calculated in-air resonance frequency for double-dipper type cymbals with varying cavity depth, showing excellent correlation

IMPACT/APPLICATIONS

Characterization of the cymbal, its modifications, and arrays of these elements will enable us to tailor the design and integrate cymbals into large area arrays and volume-restricted applications. Bandwidth, output power, efficiency, depth capability, reliability and linearity are all issues being modeled, measured and improved. The cymbal has been shown to be a promising technology for frequencies from 10 to 60 kHz. It has a total thickness of less than three millimeters and a projected cost of under $5.00 per unit. The cymbal is well suited for both send and receive applications.

Inexpensive miniaturizations of other flextensional designs may enable multi-element distributed sensor systems for harbor security. Cymbals and BBs are finding application in medical devices.

TRANSITIONS

Drs. James Tressler at NRL and Tom Howarth at NUWC are developing flat panel arrays of cymbals mounted to rigid panels for low frequency sound projection. International Transducer Corporation (ITC) is engaging in an SBIR program with NUWC to begin manufacturing cymbals.

Tiny (<1mm diameter) high frequency BB transducers were provided to Dr Gerald Lauchle, Professor of Acoustics, and Dave Van Tol at ARL for use in a three-element acoustic intensity probe. This probe takes advantage of the high sensitivity of these tiny spherical elements to resolve pressure differences at 5 mm spacings and determine the direction and intensity of incoming pressure waves at 20-30 kHz. A second set of BBs was delivered for use in five-element tetrahedral arrays.

Cymbal transducers are proving successful as drivers for transdermal drug delivery. An array of four and six cymbals has been demonstrated to expedite the progress of large molecule drugs (like insulin) through the skin. Testing by Dr. Nadine Smith of the Bioengineering Department, Penn State was successful on lab rats and rabbits and is progressing towards studies with pigs and/or sheep. Support of this work is continuing. Dr. Smith and her students conducted two other application trials using very small (down to 0.7mm diameter) very high frequency (up to 2.8 MHz) BB transducers provided by MRL. BBs served as hydrophones to map high acoustic intensity fields generated by powerful focused medical ultrasound for use in non-invasive surgery, being able to withstand four-times higher acoustic pressure than the conventional hydrophone. The second trial used the BBs themselves to perform minimally invasive hyperthermic tumor ablation. The BB performance was very promising in both trials, and follow-up studies are planned.

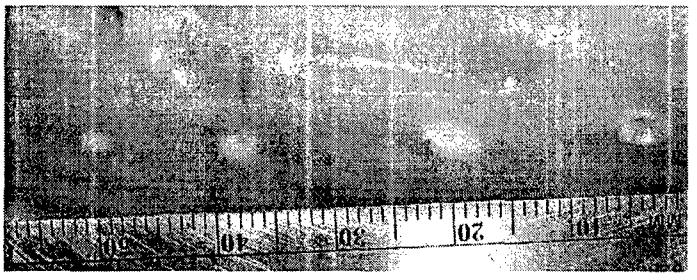

Fig. 20 Section of porcine kidney showing four ablated regions of increasing diameter with increasing insonification time using BB transducer.

Triton Systems Inc. will be testing cymbals as one possible choice for a distributed sensor system under an SBIR.

ICAT is making and testing cymbals for a vibrational energy conversion unit for Toyota. This will be incorporated into the motor mount to charge a battery off of the engine vibrations. They are attempting to get 100mW of power. The existing technology

produces less than 10mW. They are now continuing experiments with cymbal parameters to optimize the design.

Motorola, Inc. is funding a grad student through ICAT to study the use of cymbals for a high displacement undisclosed application.

RELATED PROJECTS

None

PUBLICATIONS

2001

R.J. Meyer, Jr., Technical Memorandum # 01-195, 3 August (2001).

R.J. Meyer, Jr., ARL Internal Memorandum SE#01-191, August (2001).

R.J. Meyer, Jr., ARL Internal Memorandum SE#01- 228, September (2001).

R.J. Meyer, Jr., Technical Memorandum #01-109, 15 October (2001).

Newnham R.E., "Symmetry and Antisymmetry in Ferroelectric Transducers," *Ferroelectrics*, Vol. 263, pp. 77-89 (2001).

Newnham R.E., J. Zhang, S. Alkoy, R. Meyer, W.J. Hughes, A.C. Hladky-Hennion, J. Cochran, and D. Markley, "Cymbal and BB Underwater transducers and Arrays," Proceeding of the 10th US-Japan Seminar on Dielectric and Piezoelectric Ceramics, Sept. 27-29, 2001, Providence, R.I.

Newnham, R.E., S. Alkoy, A.-C. Hladky-Hennion, W.J. Hughes, R.J. Meyer, Jr., D.C. Markley, and J. Zhang "Underwater Flat-Panel Transducer Arrays," Proceedings of MTS/IEEE Oceans 2001 Conference and Exhibition, Honolulu, HI, Vol 3, pp. 1529-35, Nov (2001).

R.E. Newnham, S. Alkoy, A.C. Hladky, J. Hughes, D. Markley, R.J. Meyer, and J. Zhang "Underwater Flat-Panel Transducer Arrays," Oceans 2001 MTS/IEEE, Honolulu, HI

Meyer, R.J. Jr. and R.E. Newnham, "Flextensional transducers with Shape Memory Caps for Tunable Devices," *Journal of Intelligent Materials Systems and Structures*, vol. 11, pp. 199-205 (2001).

Meyer, R.J. Jr., A. Dogan, C. Yoon, S. Pilgrim and R.E. Newnham, "Displacement Amplification of Electroactive Materials Using the Cymbal Flextensional Transducer," *Sensors & Actuators* A, vol.87, pp. 157-162 (2001)

Meyer, R.J. Jr., S. Alkoy, J. Cochran, T. Ritter, and R.E. Newnham, "Pre-focused Lead Titanate > 25 MHz Single Element Transducers from Hollow Spheres," *IEEE Transactions on Ultrasonics, Ferroelectrics, and Frequency Control*, vol. 48 (2), pp. 488-493 (2001).

Zhang, J., A.-C. Hladky-Hennion, W.J. Hughes, and R.E. Newnham, "Modeling and Underwater Characterization of Cymbal Transducers and Arrays," *IEEE Transactions on Ultrasonics, Ferroelectrics, and Frequency Control*, vol. 48 (2), pp. 560-568 (2001).

Zhang, J., A.-C. Hladky-Hennion, W.J. Hughes, and R.E. Newnham, " A Miniature Class V flextensional cymbal transducer with directional beam pattern: The Double-Driver," *Ultrasonics*, vol. 39, pp. 91-95 (2001)

Newnham R.E., J. Zhang, "Cymbal Transducer: A Review," *Proceedings of the 12th IEEE International Symposium on Applications of Ferroelectrics,* pp. 29-32 (2001).

Alkoy, S., R.J. Meyer, Jr., A.-C. Hladky-Hennion, W.J. Hughes, J.K. Cochran Jr., and R.E. Newnham, "Transducer Arrays from Piezoelectric Hollow Spheres," *2000 IEEE-ISAF Proceedings,* Honolulu, Hawaii, pp. 737-740 (2001).

Meyer, R.J. Jr., S. Alkoy, W. Chen, T. Ritter, J. Cochran Jr., and R.E. Newnham, "High Frequency Imaging Transducers from Hollow Spheres," *2000 IEEE-ISAF Proceedings,* Honolulu, Hawaii, pp. 741-744 (2001).

Newnham R.E. and L.E. Cross, "Symmetry and Antisymmetry in Electroceramics," *The Art of Ceramics: The Blend of Art and Science in Technology*, edited by N. Claussen (FORUM 2000), International Academy of Ceramics, Italy, pp. 205-223 (2001).

Dogan A., J. Tressler and R.E. Newnham, "Solid State Ceramic Actuator Designs," *AIAA Journal*, vol. 39, 7, July , 2001, p 1354-1362

2002

R.J. Meyer, Jr., Technical Memorandum #02-061, 23 August (2002).

R.J. Meyer, Jr., Technical Memorandum #02-099, 6 September (2002).

Meyer, R.J., Jr., W. J. Hughes, T.C. Montgomery, D.C. Markley and R.E. Newnham, "Design of and Fabrication Improvements to the Cymbal Transducer Aided by Finite Element Analysis," *Journal of Electroceramics*, Vol 8(2), pp 163-174, 2002.

Hladky-Hennion, A.-C., S. Alkoy, D.C. Markley, R.J. Meyer, Jr., W.J. Hughes, J.K. Cochran, Jr., R.E. Newnham, "Etude et realization de transducers millimetriques", Proceedings of the 6th Congress of the French Acoustical Society, April (2002).

Maione, E., K.K. Shung, N. Smith, R.J. Meyer, Jr., W.J. Hughes, R.E. Newnham, " Transducer Design for a Portable Transdermal Drug Delivery System Enhanced by Ultrasound," *IEEE Trans. on Ultrasonics, Ferroelectrics and Frequency Control*, vol. 49 (10), pp. 1430-1436 (2002)

Newnham, R.E., J. Zhang, R.J. Meyer, Jr., S. Alkoy, J.K. Cochran, Jr., D.C. Markley, "Processing of Miniature Hollow Sphere Transducers," Integrated Ferroelectrics, vol. 42/2002 p 235-243.

Uzgur E.A., A.Dogan, R.E Newnham., "Design Optimization of Piezoelectric Composite Transducers Using Finite Element Method," Key Engineering Materials, v 206-213, (2002) p 1297-1300.

Newnham, R.E., W.J. Hughes, D.C. Markley, R.J. Meyer, Jr., S. Alkoy, A.-C. Hladky-Hennion, and J. Zhang, "Cymbal and BB Flat Panel and Conformal Sonar Arrays," *Sea Technology*, pp. 29-38 (Nov, 2002).

Newnham, R.E., J. Zhang, S. Alkoy, R.J. Meyer, Jr., W.J. Hughes, A.-C. Hladky-Hennion, J. Cochran, and D.C. Markley, "Cymbal and BB Underwater Transducers and Arrays," *Materials Research Innovations*, vol.6 (3), 89-91, (2002).

Smith, N.B., R.J. Meyer Jr., R.E. Newnham, K.K. Shung, "Transducer Design for an Ultrasound Enhanced Transdermal Drug Delivery System," Proceedings of the International Association of Science and Technology for Development (IASTED), International Conference on Signal and Image Processing, August (2002).

Newnham, R.E., A. Dogan, D.C. Markley, J.F. Tressler, J. Zhang, A.E. Uzgur, R.J. Meyer Jr., A-C. Hladky-Hennion and W.J. Hughes, "Size Effects in Capped Ceramic Underwater Sound Projectors", *Proceedings of the MTS/IEEE Oceans 2002 Conference and Exhibition*, Biloxi, Miss., pp. 2315 – 2321 (Oct., 2002).

Al-Bataineh, O.M., R.J. Meyer, Jr., R.E. Newnham, N.B. Smith, "Utilization of the High-Frequency Piezoelectric Ceramic Hollow Spheres for Exposimetry and Tissue Ablation," *Proceedings of the 2002 IEEE International Ultrasonics Symposium*, 8-11 October 2002, Munich Germany, Section P3C-7.

Hladky-Hennion A.-C., S. Alkoy, D.C. Markley, R.J. Meyer, Jr., W.J. Hughes, J.K. Cochran, R.E. Newnham, "Analysis Of Transducer Arrays From Piezoelectric Hollow Spheres", *Proceedings of the 2002 IEEE Ultrasonic Symposium*, Munich, Volume 2, pp. 1239-1242 (2002).

Newnham, R.E., S. Alkoy, A.-C. Hladky-Hennion, W.J. Hughes, R.J. Meyer, Jr., D.C. Markley, and J. Zhang "Underwater Flat-Panel Transducer Arrays *Proceedings of the 6th Congress of the French Acoustical Society*, Lille, France, pp. I-VII, April (2002).

2003

Uzgur A.E., A. Dogan, E. Suvaci, R.E. Newnham, "Computational analysis on cymbal transducer," *Chemical Engineering Communications,* 190 (5-8): 853-860 May-Aug 2003.

Meyer, R.J., Jr., R.E. Newnham, A. Amin, and B.M. Kulwicki, "Flextensional Barium Strontium Titanate Actuators," *J. Amer. Cera. Soc.*, vol.86 (6) 934-38 (2003).

2004

Lee, S., Newnham, R. E., & Smith, N. B. Short ultrasound exposure times for noninvasive insulin delivery in rats using the light weight cymbal array. *IEEE Trans.Ultrason., Ferroelect., Freq.Contr.* 51[2], 176-180. (2004).

Newnham, R.E., D.C. Markley, R.J. Meyer, Jr., W.J. Hughes, A.-C. Hladky-Hennion, and J.K. Cochran, Jr., "Multimode underwater transducers," American Ceramic Society Bulletin 83 (9): 25-28, Sep 2004

Al-Bataineh OM, Markley DC, Meyer RJ, Newnham RE, Smith NB, "Feasibility of miniature high-frequency piezoelectric ceramic hollow spheres for exposimetry and tissue ablation", *Materials Research Innovations*, 8 (2): 78-83, (2004)

Kim HW, Batra A, Priya S, Uchino K, Markley D, Newnham RE, Hofmann HF, "Energy harvesting using a piezoelectric "cymbal" transducer in dynamic environment" *Japanese journal of applied physics part 1-regular papers short notes & review papers*, 43 (9A): 6178-6183 (2004)

Seungjun L, Snyder B, Newnham RE, Smith NB, " Noninvasive Ultrasonic Transdermal Insulin Delivery in Rabbits Using The Light –Weight Cymbal Array", *Diabetes Technology and Therapeutics,* 6 (6), 808-815, (2004)

Dogan A, Uzgur AE, Markley D, Meyer RJ, Hladky-Hennion AC, Newnham RE, "Materials for High Performance Cymbal Transducer", *Journal of Electroceramics,* 13, pp. 403-408, (2004)
S. E. Danley, "Thickness Dependence of the Cymbal, Ring Cymbal and Double Dipper", M.S. Thesis, The Pennsylvania State University, 2004 [published]

Uzgur, A.E., D.C. Markley, M. Guo, B. Snyder, R.J. Meyer, Jr., A. Dogan, and R.E. Newnham, "Pressure Dependence of Cymbal Transducers", *IEEE Journal of Oceanic Engineering* (2004) [in-press, refereed]

Alkoy S., R.J. Meyer, Jr., W.J. Hughes, P. Bouchilloux, J.K. Cochran Jr., and R.E. Newnham"Omnidirectional ultrasound microprobe: The "BB" transducer," Journal of Acoustical Society of America, Submitted

2005

Newnham RE, "Properties of Materials: Anisotropy, Symmetry, Structure", *Oxford University Press:New York,(* 2005)

PATENTS

R.E. Newnham, "Multimode Monolithic Transducers", PSU invention disclosure 2002-2697. Entered Sept. 24, 2002 Still under review.

Jindong Zhang, and R.E. Newnham, "Class V flextensional transducer with directional beam patterns", US Patent # 6,614,143, Sept 2, 2003.

THESIS

Danley, S. 2004 "Thickness Dependence of Cymbal, Ring and Double Dipper Transducer" *M.S Thesis*, The Pennsylvania State University, University Park.

Snyder, Benjamin M., 2004 Design, Development, and Implementation of The 3x3 Cymbal Array for Transdermal Insulin Delivery, *M.S Thesis*, The Pennsylvania State University, University Park.

Lee, S, 2004, Ultrasound-Mediated Transdermal Insulin Delivery and Glucose Measurement Using the Cymbal Array, *Ph.D Thesis*, The Pennsylvania State University, University Park.

HONORS/AWARDS/PRIZES

Army Research Laboratory Certificate of Merit , 2001

David Kingery Award, American Ceramic Society, 2001

Honorary Member, Ceramic Society of Japan 2002

George Weatherly Distinguished Lecturer, Canadian Ceramic Society, 2003

Benjamin Franklin Medal for Electrical Engineering, Franklin Institute, 2004

Fellow, IEEE, 2005

Academician, World Academy of Ceramics, 2005

R.J. Meyer, Jr. -

FY03 ONR Young Investigator

APPENDIX
I

SIZE AND MATERIAL EFFECTS ON CYMBAL TRANSDUCERS FOR UNDERWATER APPLICATIONS: HYDROPHONES AND PROJECTORS

A. Dogan, J. Tressler, E. Uzgur
D. Markley, R. Meyer, Jr., A.C. Hladky-Hennion, J. Zhang, R. E. Newnham

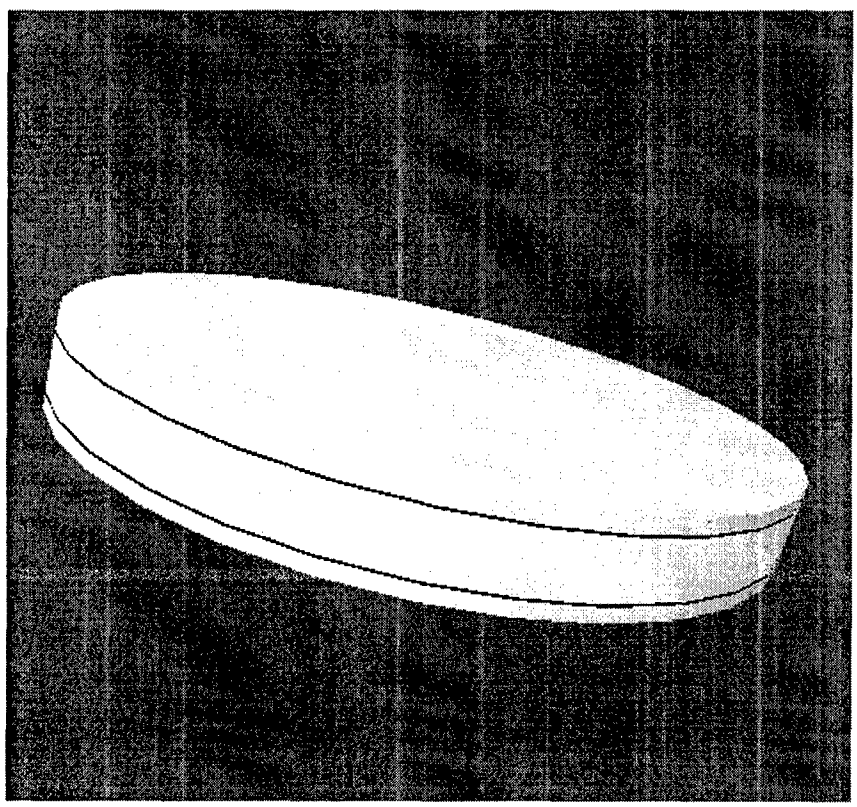

Contact:

Dr. Robert E. Newnham
251-A Materials Research Laboratory
The Pennsylvania State University
University Park, PA 16802-4801 USA
Tel:(814)865-1612
Fax:(814)865-2326
bobnewnham@psu.edu

Douglas C. Markley
254 Materials Research Laboratory
The Pennsylvania State University
University Park, PA 16802-4801 USA
Tel:(814)863-0180
Fax:(814)865-2326
dcm13@psu.edu

SIZE AND MATERIAL EFFECTS ON CYMBAL TRANSDUCERS FOR UNDERWATER APPLICATIONS: HYDROPHONES AND PROJECTORS

A. Dogan[1,3], J. Tressler[2], E. Uzgur[1,3]
D. Markley[1], R. Meyer, Jr. [4], A.C. Hladky-Hennion[5], J. Zhang[6], R. E. Newnham[1]

[1]The Pennsylvania State University, Materials Research Institute, University Park, PA 16802
[2]Naval Research Laboratory, Washington D.C.
[3]Anadolu University, Eskisehir TURKEY
[4]Applied Research Laboratory, University Park, PA
[5]ISEN, Lille, France
[6]Kulicker & Soffa, Willow Grove, PA

ABSTRACT

Cymbal transducers are small, thin Class V flextensional transducers. A single cymbal element consists of a piezoelectric disk sandwiched between two metal cymbal-shaped endcaps which serve as mechanical transformers, converting the low impedance, small extensional motion of the ceramic into high impedance, large flextensional motion of the endcap. A cymbal transducer element is very small, with a thin profile. A single element is characterized by high Q, low efficiency, and medium power capability. When comparing cymbals to other transducers, the designer should consider their use in large flexible, low cost arrays.

The effects of changes in materials and dimensions on the cymbal-type flextensional transducers, in-air and water-loaded, were examined experimentally and through finite-element-analysis (FEA). Experimental and FEA calculated results matched quite well. After gaining experience and confidence in the FEA models, extensive parametric studies were performed using FEA to investigate the size and material effects on cymbal transducer characteristics. The scaling factor (i.e., overall

size), endcap stiffness, and cavity design have the strongest influence on resonance frequency. Adjusting the dimensions and materials used for drivers and endcaps provides a range in the fundamental flexural frequency from about 3 to 250 kHz in water. These results also indicate trends that can be used to extend the ranges further. The scaling factor, cavity depth, and PZT thickness had the strongest effects on the projector/receiver performance (TVR/FFVS). Investigations are underway to combine and optimize some of these parameters for potentially significant improvements in bandwidth and efficiency.

I. INTRODUCTION

A. Composite Transducers

A number of materials exhibit piezoelectric behavior including ceramics, polymers, and their composites. Conflicting requirements in optimum transducer physical and electromechanical properties have led researchers to focus on composite materials, which enhance favorable properties and reduce undesirable effects.

Superior properties have been obtained with several types of piezocomposites. Microstructural arrangement of component phases in the composite, sometimes referred to as connectivity [1], is a critical parameter for the electromechanical performance of the composite. For a composite containing two phases, there are ten important connectivity patterns. Over the last few decades, researchers have investigated various methods to process piezocomposites and improve their properties. Simple connectivities such as 0-3, 1-3, and 2-2 etc. have been studied intensively. There are several excellent review papers on connectivity patterns, and the processing techniques used to form piezocomposites from active piezoelectrics and inactive polymers [1], [2]. The various composites have

different applications due to enhancement of different physical parameters. For example, 1-3 composites, which have been widely commercialized, use piezoelectric ceramic rods or fibers arranged parallel to the poling direction and embedded within a polymer matrix. A decoupling of the d_{33} and d_{31} coefficients enhances the d_h. Competition continues for the composites with the best electromechanical performance for each application.

Ceramic-metal composites generally have a simple design [3]. Multilayer actuators consist of alternating thin ceramic and metal electrode layers stacked together to provide large displacements with relatively low electric fields. Bimorph actuators are made by bonding two piezoelectric ceramic plates on either side of an elastic shim. The ceramics are driven with opposing electric fields, or are poled in opposing directions to provide a bending motion to the device.

Flextensional transducers are another example of a ceramic-metal composite, with metal faceplates, shells or caps that couple to both the ceramic and the surrounding medium. The metal component transfers the incident stress to the ceramic or the displacement to the medium. A new generation of miniature flextensional piezocomposites began with the "moonie" and continued with the "cymbal", both with 2-(0)-(2) connectivity [4-8]. In flextensional transducers, the flexural vibration of the metal shell causes an extensional vibration of the piezoelectric ceramic, or vice versa. Cymbal elements are then positioned into arrays with thin cross-section by distributing the cymbals in a planer arrangement and surrounding them with polymer. Cymbal arrays are basically 1-3 composites with the rods or fibers replaced by cymbals. The individual cymbals can be wired in parallel, in series, or independently. The entire assembly is

"potted" in compliant polymers for waterproofing and acoustic matching to the target medium [9].

B. Cymbal Transducer Principle:

Each element of a cymbal array consists of a piezoelectric disk, sandwiched between two truncated conical endcaps made of metal, ceramic or plastic, with shallow cavities on their inner surface. These are then positioned in arrays. Cymbal transducers can be built using circular, rectangular or ring shaped ceramics. The design of the cymbal transducer is illustrated graphically in Figure 1. For a simple ceramic disk the hydrostatic piezoelectric coefficient d_h can be defined by

$$d_h = (2d_{31} + d_{33}) \qquad (1)$$

Lead-zirconate-titanate (PZT) ceramics have large d_{31} and d_{33} coefficients, but they are of opposite sign, so the resulting d_h values are low. The presence of the cavities in a cymbal allows the metal endcaps to serve as a mechanical transformer for transforming and amplifying a portion of the incident axial stress into radial stresses of opposite sign. Thus, the d_{33} and d_{31} contributions of the PZT now add together (rather than subtracting) in the effective d_h value of the device, such as a hydrophone or accelerometer. Conversely, radial motion of the ceramic driving element is transferred and amplified by the metal endcaps into a large motion in the axial direction. In this way, cymbals can be used as both sensors and actuators. The amplification factor is approximately equal to the radius of the cavity divided by the height of the cavity.

Piezoelectric, electrostrictive, and antiferroelectric-ferroelectric switching types of materials can be used as the driving element in either single layer or multilayer form [10-

12]. In the cymbal and moonie transducer designs, the flexibility and durability of the metals and the driving power of the ceramic element are combined.

Poled ferroelectric ceramics (Curie group ∞m) possess three independent piezoelectric coefficients: d_{31}, d_{33}, and d_{15}. Each of the piezoelectric coefficients can be used as the driving element of a composite cymbal transducer. Polarization and electric field directions of the samples can be altered systematically to make use of the three different piezoelectric coefficients.

The cymbal is a versatile performer. Research trials have been successfully conducted using cymbals in large 100 and 200 element sonar arrays. In the biomedical field cymbal arrays have been used in trials as ultrasonic drivers for transdermal drug delivery, and miniature single elements as aural implant devices for hearing restoration. Their large displacement (10 - 100 μm for a half-inch diameter cymbal, depending on parameter adjustment) and good force (15N under static drive of 1 kV_p/mm) [13] makes them applicable to trials as drivers for mini-pumps, or as positioning actuators for optical systems. Stacking the cymbals provides an additional n-times displacement. Other potential applications are detailed in the original cymbal patent [8].

Desired actuation and sensing performance can be tailored by engineering the flexibility of the endcaps or changing the dimensional parameters of the components. In this report, the effect of materials and dimensional design parameters on the resonance frequency, TVR, FFVS, hydrostatic pressure dependence, and reliability of the cymbal will be reported.

C. Essential Parameters for Underwater Transducers:

Cymbal transducers can be used as both underwater sound projectors and sound receivers. The most important parameters required in characterizing an underwater transducer are resonance frequency (f_r), mechanical quality factor (Q_m), electroacoustic efficiency (η), electromechanical coupling coefficient (k_{eff}), acoustic directivity, and free field voltage sensitivity (FFVS) for hydrophones, and transmitting voltage response (TVR), source level (SL) and drive limits for projectors. Each application carries its own requirements for effective performance. With these factors in mind, parametric characteristics of the cymbal for underwater transducer applications were investigated over a range of sizes and materials.

For hydrophones, the free field voltage sensitivity is equal to the voltage measured across the open circuit terminals of the hydrophone subjected to an incident plane wave of unit acoustic pressure. The results are usually reported in units of dB referenced to one volt per micro-Pascal.

To a first approximation, the acoustic performance of the projector can be gauged by the transmit voltage response (TVR). TVR is equal to the sound pressure produced at a distance of one meter by the transducer with one-volt input. It is typically reported in decibels referenced to a pressure of one micro Pascal. This easily measurable quantity can be used to compare variations of a transducer design and can provide an estimate of device performance. TVR is a function of the conductance (G), directivity index (DI) and the transducer efficiency (n), as given by Equation 2.

$$TVR = 10 \log (G)+DI+10 \log (n)+170.8 \qquad (2)$$

To predict the performance of the transducer in an underwater application, the transducer's source level (SL) is needed. A key parameter in this report is the thickness of the ceramic disk driver. Using established maximum driving criterion to obtain maximum expected drive voltage, peak values of SL were calculated. The source level (SL) can be obtained from the TVR by scaling it with the input drive voltage. To do this, the transducer must behave linearly. The relationship between source level and TVR is given in Equation 3.

$$SL = TVR + 20 \log Vrms \qquad (3)$$

The acoustic performance of an array of elements can be estimated from the TVR of a single element using Equation 4. Great care must be used in this scaling as it is only valid if the array is acoustically loaded. It also does not consider interactions between the elements of the array. In our experiments many of the transducer designs are small compared to the wavelength. If the single element beam pattern is omnidirectional, this scaling may not be accurate.

$$(TVR)_{array} = (TVR)_{element} + 20 \log N \qquad (4)$$

II. EXPERIMENTAL PROCEDURE

A. Fabrication of the Cymbal Transducer

A schematic drawing of a cymbal is shown in Figure 1. The dimensions shown in this figure define what will hereafter be referred to as a "reference size" cymbal. Cymbal

transducers were fabricated by punching disks from sheet metal and then molding the punched disks into caps of the desired shape using a die press. A cost effective mass production method for reference-size samples has also been developed by simultaneously punching and shaping sheets of metal foil, typically 0.25 mm thick, using a specially designed die-punch apparatus. For the reference-size cymbal the endcaps are 12.7 mm in diameter with a base cavity diameter of 9.0 mm and an apex diameter of 3.0 mm. For bonding purposes, the endcap flange width is kept constant at 1.85 mm, but the cavity depth is adjusted from 120 μm to 600 μm, with a reference cavity depth of 250 μm. The final stage in the preparation of the endcaps is to roughen the bonding surface of the endcap flange using 600 grit sand paper (3M), followed by cleaning with acetone. The flanges of the endcaps are bonded to poled hard or soft PZT ceramics (provided by Piezo Kinetics, Inc. Bellefonte, PA) using a very thin (~20μm) layer of insulating epoxy (Eccobond 45LV/ Catalyst 15LV, 3:1, provided by Emerson and Cuming Inc., Woburn, MA). The pre-poled ceramic disks used throughout these experiments were 12.7 mm in diameter and 1.0 mm thick. To enhance the bonding, the transducers were allowed to cure at room temperature for at least 24 h (or 70°C for > 4hrs.) under moderate pressure. Based on microscopic observations, the bonding layer is approximately 20 μm thick [13] and has a width around 1.85 mm. In some cases, an additional layer of epoxy was added to the outer rim of the transducer to prevent fluid leakage into the cavity during underwater testing, especially during hydrostatic pressure tests. The relevant physical properties of the piezoelectric ceramics and endcap materials, along with bonding material are listed in Tables I and II, respectively [14-17].

The transducer dimensions for the parametric studies are listed in Table III. The 12.7 mm diameter cymbal was selected as the reference size. Sizes larger or smaller than the reference size were fabricated following the same procedure. Extensive experimental and FEA studies were performed on the reference size cymbal transducer. After establishing confidence in the FEA models, systematic calculations were performed on a range of transducer diameters from 3.2 mm to 35 mm.

B. Measurement Systems

Admittance characteristics, both in air and in water, together with the resonant frequency, effective coupling factor, mechanical quality factor, and electroacoustic efficiency were measured using an HP 4194A impedance/gain phase analyzer at room temperature and atmospheric pressure.

To determine the effect of water (mass) loading on the admittance spectra, effective coupling coefficient, and Q_m of single element cymbal transducers, measurements were made using a small container filled with de-ionized water. The internal dimensions of the container were 55 cm long, 55 cm wide, and 7 cm deep, taking into account the 12.7 mm thick Sorbothane liner used to absorb sound waves and minimize reflections, which would otherwise form standing waves. Reflections from the surface are unavoidable. A special sample holder was used to assure that the measurements were always made at the same depth (2.5 mm) keeping the face of the transducer parallel to the surface. The results obtained from these measurements were compared with those calculated from FEA codes.

Underwater performance was further evaluated in an anechoic water tank at Penn State's Applied Research Laboratory. The tank has the approximate dimensions of 5.5 m

depth, 5.4 m width, and 7.9 m length. The inside of the tank is lined with a resonant absorber, Saper-T, to minimize sound reflections. The water is maintained at 22°C with thermoclines minimized by constant circulation of the pump-driven water. The test frequency range extends from 2 kHz to 500 kHz. Pulsed signals were used to eliminate the effects of transducer rise-time and multipath reflections. Normally, transducers are tested using a gated 2 ms sinusoidal pulse. The receive signal is captured by an F33 standard hydrophone and processed through an HP465A amplifier connected to an HP 89410A vector signal analyzer.

C. Scaling

The 12.7 mm diameter reference-size cymbal transducer was studied extensively. Effects of bonding layer thickness, cavity depth, cavity diameter, PZT type and thickness, endcap thickness and material, and apex diameter have been investigated. Transducer parameters were evaluated for five different transducer sizes using FEA techniques. Table III lists the dimensions of the reference sample in bold, and the larger and smaller scaled transducers to be used as new controls. Unless otherwise mentioned, the piezoelectric driving element was PZT-5H, the bonding layer was Emerson and Cuming epoxy, and brass was used as the endcap material.

III. ANALYTICAL THEORY AND FINITE ELEMENT MODELING

Analytical methods derived from shallow shell theory [18] were originally used to calculate resonance frequencies. The fundamental resonance frequency in air, f_r, is governed principally by the endcap dimensions and elastic constants.

$$f_r \propto \sqrt{\frac{E}{\rho}\left[\frac{1}{\varnothing_c^2(1-\sigma^2)}+\frac{1}{R^2}\right]} \qquad (5)$$

where, ρ is the endcap material density

$\varnothing_c$ is the diameter of the cavity at its base

R is the endcap radius

E is Young's modulus of the endcap

σ is Poisson's ratio.

Thus, for transducers made with different metals, the first resonance frequency should be proportional to the term $[E/\rho\,(1-\sigma^2)]^{1/2}$ which has units of meters per second (m/s) and is related to the sonic velocity of the endcap material.

The relationship between the water-loaded and in-air resonance frequencies of the cymbal transducer is given by the equation

$$f_{r,w} \approx \frac{f_{r,a}}{\sqrt{1+\left(\frac{8a}{3\pi}\right)\left(\frac{\rho_w}{\rho_p}\right)\left(\frac{0.7885}{t}\right)}} \qquad (6)$$

where $f_{r,a}$ is the measured in-air resonance frequency

a is the radius of the cavity

ρ_w is the water density

ρ_c is the endcap material density

t is the endcap thickness.

This equation is based on the curve deflection theory for a thin plate clamped around its rim [19]. The coefficient 0.7885 in the above equation is calculated from this boundary condition. The equation also contains dimensional terms, and a relative density term.

When operated near resonance the cymbals are usually small compared to the wavelength (ka <<1), so that the imaginary part of the radiation impedance (radiation reactance) can be approximated as:

$$X_r = \rho_w c A \frac{8ka}{3\pi} \tag{7}$$

where $k = \omega / c = 2\pi / \lambda$, a is the radius of the cymbal, and area $A = \pi a^2$

The radiation reactance X_r can be regarded as an additional vibrating mass (M_r) given by:

$$M_r = \frac{X_r}{\omega} = \frac{8}{3}\rho_w a^3 \tag{8}$$

This mass is equivalent to that of a cylinder of water having the same cross sectional area as the piston (cymbal) and a length of $8a/3\pi$. For a 12.7 mm diameter cymbal transducer, the mass of the water associated with the radiation reactance is 0.7 g, which is over half the mass of the cymbal transducer itself (1.3 g). This "associated mass" has a very significant effect on the cymbal transducer. The amplitude of the resonance frequency is greatly reduced. For transducers having a radiation impedance that is highly reactive, the transducer's energy is not transferred to the water. The acoustic power of the transducer is equal to the real part of the radiation impedance times the square of the vibration velocity.

In an evolution from the analytical approach, finite element analysis was also used to calculate resonance frequencies, TVR, FFVS, k_{eff} and Q_m. The finite-element-method (FEM) is a numerical analysis tool for obtaining approximate solutions to geometrically complex engineering systems. A geometrically complex region defining a continuum is divided into small geometrical units called finite elements that are connected to one another by a finite number of points called nodal points. The material properties and governing equations are applied to these elements and expressed as unknown values at the nodal points of these elements. Incorporating the loading and boundary conditions, a global set of equations is assembled. Solving these equations gives the approximate behavior of the continuum [20].

In this study, ANSYS and ATILA FEM codes were used extensively for the analysis of the in-air vibration modes and associated resonance frequencies, as well as the in-water sonar performance of the cymbal transducer. Initial studies of the cymbal's in-air performance began with the ANSYS software package (version 5.1; followed by version 5.6) (Swanson Analysis Systems, Inc). Later the ATILA code (Magsoft Corporation) was used to run in-air *and* underwater characterizations of the cymbals. The ATILA finite element analysis code for sonar transducers was developed at the Acoustics Department at Institute Superior d'Electronique du'Nord – France. Modal analysis can be carried out to identify the vibration modes and determine their resonance frequencies and associated coupling factors. In-air or in-water impedance and displacement field, transmit voltage response, and sonar directivity patterns can be modeled using a harmonic analysis procedure [21-24]. The results were compared with

the experimental measurements obtained using an HP 4194-A Impedance/Gain Phase Analyzer, as well as with the underwater tests.

In elastic materials there are three degrees of freedom attached to a node, with an additional electrical degree of freedom added for piezoelectric materials. The classical set of equations, in matrix form for a coupled piezoelectric-solid structure is given in Equation 9 [25].

$$\begin{bmatrix} [K_{uu}]-\omega^2[M] & [K_{u\phi}] \\ [K_{u\phi}]^T & [K_{\phi\phi}] \end{bmatrix} \begin{pmatrix} \mathbf{U} \\ \mathbf{\Phi} \end{pmatrix} = \begin{pmatrix} \mathbf{F} \\ -\mathbf{Q} \end{pmatrix} \tag{9}$$

where $[K_{uu}]$ is the structure stiffness matrix

$[M]$ is the structure mass matrix

$[K_{u\phi}]$ is the piezoelectric stiffness matrix

$[K_{\phi\phi}]$ is the dielectric stiffness matrix

ω is the angular driving frequency

U is the vector representing the nodal values of displacement

Φ is the vector representing the nodal values of electrical potential

F is the vector representing the nodal values of applied forces

Q is the vector representing the nodal values of electrical charge.

Superscript T stands for matrix transposition.

The underwater performance of a transducer can be computed by modeling a structure containing a piezoelectric part and a non-piezoelectric solid part (such as metallic or polymeric parts of a device) immersed in fluid. The notations for such a

structure are defined in Figure 2. Electrical and mechanical fields are coupled inside the piezoelectric domain, Ω_p. The solid structure, Ω_s, which includes Ω_p, is in contact with the infinite fluid domain, Ω_f, through the surface S_i. The fluid domain is limited by the surface S_r, on which a non-reflecting boundary condition is applied.

The physical quantities of interest in this case are the displacement field, u, in the solid domain and the pressure field, p, in the fluid domain. Their nodal values are unknowns and are arranged into vectors **U** and **P**, respectively. The whole system equation for this solid-fluid domain can be written as follows [26]:

$$\begin{bmatrix} [K_{uu}]-\omega^2[M] & -[L] \\ -\rho^2 c^2 \omega^2 [L]^T & [H]-\omega^2[M_1] \end{bmatrix} \begin{pmatrix} \mathbf{U} \\ \mathbf{P} \end{pmatrix} = \begin{pmatrix} \mathbf{F} \\ \rho c^2 \varphi \end{pmatrix} \tag{10}$$

where $[H]$ is the fluid compressibility matrix

$[M_1]$ is the coherent mass matrix

$[L]$ is a connectivity matrix that represents the coupling between the structure and the fluid.

ρ is the fluid density

c is the sound speed

φ is the vector representing the nodal values of the pressure gradient normal to the fluid domain boundary

The non-reflecting boundary condition applied on the S_r surface allows the user to limit the finite element mesh of the fluid. When this surface is assumed to be in the far field, the relation between φ and $\mathbf{P}_\infty$ at the external fluid boundary S_r is [24]:

$$\varphi = -[\alpha + jkR][D]\frac{\mathbf{P}_\infty}{R} \tag{11}$$

where R is the radius of the external fluid boundary

k is the wave number

$[D]$ is the monopolar radiating matrix

α is equal to 1 when the structure is three-dimensional, or axisymmetrical, and ½ in the case of a plane strain analysis.

The nonreflecting condition is valid if the external fluid boundary is inside the far field area (kR»1). Considering an external excitation such as a prescribed displacement or force, and including the monopolar radiating condition, the system of equations given in Equation 10 becomes [24]:

$$\begin{bmatrix} [K_{uu}] + j\omega[C_{uu}] - \omega^2[M] & -[L] \\ -\rho^2 c^2 \omega^2 [L]^T & [H] - \omega^2[M_1] + \frac{\rho c^2}{R}[\alpha + jkR][D] \end{bmatrix} \begin{pmatrix} \mathbf{U} \\ \mathbf{P} \end{pmatrix} = \begin{pmatrix} \mathbf{F} \\ \mathbf{0} \end{pmatrix}$$

A 2-D axisymmetric model was used in the modal and harmonic analyses. For simplicity only one half of the cymbal was meshed. The mechanical boundary conditions of the cymbal were set free in both the in-air and in-water modeling. The thickness of the epoxy layer was 0.04mm. In the underwater simulation, a dipolar-damping element was employed. Therefore the boundary of the fluid domain can be placed in the near-field region, reducing the size of the model. The in-water mesh pattern is shown in Figure 3.

FEA and the analytic expression give results that generally correlate well with the measured data. Discrepancies mainly arise from experimental error, mesh fineness limitations, and the fact that FEA calculates for discrete frequencies, not a continuum. Material property data input sets are limited to linear region properties, leading to some additional discrepancy.

The experimentally measured admittance spectrum for a reference brass-capped cymbal in the neighborhood of the fundamental (first) resonance frequency in-air is compared to the FEA calculated curve in Figure 4. Less than 5% difference in resonance frequency is observed between the two, indicating that FEA codes adequately model the behavior of the cymbal in air. Table VI shows the calculated in-air and in-water fundamental resonance frequencies for the five scaled cymbal sizes.

IV. RESULTS AND DISCUSSION

A. Size and Materials Effect on The Resonance Frequency of Cymbal

1. Vibration Modes

Figure 5 shows the first three resonance modes of the reference cymbal transducer under mechanically free conditions. In the node notation (m, n), integer m is the number of radial node lines and integer n is the number of azimuthal nodal circles. m is 0 for a two dimensional axisymmetric body. The first three modes come from the resonance of the metal endcaps. The first one is a pure flexural mode in which all parts of the endcaps move in phase. At the second resonance, there are two nodal rings with the dome region and the shoulder region moving out of phase. The total pressure generated will be partly cancelled out which will be evident later in the underwater TVR response of the cymbal.

The third mode occurs at much higher frequency, and will not be considered in this report. It may become of interest if very large-sized, low fundamental resonance cymbals are to be made.

2. Scaling Factor

Figure 6 compares the FEA calculated in-air and water-loaded first resonance frequency for brass-capped cymbals whose sizes were increased or decreased by multiplying all parameters of the reference size cymbal by a scaling factor. Increasing device size increases the R (endcap radius) and $Ø_c$ (cavity diameter) terms in Equation 5, effectively decreasing the resonance frequency. As Equation 6 shows, the water-loaded resonance frequency is controlled by the radius/thickness ratio of the endcap and the relative densities of the endcap material and water. When a direct scaling factor is used to change the radius and thickness for a given endcap material, the difference between in-air and in-water resonance is a constant. Adjustment of the scaling factor from 0.25 to 2.75 provided a range in the fundamental resonance frequency of from 9.4 kHz – 85.6 kHz in air, and 6.4 kHz - 58.2 kHz in water.

3. Effect of Epoxy Thickness

In-air calculations using the FEA modeling indicate that, relative to other parameters studied, the thickness of the epoxy layer has only a small effect on the first resonance frequency, in an inversely proportional relationship (Figure 7). If we assume the endcap flange is bonded directly to the disk (zero thickness epoxy adhesive layer), the calculated resonance frequency is ~27 kHz for a reference-sized cymbal. For an epoxy layer thickness of 1000 μm (1 mm), the resonance frequency decreases to 22 kHz, a change of 20%. Realistically, the epoxy layer thickness would be between 10 μm and 100

μm, so even over this broad range, a variation in resonance frequency of less than 5% is expected. A thinner bonding layer causes adhesion and endurance problems; a thicker bonding layer leads to high compressibility of the bonding material resulting in stress transfer losses across the layer. In all of our experimental studies, bonding layer thicknesses were kept between 20-40 μm. In some cases a secondary epoxy layer was applied to the rim of the transducer to protect against water penetration into the cavity. An approximately 1-2 mm thick epoxy seal around the rim of the transducer stiffens the structure and typically increases the resonance frequency by 3 to 4 kHz for a reference size cymbal.

4. Effect of PZT Thickness and Material

The effect of PZT thickness on the first resonance frequency is plotted in Figure 8 for various transducer sizes. Approximate resonance frequencies can be obtained from this figure. However, if we focus on a particular transducer diameter (e.g. reference size) we see that the resonance frequency approaches a constant value after a certain thickness (Figure 9). The saturation thickness is around 2.5 mm and can be scaled using the following expression for all transducer sizes:

$$\frac{\text{PZT Thickness}}{\text{Total Thickness}(\text{apex}-\text{to}-\text{apex})-\text{PZT Thickness}} \approx 2.5 \qquad (12)$$

The clamping effect of the metal endcaps becomes more significant as the PZT thickness gets smaller because the cap/ceramic stiffness ratio increases. The coupling coefficient, k_{eff}, decreases very slightly as PZT thickness increases.

Changing the PZT driving element composition has a small effect on the first resonance frequency of the cymbal transducer. In-air, the cymbals driven by a hard PZT ceramic (e.g. PZT-4 or PZT-8) exhibit a 1 kHz higher resonance frequency than those driven by a soft PZT (e.g. PZT-5A or PZT-5H) for various PZT thicknesses (Figure 9). In general hard PZT ceramics have higher Young's modulus than soft PZT ceramics. Thus, the first flextensional resonance of cymbal transducers with hard PZT materials occurs at slightly higher frequency.

Table IV [9] compares the experimentally measured characteristics of in-air and water-loaded reference size brass-capped cymbals with those obtained from the FEA and *in-air* analytical results (Equations 6 and 8). First resonance frequencies of cymbal transducers in-water (for various PZT driving elements) are roughly 40% lower than in air, due to the water-loading effect. On the other hand, water-loading increases the effective coupling factor, and the measured coupling coefficients for the water-loaded single elements show an increase of 25-60%. This effect is not fully understood at this time. In Table IV, the numbers in parentheses represent the percent change from the in-air values.

5. Effect of Endcap Material

The resonance frequencies for cymbals capped with different metals are plotted as a function of ultrasonic velocity of the endcap material in Figure 10. These results show that for a transducer of fixed size, the first resonance frequency can be adjusted simply by changing the endcap material. The calculated admittance in the neighborhood of the first resonance associated with each endcap metal showed that the amplitude of the admittance is nearly independent of the endcap material used [9]. The measured k_{eff} for various

endcaps in-air is around 0.20±.01. Therefore, the resonance frequency can be adjusted without affecting the amplitude of admittance.

Resonance frequencies for the water-loaded conditions must be examined carefully. The characteristics of the water-loaded cymbals made with different endcap metals are presented in Table V. In most cases, less than 10% difference is observed between the measured and FEA results, for the fundamental resonance frequencies. The magnitude of the effect of water-loading depends on the endcap material. The variation in differences between the in-air and in-water resonance frequencies can be explained from Equation 6. Cymbals made with endcap metals closer in density to water (i.e. having a better acoustic impedance match) exhibit a much larger resonance frequency shift than cymbals having endcaps with higher densities. When this percent change in resonance frequency is plotted versus the ratio of water density to endcap density, the reciprocal square root behavior is observed, Figure 11 (Equation 6). For underwater applications the highest coupling coefficient was obtained using titanium endcaps. The amplitudes of the admittance curves do not change significantly for different endcap materials, as in the in-air case.

6. Effect of Endcap Thickness

Figure 12 shows the calculated admittance spectra near the first resonance for water-loaded brass-capped reference cymbals with varying endcap thickness. Though they appear similar to in-air spectra, the resonance frequencies are depressed because of mass-loading effects. Figure 13 shows the influence of endcap thickness on the first resonance frequency for different endcap metals for a reference-sized cymbal. The water-loading effect is more significant for thinner endcaps. For a given endcap

thickness, the resonance frequency increases with increasing endcap stiffness. The endcap thickness plays an important role in determining how much the resonance frequency will decrease in water. Equation 6 indicates that as endcap thickness increases, the difference between the in-air and in-water resonance frequencies becomes smaller. This is confirmed by the results presented in Figure 13. The effect of endcap thickness on the resonance frequency for various transducer sizes is shown in Figure 14. For all transducer diameters, a nearly linear relation exists between the endcap thickness and the first resonance frequency and is most significant for the smaller, 3.2 mm diameter samples. For the reference transducer the effective coupling coefficient does not show such a substantial change with endcap thickness (Figure 15). The curve shows a maximum, which may be a compromise between having enough stiffness to overcome the water-loading, while remaining sufficiently compliant to be an efficient flextensional transformer.

7. Effect of Cavity Depth

FEA results of the in-water first resonance frequency for reference sized cymbals with different endcap materials of varying cavity depths are shown in Figure 16. With increasing cavity depth, substantial increases are observed in resonance frequency for all endcap materials. Again, the first resonance frequency increases with the modulus of elasticity of the endcap. A similar effect is apparent for various transducer diameters (Figure 17). The effect of the cavity depth on resonance frequency is most significant for the smaller transducer.

Figure 18 shows the in-air admittance spectra in the neighborhood of the first resonance for reference cymbals with different cavity depths. The resonance frequency

decreases for shallow cavities. On the other hand, the amplitude of the admittance curve gets smaller with decreasing cavity depth. Figure 19 shows that the effective coupling coefficient, k_{eff} increases with increasing cavity depth. Measured in-air k_{eff} values for reference size cymbals are generally around 0.25. If cavity depth is reduced to adjust the resonance frequency, a slight sacrifice must be made in k_{eff}. The FEA results again correlate well with the measured results, with a 10% - 20% underestimation.

8. Effect of Cavity Diameter

The effect of cavity diameter on the first resonance frequencies for water-loaded brass-capped cymbals with different cavity depths is shown in Figure 20. For all cavity depths, increasing cavity diameter causes a decrease in the first resonance frequency. The trends in the results mirror those of the in-air case, but with the resonance frequency shifted down roughly 30%. Figure 21 shows the effect of cavity diameter on the first resonance frequency for various transducer sizes. Smaller transducer sizes lead to an increase in the first resonance frequency. First resonance frequency decreases with increasing cavity diameter, but the decrease is more significant for the smaller size transducers. In other words, as the ratio between the cavity depth and cavity diameter (which is related to the tangent Θ of the cavity angle) gets smaller, the changes in the cavity diameter have a more significant effect on the first resonance frequency. Changing the cavity diameter also has an effect on the radiating surface area.

9. Effect of Apex Diameter

The effect of changing apex diameters for various cavity diameters in reference-sized cymbals is shown in Figure 22. For the larger cavity diameters the maximum resonance frequencies are observed near an apex diameter of 4.5 mm. There is a steady

increase for the samples with small apex diameters. Figure 23 shows the resonance frequency versus apex diameter relation for various transducer sizes (assuming scaled cavity diameters). A shallow bell shaped curve is generally observed for all sizes. The maximum resonance frequencies and k_{eff}, and minimum Q_m are achieved for an aspect ratio of 1:3 between apex diameter and transducer diameters. This relationship is another parameter that can be adjusted to help tailor the resonance frequency.

B. Size and Material Effects on Sensing and Projecting Performance (Beam Patterns, TVR and FFVS)

1. Directivity Beam Patterns

The measured (ARL anechoic test tank) and FEA calculated directivity patterns of a cymbal transducer under free mechanical conditions are shown in Figure 24. These patterns were generated for the plane normal to the cymbal disk. The peak value is set equal to zero, and any diminution of value is shown normalized as dB reductions relative to the angle measured. Near the first resonance frequency and at higher frequencies, near 30 kHz and 50 kHz, omnidirectional patterns were observed in the potted cymbal case and in the calculation. The mechanical conditions and test fixtures have a very pronounced effect on the performance of cymbal transducers, especially at higher frequencies. The test fixtures must be carefully chosen during the test to avoid interference with the transducer performance [27].

2. TVR & FFVS

Reference size cymbals are essentially omnidirectional up to their resonance frequency. Increasing device diameter decreases the resonance frequency. TVR and FFVS become directional properties if the devices are larger than the wavelength.

Performance estimates are presented here over a broad frequency range, so as size to wavelength ratio changes a difference in directivity index (DI) may affect results in ways not reflected here. For purposes of this report, the values presented are taken in the plane normal to the ceramic disk. When evaluating TVR and FFVS for scaled-up cymbals with larger diameters, directivity should be considered.

A very good match was obtained between the FEA calculations and the experimental TVR values shown in Figure 25. Just below the first flextensional resonance, the TVR increases linearly with frequency and follows the pattern of a typical piezoelectric transducer as predicted using a simple mass-spring model. Well above the first resonance but below the (0,2) resonance, the TVR drops to about 112 dB, as predicted by the model. There was a sharp dip around 65kHz associated with the (0,2) mode of the metal endcap. As shown in Figure 5, the two portions of the endcap vibrate out of phase in this mode. The pressures from different portions of the metal endcaps cancel and lead to a sharp drop in response. There is a dip in the TVR measured value at about 20 kHz that has been explained by Meyer [28] to be caused by an asymmetric bending mode related to imperfectly matched endcaps. The mechanical Q-factor is around 14 for the single cymbal transducer, which is rather high compared to other flextensional transducers because of its small size and weight. Because of the high Q it will be difficult to use cymbals as single element sound projectors, but small size, low weight, and low cost make cymbals attractive for incorporation into arrays tailored to achieve the desired power and beam pattern.

a. Scaling Factor

To some extent the frequency of a cymbal transducer can be adjusted by changing endcap material and endcap shape, but if we wish to make a large change in the first resonance frequency, the only option is to change the size of the cymbal transducer. Currently there is an interest in using cymbal transducers at very low frequencies for oil industry exploration and in very small sizes for hearing aid devices. Preliminary calculations were carried out using ATILA to determine the underwater response of different sized cymbal transducers. Figure 26a shows the calculated TVR of cymbal transducers of different sizes made by scaling the geometry in proportion to the reference 12.7 mm diameter cymbal. Note that the TVR peak amplitude is about the same for large and small cymbals, regardless of resonance frequency. For a 35 mm diameter cymbal (2.75x scaling factor), the first resonance frequency is about 6 kHz. The calculated Q factor is around 15. At this size, the structure becomes very compliant and (0,1) and (0,2) modes approach one another closely. To avoid interference from the higher frequency vibration modes, a cymbal of this size must be operated near the first flextensional resonance mode.

As size decreases the resonance frequency in-water increases. For a one-eighth-inch diameter (3.2 mm) cymbal the resonance frequency increases to around 63 kHz with a Q factor around 14.

The FFVS below resonance decreases gradually in proportion with the size (Figure 26b).

b. Effect of Epoxy Bonding Layer Thickness

Figure 27 shows that the epoxy bonding layer thickness has little effect on the underwater characteristics of the cymbal transducer. Experimentally, the bonding layer thickness of the cymbal samples was measured to be around 20 μm. For simplicity, and to reduce the required total number of nodes, a 40 μm thick bonding layer was chosen for the FEA calculations. For bonding layers between 20 to 40 μm, the performance is almost unaffected except for a 5% decrease in the (0,2) resonance frequency. Further increases to the epoxy layer thickness increase the effective compliance of the cymbal structure. Thick epoxy layers will result in a transducer failure. Under high drive conditions, the losses in the glue layer convert energy to heat which can result in thermal runaway.

c. Effect of PZT Material and Thickness

In the cymbal structure, the only active element is the poled PZT ceramic, while the epoxy layer and metal endcaps serve as mechanical transformers. Therefore, the underwater characteristics of a cymbal are mainly determined by the PZT driving element, more specifically by the piezoelectric coefficients leading to radial motion (d_{31}). Figure 28a shows the calculated TVR of cymbals using various PZTs. The resonance frequency remains almost the same because it is governed by the mechanical resonance of the endcaps and depends mainly on the endcap material and geometry. Cymbals driven by soft PZT with a high d_{31} piezoelectric coefficient (e.g. PZT5H) yield higher TVR values than those driven with hard PZTs (e.g.PZT4 and PZT8). This result may be deceiving. Although the per-volt performance is higher, the maximum source-level (SL) has to be considered. The higher loss tangent and the lower coercive field of PZT 5H

limit the drive level for this material. Typical rule of thumb drive levels for PZT 5H, PZT 4, and PZT 8 are 4, 7 and 10 V/mil rms. Applying these limits, peak SLs using these materials are: PZT 8, 176.4; PZT 4, 174.8; and PZT 5H, 175.9.

Changing the PZT driving element only alters the amplitudes of the TVR and FFVS spectra and the second mode resonance frequencies; the fundamental resonance frequencies remain constant. Figure 29 shows the measured TVR curves near resonance for cymbals made with different PZTs. FEA and measured results are in good agreement.

The calculated FFVS of cymbals with hard and soft PZTs are shown in Figure 28b. There was not much increase in sensitivity in using soft PZT with larger d coefficients. Since the FFVS is the open-circuit voltage output of the hydrophone, this can be understood by examining the figure of merit of the material:

$$FOM = \frac{d_h g_h}{\tan \delta} \tag{13}$$

where d_h is the hydrostatic piezoelectric strain constant, tanδ is the electrical dissipation factor and g_h is the hydrostatic piezoelectric voltage constant ($g_h = \frac{d_h}{\varepsilon_{33}^T}$). Although soft PZTs have higher d coefficients, they also have higher dielectric loss and higher dielectric constants, which reduce their figure of merit. Therefore, soft PZT does not necessarily have higher sensitivity. On the other hand, the capacitance of a hydrophone is important in that a high capacitance permits a lower limit to the operating frequency band, for a given input resistance to the amplifier. For this reason soft PZT is preferred in hydrophone applications. Trade-offs often must be made between output voltage sensitivity and capacitance. Since we are intending to use the cymbal transducers as both

projectors and receivers, they must be driven hard at resonance, and soft PZTs are rejected because of their higher dielectric loss. As a trade-off, PZT4 was selected over PZT 8 for its higher capacitance and sensitivity. For a half-inch cymbal transducer made of PZT4, the capacitance is about 1.5 nF and a satisfactory electrical impedance match can be obtained.

Figure 30a shows the effect of ceramic thickness on the transmit voltage response of a single element transducer. The geometry is that of the reference design with PZT-5H as the driver material. The thickness was varied from 0.1 mm to 3.0 mm. As expected from Equation 12, the fundamental resonance frequency increased up to a thickness of approximately 2 mm. Thicker driving elements provide a stiffer boundary condition for the endcap which shifts the fundamental resonance to slightly higher frequencies. For larger thickness the resonance frequency remained relatively unchanged. Increasing the thickness caused a small change in the second vibration mode of the endcaps. For thicker drivers this mode shifts to lower frequencies.

The TVR level drops with the larger thickness because of a change in impedance. To determine if there is any significant effect on the TVR level, the electric field limits for PZT-5H can be applied, which takes into account the change in impedance (Table VII). Increasing the ceramic disk thickness allows the device to be driven at much higher voltage and the resulting increase in source level is significant. The presence of an apparent optimum SL at 2 mm thickness and the different shape of the TVR and FFVS curves for the 3 mm thickness will be investigated further. The latter to determine if there is an effect that can be exploited for increased bandwidth (by bringing the first and second modes closer together), or a condition that must be avoided.

For the free field voltage response, shown in Figure 30b, the magnitude of the sensitivity was relatively unchanged around the fundamental resonance. A slight increase was observed for the thicker drivers with again, a maximum appearing around 2mm for the below resonance sensitivity.

d. Effect of Endcap Material

Figure 31 shows the TVR and FFVS for cymbal transducers made with different endcap metals. Both the (0,1) and (0,2) mode frequencies increased as the modulus increased, and the difference between them also increased. For cymbal transducers, the difference in frequency between the (0,1) mode and the (0,2) mode determines the usable frequency range for underwater applications. Therefore there is a larger usable frequency range for cymbal transducers with high modulus endcaps.

The magnitude of TVR and FFVS values depend only slightly on endcap material. Higher modulus endcaps yielded higher TVR but lower FFVS. High modulus materials are preferred because of greater pressure tolerance and the wider frequency range.

e. Effect of Endcap Thickness

Figure 32a shows the TVR as a function of endcap thickness for brass endcaps. As expected, the thicker endcaps have higher resonance frequency. Thicker endcaps have higher stiffness, which raises the resonance frequency significantly. The fundamental resonance can be tuned from 10 kHz to 50 kHz by changing the thickness from 0.12 mm to 1.0 mm. The magnitude of the TVR shifts slightly higher, which may represent an improvement in the real part of the radiation impedance. In this case, the change in directivity should be larger than the observed increase in TVR. This suggests that the thicker endcaps are not as efficient in transferring the radial motion of the endcaps into an

axial displacement. The FFVS, shown in Figure 32b, decreases in magnitude for thicker endcaps. Therefore, as the transmit case suggested, thicker endcaps do not transfer the incoming pressure wave to the ceramic as efficiently.

f. Effect of Cavity Depth

The effect of cavity depth on the underwater characteristics of a cymbal transducer is shown in Figure 33. Of all the parameters considered, cavity depth had the most profound effect on the amplitude of the TVR and FFVS. As the cavity depth increased from 0.1 mm to 1.0 mm, the amplitude of TVR increased by about 25 dB over the frequency range between the (0,1) mode and (0,2) mode. At the same time, the resonance frequency of the cymbal increased from 12kHz to 39kHz. As the cavity depth increased, the effective Q decreased significantly resulting in a broader bandwidth (Figure 19). Both measurement and simulation show that as cavity depth increases, the electromechanical coupling coefficients of the cymbal transducer increase. The increase in TVR and FFVS was mainly due to the increase in electromechanical coupling coefficient of the cymbal transducer.

g. Effect of Cavity Diameter

The transmit and receive characteristics of a reference size cymbal transducer with varying cavity diameter are shown in Figure34. By varying the cavity diameter, the angle between the endcap arm and the ceramic changes, along with the flange width. Also, the length of the endcap arm changes as a function of angle. For a 12.7 mm diameter cymbal, the maximum cavity diameter was limited to 12.0 mm. This leaves only a 0.7 mm rim for bonding. From the TVR curves, as the cavity diameter was increased from 4.5 mm to 12.0 mm, the fundamental resonance frequency changed from 10 kHz to 70

kHz, respectively. This is a factor of 7 change in resonance frequency for a factor of 3 change in cavity diameter. The FFVS below resonance showed 30 dB higher sensitivities for the larger cavity diameters while the magnitude of the TVR at resonance remains relatively constant for the different cases. So for a given apex diameter, more efficient stress transfer to the ceramic occurs at smaller angles. The second mode of the endcaps was also affected. The longer arm length reduced the ratio of the second mode to the fundamental mode by 39%.

h. Effect of Apex Diameter

In the previous section, the cavity diameter was altered while maintaining a fixed apex. Next, the apex diameter was adjusted with a constant cavity diameter of 9.0 mm. As with the previous case, changing the apex diameter altered the angle between the conical dome and the ceramic and changed the length of the arm. In this case, the change in fundamental resonance frequency was not nearly as significant. Only a 33% change was observed. The magnitude of the TVR was relatively constant, as shown in Figure 35a. Also, the various apex diameters seemed to provide similar displacements below resonance since the TVR values are nearly identical for the different cases. A similar change in the second resonance of the endcap was observed. This frequency shifted downward from 62 kHz to 40 kHz, a change of 35%. This change has a bigger influence on the operating bandwidth of the device. For larger bandwidths, the apex diameter should be reduced. Little difference was seen in the receive sensitivity except near the second vibration mode. The FFVS is shown in Figure 35b.

V. HYDROSTATIC PRESSURE DEPENDENCE

This section shows how the cymbal transducer performs under hydrostatic pressures of up to 1000 psi (7 MPa). The influence of endcap materials, endcap geometry and dimensions, as well as the type of PZT on performance will be shown. The means by which the transducer fails under hydrostatic pressure will be clarified. (See further discussion under Section VII. Reliability). Unless otherwise indicated, all cymbal transducers tested in this chapter are brass-capped PZT-5H with the reference dimensions described earlier (Figure 1).

The magnitude of hydrostatic pressure that a transducer can withstand without degradation in performance is an essential parameter. This must be investigated before a prototype underwater transducer can be placed into service. So-called shallow water projectors are typically only required to withstand pressures on the order of 250 psi (1.75 MPa), which is equivalent to about 500 ft. (175 m) of depth. As a rule of thumb, 1 psi is $\cong 7 \times 10^{-3}$ MPa, and 1 MPa pressure corresponds to 100 meters of water depth.

The d_h measurements reported below represent the first cycle under elevated pressure for the specific samples involved. The maximum pressure that can be cyclically applied to cymbals of various dimensions without inducing irreversible reduction in properties (walkoff) is under investigation. One such test is described under Section VII B. We also plan to study whether an initial cycle is required to stabilize the sample prior to repeated cycling, and what pressure and hold-time are required to insure stable, reversible, repeatable results.

A. Measurement

The pressure dependence of a cymbal transducer was determined by measuring its effective d_h coefficient as a function of hydrostatic pressure [9, 27, 29]. The units of d_h are typically reported in terms of 10^{-12} C/N or simply pC/N. The piezoelectric voltage coefficient, g_h, can be calculated from the charge coefficient through the relation; $g_h = (d_h/\varepsilon)$, where ε is permittivity in farad/m.

The g_h coefficient is reported in terms of 10^{-3} V•m/N (or mV•m/N). The hydrophone sensitivity is equal to the product of the g_h coefficient and the transducer thickness; thus, the g_h coefficient is really the most direct and important factor to consider when designing high sensitivity hydrophones.

Different hydrophone materials are often compared using a figure-of-merit (FOM) which is the product of the d_h and g_h coefficients [30]. It is generally reported in units of 10^{-15} m^2/N or fm^2/N. Sometimes the dielectric loss is taken into account and the FOM is then taken to be $d_h \bullet g_h/\tan\delta$ [31]. When loss is accounted for, the figure-of-merit is reported in units of 10^{-13} m^2/N. The figure-of-merit measurement is perhaps more useful in determining the type of amplifier to use in the electronic circuitry and, in the case of composites, should be normalized by the volume of the device in order to make an accurate comparison [32].

B. Effect of Endcap Materials/Dimensions on Pressure Dependence

Adjustment of the various parameters allows cymbals to be tailored to withstand high hydrostatic pressures. The pressure dependence is independent of the type of PZT used as the active element. Figure 36 shows that for reference size, brass-capped

cymbals made with different driver materials the effective d_h remains flat out to about 2.5 MPa hydrostatic pressure. The d_h of each of the samples dropped off above this pressure.

Improving the performance of the cymbal under hydrostatic pressure depends upon the endcap material, endcap thickness and cavity depth since these three attributes all affect the effective endcap stiffness. Higher Young's modulus metals, thicker endcaps, and endcaps with deeper cavities can all withstand higher pressures before loss of properties. Potting the entire device in a stiff polymer also increases the pressure tolerance.

The pressure dependence of a reference size, brass-capped cymbal potted in a stiff polyurethane enclosure 6 mm in thickness and 34 mm in diameter is compared to an unpotted sample in Figure 37. The drop-off in d_h is much more gradual than in the unpotted sample with the largest drop occurring after 4 MPa. The difference in effective d_h between the potted and unpotted sample is small, indicating that potting the hydrophone in polyurethane allows its use range to be extended from ~2.5 MPa to nearly 4 MPa (i.e. an extra 150 m of water depth) without a large difference in performance. As stated above, the reversibility of the effect is being studied (see Section VII, B).

Figure 38 shows the pressure dependence of the effective d_h and g_h coefficients of same-size cymbal transducers with different endcap materials. These data clearly show that endcaps made of stiffer metals are capable of withstanding higher pressures without a degradation in performance. Stiffer endcaps are not as efficient in transferring stress to the piezoceramic, which is why the effective d_h coefficient drops for cymbals with higher Young's modulus endcaps.

Figure 39 shows how the hydrostatic performance of the cymbal is affected by varying endcap thickness (brass endcaps). Again, the effective stiffness increases for thicker endcaps, resulting in higher pressures that can be withstood, but at the expense of lower effective d_h. Figure 40 shows the pressure dependence of effective d_h for various cavity depths (a. brass endcaps, unpotted, b. Ti endcaps potted in urethane). Shallow cavities act as very good stress transformers but are more susceptible to the pressure load. Endcaps with deep cavities approach a dome-like configuration and are capable of withstanding much higher pressures. Much of the incident axial direction stress is transferred axially into the ceramic rather than being transformed into the radial direction. This accounts for the lower observed effective d_h values. Nevertheless, these results show that cymbal transducers with deep cavities, especially when combined with a stiff metal endcap and polymer potting, may tolerate hydrostatic pressures up to and even exceeding 7 MPa without a degradation in their performance while still maintaining a d_h value many times that of the uncapped PZT disk.

VI. ACTUATOR PERFORMANCE

A. Displacement

Figure 41 shows the effect of the cymbal overall size on the measured displacement. The displacement increases with size in a linear relationship. For each parameter configuration there is a different slope to the increase in displacement with voltage. For example, the brass capped 1-inch diameter cymbal goes from 6.1 at 100V to 90.2 at 1000V, not 61 as would be expected from a voltage-based extrapolation. On the other hand, the 5/8-brass version does scale with voltage. Samples made with titanium

endcaps had slightly reduced displacement magnitude, but, showed slopes that were nearly identical to those for brass, for each size, indicating that the effect is primarily governed by the geometry of the device.

B. Generative Force

A load-line showing the relationship between generative force and displacement is shown in Figure 42 for three different sized cymbals. These data were calculated using the ANSYS FEA program. Each cymbal is made with PZT 5H and brass endcaps, with all parameters scaled for the different device diameters.

VII. RELIABILITY

A. Material and Design Factors

Figure 36 shows the pressure dependence of the measured effective d_h coefficients of four samples exposed to hydrostatic pressure with measurements usually made at intervals of 0.35 to 0.7 MPa. All four transducers exhibit similar pressure dependence, with d_h dropping off at about 3 MPa. Since the 'hard' PZT-4 and PZT-8 should be capable of withstanding higher stresses (and consequently higher pressures) before depoling, this indicates that the effect is not due to depolarization of the ceramic. Removing the cymbal endcaps from both the hard and soft PZT and remeasuring the d_{33} coefficients showed no significant changes in their values confirming that no depoling occurred in the PZT.

Resonance spectra for the cymbals were measured both before and after the high-pressure tests. After being exposed to high pressure, the radial mode of the ceramic is still quite strong and the fundamental mode from the endcap, the flexural mode (first

resonance mode) is still observed, albeit at a lower frequency and with a reduced amplitude. The presence of both vibration modes and the absence of any additional spurious resonances after testing indicate that the bonding layer remains intact.

For reference size cymbals, the shape of the endcaps both before and after being subjected to a hydrostatic pressure of 7 MPa was profiled using a Tencor Instruments Alpha-Step 200 Profilometer. Partial collapse of the endcaps took place during the pressure testing. The apex at the top of the endcap was indented and the cavity was somewhat shallower. This explains the downward shift in the resonance frequency, since cymbal transducers with shallow cavities exhibit lower resonance frequencies than those with deeper cavities.

Figures 37 through 40 show improvements obtained by "potting" the cymbal in polyurethane prior to pressure testing, by using stiffer metal endcaps, by increasing the endcap thickness, or by increasing cavity depth.

B. Pressure and Electric Field Fatigue Test:

If the hydrostatic pressure seen by the cymbal is kept below the failure pressure, there is no significant degradation in performance after at least eight days at 2.4 MPa (240 m depth undersea), or after being cycled at least 40 times between 0 and 2.75 MPa (Figure 43). Additional studies are planned for determination of the maximum cycling pressure tolerance for different parametric conditions without degradation of properties, and if additional stability can be attained by pre-stressing (conditioning) the cymbals.

To investigate the mechanical fatigue characteristics of a cymbal, an electric field of 1kV/mm (peak to peak) at 100 Hz was applied in air. Experiments were performed at room temperature (25° C ±2). After cycling 10^8 times, a deviation in apex displacement

of only ± 0.8 % was observed. The reason for the deviation is probably the room temperature fluctuation and experimental error. Before and after the cycling test, the admittance spectra of the actuators were recorded. The admittance spectrum is very sensitive to any destruction in the bonding layer and to sample imperfections. For this reason, it is used as a nondestructive test method. After the fatigue tests, no significant changes were observed. The resonant and antiresonant frequencies as well as their peak amplitudes were the same as the original values found before the fatigue tests.

C. Performance Under High Drive Level

Figure 44 shows TVR vs. elapsed time results as drive level increases for a 3X3 cymbal array made from titanium endcaps with 150 μm cavity depth, using 1 mm thick PZT 4. The array was potted in EN-9 polyurethane prior to testing. The TVR was measured using 15 kHz pings 5 ms on; 67 ms off (7.5% duty cycle) sampled every two minutes with a 2 ms gated pulse. The TVR remains essentially constant up to about 53 dB. To convert drive level in dBV to the drive level in voltage (V) use:

$$dBV_{drive,\,rms} = 20 \cdot \log V_{drive,\,rms} \qquad (14)$$

Therefore, 53 dBV_{rms} corresponds to 447 V_{rms}, or an electric field of about 11 V/mil, which is well above the 7 V/mil maximum usually recommended for PZT 4. This array shows stable behavior while being driven at this high level for 30 minutes.

A similarly constructed array was tested for its frequency response under increasing drive level (Figure 45) up to 53 dBV. The frequency sweeps were performed using 2 ms pulses every 1 second at 200 Hz steps. Drive level in dBV is listed in the

legend. The frequency and resonance behavior is essentially unchanged with increasing drive.

Driving at higher levels may result in failure due to depoling of the ceramic, metal fatigue, excessive heating, or stress fractures in the ceramic or bonding layer epoxy.

VII. CONCLUSIONS

Benefiting from their very high piezoelectric charge coefficients, cymbal arrays can be used as very effective under-water transducers. The advantages of the cymbal type of hydrophone include very large d_h (hydrostatic charge) and g_h (hydrostatic voltage) coefficients, very thin profile, lightweight, and inexpensive fabrication. The moderate TVR exhibited by a single device can be greatly enhanced by incorporating cymbals into thin, flat, close-packed, flexible, and conformal arrays [27,33]. Hydrophone figures of merit ($d_h.g_h$) of some of the widely used composites and single element transducers are compared in the plot in Figure 46. Due to the size dependence of some transducers, the figure of merit is calculated for a 1-cm^2 transducer for a valid comparison. Cymbals exhibit the highest figure of merit among all of the listed composites.

The fundamental resonance frequency of cymbals can be readily tailored to specific applications by control of the numerous available dimensional parameters, offering great flexibility in design. Adjustment of the dimensions and materials used for drivers and endcaps provided a range in the fundamental resonance frequency of from 3.5 kHz - 252.4 kHz in water. These results also indicate trends that can be used to extend the ranges further. The scaling factor, cavity depth, and PZT thickness had the strongest effects on the projector/receiver performance (TVR/FFVS) while pressure tolerance was

most influenced by endcap design. Array performance indicates that cymbals are stable under high electrical driving conditions, up to 53 dBV (11V/mil), and cycling a single element with a 100 Hz, 1kV/mm field had no significant effect after 10^8 cycles. When cycled under a hydrostatic pressure of 0 to 2.75 MPA, a stable dh was measured after initial conditioning cycles.

The results collected in this report provide direction for the next phase of cymbal optimization. For example, the use of 1 mm thick ceramic disks has been the norm for cymbal research trials to date. It is now apparent that greatly increased source levels can be attained with thicker disks. Some of the TVR curves show a TVR peak near the second mode instead of the trough typically seen at this mode. By combining thicker disks, larger cavity depths, and thinner endcaps, it may be possible to draw the first two resonance modes together and provide increased bandwidth.

Application requirements must be specified before the cymbal design can be optimized to fit a given need. The parametric study detailed in this report provides guidance for tailoring dimensions of single cymbal elements. For most applications, cymbals are much more effective when combined into thin, flexible, low-profile arrays taking advantage of their high power to thickness ratio. To study array behavior, a large 6X34 element array was constructed with each element individually wired. The performance of this array is currently under evaluation.

VIII. ACKNOWLEDGEMENTS

This report represents the work of eight researchers over a period of several years. The authors would like to acknowledge the technical assistance provided by Dr. Kenji

Uchino, Paul Moses, Jeff Long, Joe Kearns, Susan Danley, Wipha Yimnirun, Dick Brenneman, Gaylord Shawver and Chris Jabco at the Materials Research Laboratory. Also Dr. Jack Hughes, Dr. Tom Montgomery, Bob Dashem, Greg Granville, and Mark Geleskie at the Applied Research Laboratory, and Dr. Philippe Bouchilloux at Magsoft (ATILA support). The authors are especially grateful for the support and encouragement of Dr. Jan Lindberg and Dr. Wallace Smith at the Office of Naval Research. The work was funded by the Office of Naval Research and Advanced Research Projects Agency, and the National Science Foundation.

IX. REFERENCES

1. Newnham R.E., Skinner D.P. Cross L.E., "Connectivity and Piezoelectric-Pyroelectric Composites," *Mater Res Bull* 1978, 13, 525
2. Gururaja, T.R., A. Safari, R.E. Newnham and L.E. Cross, "Piezoelectric Ceramic-Polymer Composites for Transducer Applications," *Electronic Ceramics*, Edited by L.M. Levinson. Marcell Dekker. Inc., New York, 92 (1987)
3. Kenji Uchino, *Ferroelectric Devices.* Marcel Dekker, Inc., New York, NY 2000
4. Sugawara, Y., Onitsuka, K., Yoshikawa, S., Xu, Q. C., Newnham, R. E., and Uchino, K., "Metal-Ceramic Composite Actuator," *Journal of the American Ceramic Society*, Vol. 75, No. 4, 1992, pp. 996–998.
5. Newnham, R. E., Xu, Q. C., and Yoshikawa, S., *U.S. Patent*, # 999 819, 1991.
6. A. Dogan, S. Yoshikawa, K. Uchino, R.E. Newnham, "The Effect of Geometry on the Characteristics of the Moonie Transducer and Reliability Issue", IEEE *Ultrasonic Symposium Proceedings,* Vol. II. pp. 935-939, 1994

7. Dogan A., Uchino, K., and Newnham, R. E., "Composite Piezoelectric Transducer with Truncated Conical Endcaps, Cymbal," *IEEE UFFC*, Vol.44, No. 3, 1997, pp. 597-605.

8. A. Dogan and R.E. Newnham "Metal-Electroactive Ceramic Composite Transducer" U.S. Patent No. 5,729,077, 1998

9. Tressler, J.F. 1997. "Capped Ceramic Underwater Sound Projector the 'Cymbal'," *Ph.D. Thesis*, The Pennsylvania State University, University Park.

10. A. Dogan, J. Tressler, R. E. Newnham, "Solid State Ceramic Actuator Designs" AIAA Journal Vol. 39, No. 7, pp.1354 -1362, July 2001.

11. R.J. Meyer Jr., A. Dogan, C. Yoon, S. Pilgrim and RE. Newnham, "Displacement Amplification of Electroactive Materials Using the Cymbal Flextensional Transducer," Sensors and Actuators, A 87 pp.157-162, 2001.

12. A. Dogan, K. Uchino, and R.E. Newnham, "Flextensional Composite Transducers: Designing fabrication and Application" Kluwer Academic Publisher NATO Science Series 3, 76, pp.357-374, 1999.

13. A. Dogan, Ph. D. Thesis, "Flextensional 'Moonie and Cymbal' Actuators", Materials Program, The Pennsylvania State University, 1994.

14. Vernitron Piezo-electric Division, "Piezoelectric Technology - Data for Designers".

15. *Smithell's Metals Reference Book, 6th edition.* Edited by E.A. Brandes, Butterworth & Co., NY, 1983.

16. L.L. Harner, "The Use of Fe-29Ni-17Co Alloy in the Electronics Industry"; pp. 3-16 in *Low Thermal Expansion Alloys and Composites*. Edited by J.J. Stephens and D.R. Frear, The Minerals, Metals, and Materials Society, Warrendale, PA, 1994.

17. Emerson and Cuming Inc., Woburn, MA (Eccobond 45LV/ Catalyst 15LV)

18. E. Reissner, "On Axi-Symmetrical Vibrations of Shallow Spherical Shells," *Quart. Appl. Math*, 13 279 (1950).

19. R.S. Woollett, "Theory of the Piezoelectric Flexural Disk Transducer with Applications to Underwater Sound," *USL Research Report No. 490, S-F001 03 04-1*, U.S. Navy Underwater Sound Laboratory, Fort Trumbull, New London, CT, 5 December 1960.

20. Chandrupatla, T.R. & A.D. Belegundu. 1997. In *Introduction to Finite Elements in Engineering*, Prentice-Hall, Inc, Upper Saddle River, NJ

21. Hamonic, B., J.C. Debus, J.N. Decarpigny, D. Boucher & B. Tocquet. 1989. "Analysis Of A Radiating Thin-Shell Sonar Transducer Using The Finite Element Method," *J. Acous. Soc. Am.*, 86, (4), pp.1245-1253

22. Hladky-Hennion, A.C., & J.N. Decarpigny. 1991. "Application Of The Finite Element Method To The Modeling Of 2D And 3D Passive Or Active Structures," *Ultrason. Int. Conf. Proc.*, pp.415-418

23. Hladky-Hennion, A.C. & J.N. Decarpigny. 1993. "Finite Element Modeling Of Active Periodic Structures: Application To 1-3 Piezocomposites," *J. Acous. Soc. Am.*, 94, pp.621-635

24. Hladky-Hennion, A.C., R. Bossut & M.D. Billy. 1998a. "Time Analysis Of Immersed Waveguides Using The Finite Element Method," *J. Acous. Soc. Am.*, 104, pp.64-71

25. Decarpigny, J.N., J.C. Debus, B. Tocquet & D. Boucher. 1985. "In-Air Analysis Of Piezoelectric Tonpilz Transducers In A Wide Frequency Band Using A Mixed Finite Element-Plane Wave Method," *J. Acous. Soc. Am.*, vol. 78, no 5, pp.1499-1507

26. Bossut, R. & J.N. Decarpigny. 1989. "Finite Element Modeling Of Radiating Structures Using Dipolar Damping Elements," *J. Acous. Soc. Am.*, vol. 86, no 4, pp. 1234-1244

27. Tressler, J.F., Newnham R.E., Hughes, W. J, 1999. "Capped Ceramic Underwater Sound Projector the 'Cymbal' transducer," *J. Acous. Soc. Am.*, vol. 105, no 2, pp.591-600.

28. Meyer, R.J., Jr., W.J. Hughes, T.C. Montgomery, D.C. Markley and R.E. Newnham, "Design of and Fabrication Improvements to the Cymbal Transducer Aided by Finite Element Analysis," *Accepted by the Journal of Electroceramics*, April 2002

29. Zhang, J. 2000 "Miniaturized Flextensional Transducers and Arrays," *Ph.D. Thesis*, The Pennsylvania State University, University Park.

30. S. Hanish, *A Treatise on Acoustic Radiation, Volume II - Acoustic Transducers*, Naval Research Laboratory, Washington, DC, 1983.

31. A.S. Bhalla and R.Y. Ting, "Hydrophone Figure of Merit," *Sensors and Materials*, 4, 181-185 (1988).

32. T.B. Gabrielson, "Limitations of the $d_h g_h$ Figure of Merit." Presented at the 1997 ONR Transducer Materials and Transducers Workshop, The Pennsylvania State University, April 1997.

33. Zhang J., W. Jack Hughes, R. J. Meyer Jr., K. Uchino, and R. E. Newnham, "Cymbal Array: A Broad Band Sound Projector," *Ultrasonics,* vol. 37 (8), pp. 523-529 (2000)

FIGURES and TABLES

Table I

Physical and piezoelectric properties of the PZT compositions used in this study [14]

Property	Symbol/units	PZT 5H	PZT 5A	PZT 4	PZT 8
Density	$\rho(kg/m^3)$	7500	7750	7600	7500
Young's Modulus	E (GPa)	48.3	52.0	65.0	71.0
Piezoelectric Strain Charge Coefficients	d_{31} (pC/N)	-274	-171	-123	-97
	d_{33} (pC/N)	593	374	289	225
	d_{15} (pC/N)	741	584	496	330
Permittivity	ε_{11}^S(X 10^{-8} F/m)	1.50	0.811	0.797	0.646
	ε_{33}^S(X 10^{-8} F/m)	1.30	0.735	0.531	0.562
Dielectric Loss	tan δ	0.013	0.01	0.004	0.004
Elastic Stiffness	c_{11}^E(X 10^{10} N/m^2)	12.72	12.03	14.69	13.90
	c_{12}^E(X 10^{10} N/m^2)	8.02	7.51	8.11	7.78
	c_{13}^E(X 10^{10} N/m^2)	8.47	7.51	8.11	7.43
	c_{33}^E(X 10^{10} N/m^2)	11.74	11.09	13.17	11.54
	c_{44}^E(X 10^{10} N/m^2)	2.30	2.11	3.13	2.65
	c_{66}^E(X 10^{10} N/m^2)	2.35	2.26	3.29	3.06
Mechanical Quality Factor	Q_m	65	75	500	1000

Table II
Physical properties of the metals for endcaps and epoxy for bonding layer

Material	Young's Modulus E (GPa)	Density $\rho(kg/m^3)$	Poisson's Ratio σ	Reference
Brass	100.6	8550	0.35	[15]
Titanium (Ti)	120.2	4500	0.361	[15]
Kovar	137.9	8360	0.32	[16]
Steel	207	7860	0.3	[15]
Molybdenum (Mo)	324.8	10200	0.293	[15]
Tungsten (W)	411	19300	0.28	[15]
Eccobond 3/1	2.5	1430	0.40	[17]

Table III

Scaled sizes of cymbal transducers tested in this study (bold print for reference cymbal)

Scaling Factor	Transducer Diameter (mm)	Cavity Depth (mm)	Cavity Diameter (mm)	Endcap Thickness (mm)	Apex Diameter (mm)	PZT Thickness (mm)
2.75	35	0.68	24.80	0.68	8.26	2.75
1.25	15.8	0.31	11.20	0.31	3.73	1.25
1.0	**12.7**	**0.25**	**9**	**0.25**	**3**	**1**
0.75	9.5	0.18	6.73	0.18	2.24	0.75
0.25	3.2	0.06	2.26	0.06	0.75	0.25

Table IV

Comparison of the characteristics of water-loaded reference size brass capped cymbals driven by various PZT types (The percentage changes from in-air values are given in parantheses).

PZT Type		PZT 5H	PZT 5A	PZT 4	PZT 8
f_r (kHz)	**Measured**	16.5 (-37%)	16.2 (-38%)	16.3 (-38%)	15.0 (-42%)
	FEA	16.5 (-30%)	16.1 (-32%)	16.3 (-32%)	17.5 (-32%)
	Analytical	16.0±2	17.0±2	16.7±2	16.6±2
k_{eff}	**Measured**	0.25 (+25%)	0.27 (+25%)	0.27 (+58%)	0.24 (+60%)
	FEA	0.22±.09	0.24±.03	0.24±.05	0.18±.07

Table V

Comparison of the characteristics of water-loaded
reference size cymbals with PZT 5H of various cap types
(numbers in parentheses are percent difference from in-air values).

Cap Material		Brass	Titanium	Kovar	Molybdenum
f_r (kHz)	**Measured**	16.5 (-37%)	20.5 (-48%)	18.2 (-36%)	24.3 (-30%)
	FEA	16.5 (-30%)	20.0 (-43%)	18.6 (-30%)	26.2 (-28%)
	Analytical	16.0±2	20.5±2	16.5±2	20.6±2
k_{eff}	**Measured**	0.25 (+25%)	0.30 (+43%)	0.28 (+22%)	0.24 (+14%)
	FEA	0.22±.09	0.24±.04	0.25±.04	0.22±.06

Table VI

FEA calculated first resonance frequency for air and water-loaded cymbal of different overall size .

Scaling Factor	Device Diameter (mm)	First Resonance Frequency (Air-Calculated)	First Resonance Frequency (Water-Calculated)
0.25	3.2	85.57	58.18
0.75	9.5	33.09	22.50
1.00	12.7	23.5	16.5
1.25	15.8	20.21	13.74
2.75	32.7	9.40	6.39

Table VII

Calculated Available Source Power Levels Based on TVR Peaks and Using 4V/mil Drive Limit for PZT 5H (SL = TVR + 20 logV)

Disk Thickness (mm)	Max. Applied Voltage (V)	20 log V	TVR Peak (dB re 1 µPa/V @ 1m)	Peak Source Level (dB)
0.1	15.75	23.95	138.25	162.2
0.5	78.74	37.92	134.91	172.8
1.0	157.48	43.95	132.01	176.0
2.0	314.96	49.97	128.22	178.2
3.0	472.44	53.49	123.77	177.3

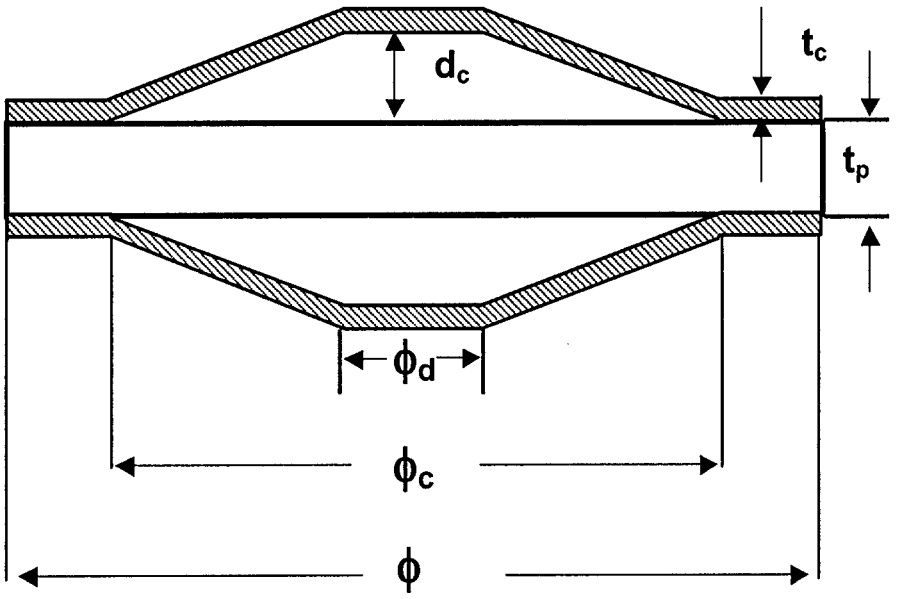

Parameter	Symbol	Reference dimension (mm)
Cap Thickness	t_c	0.25
Cavity Diameter at Base	ϕ_c	9.00
Cavity Depth at Apex	d_c	0.25
PZT Thickness	t_p	1.00
Device Diameter	ϕ	12.70
Apex Diameter	ϕ_d	3.00

Figure 1. Cross-sectional view of the cymbal transducer along with the reference-size dimensions and their respective symbols used throughout the report

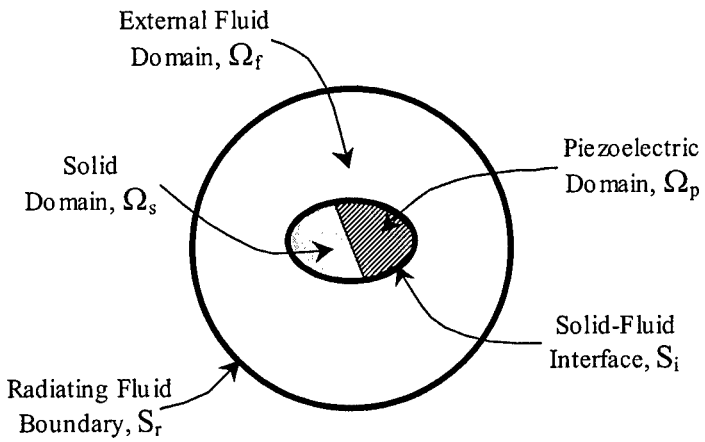

Figure 2 Various domains modeled by the finite element method.

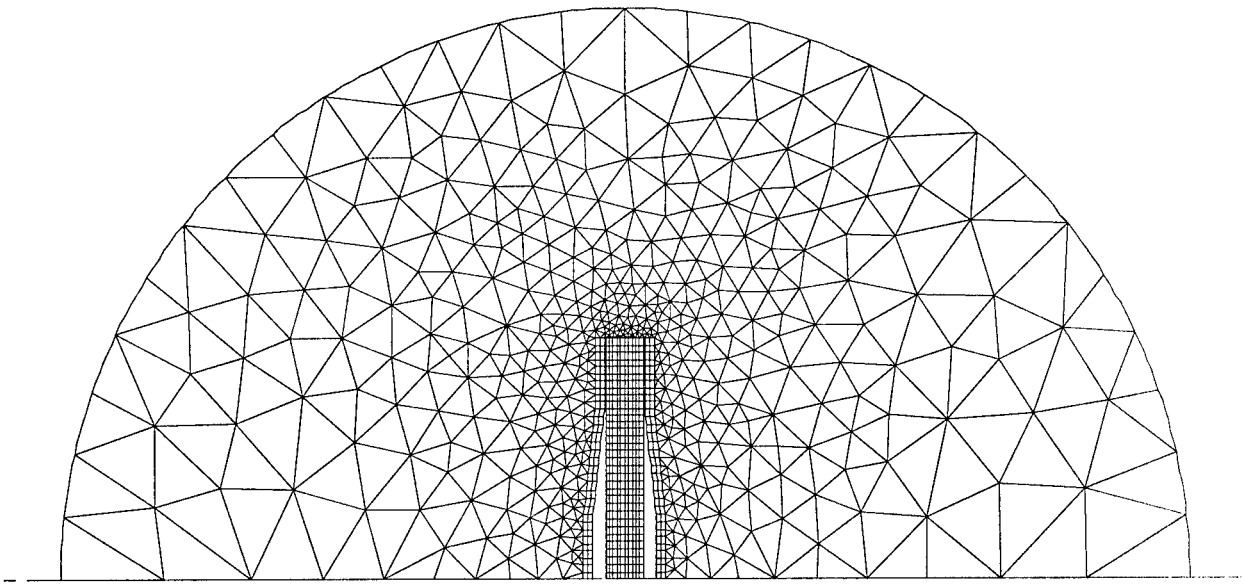

Figure 3. The in-water ATILA FEA mesh of a reference cymbal transducer

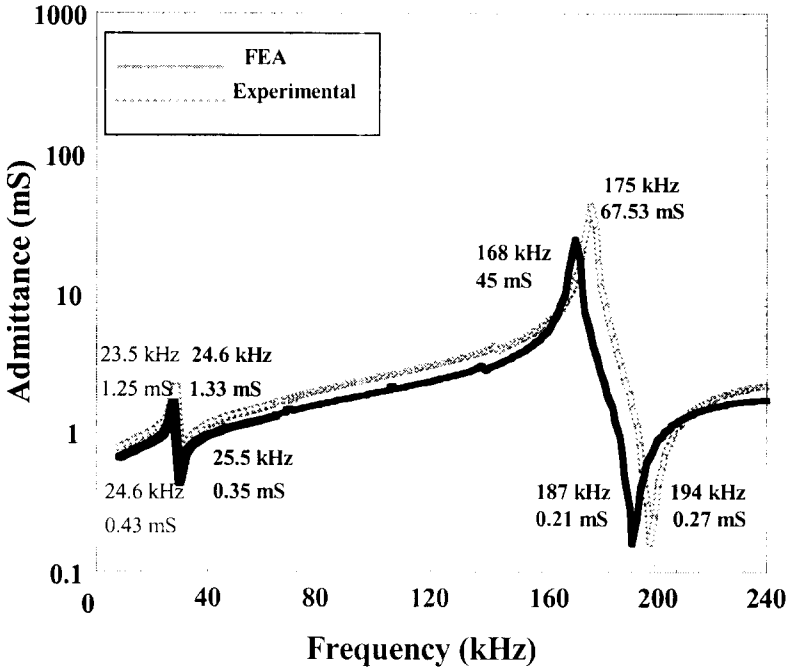

Figure 4. FEA result and experimentally measured admittance spectrum for a reference cymbal transducer

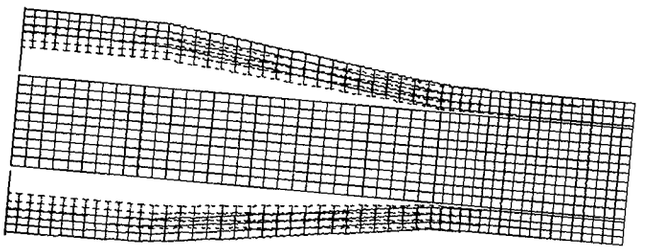

(0,1) mode

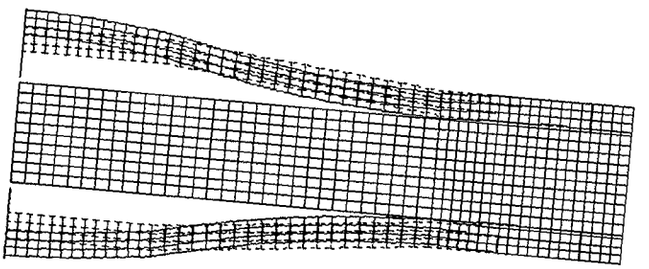

(0,2) mode

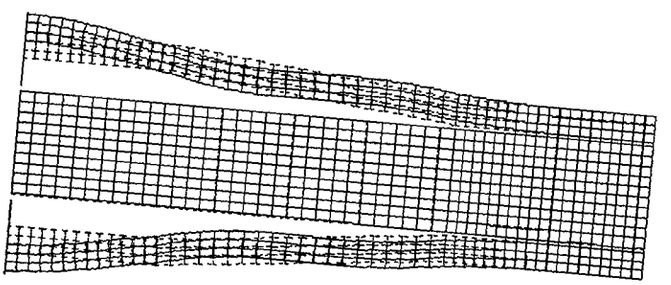

(0,3) mode

Figure 5. ATILA calculated vibration modes of the cymbal transducer. Dashed lines represent the at-rest state, solid lines represent the displaced postions of the FEA nodes.

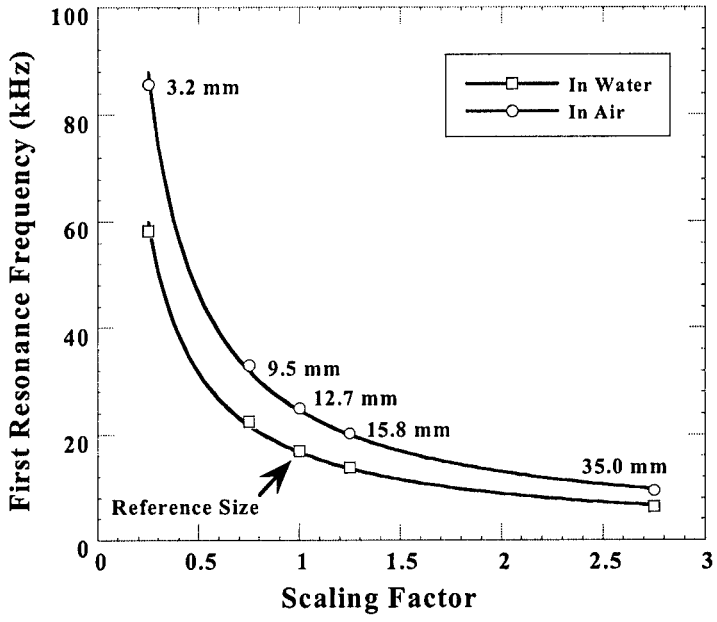

Figure 6. FEA calculated first resonance frequency for air and water loaded cymbals of different overall size, in which each parameter is multiplied by a scaling factor. PZT 5H disks and brass endcaps were used. The device diameter is given in millimeters for each data point.

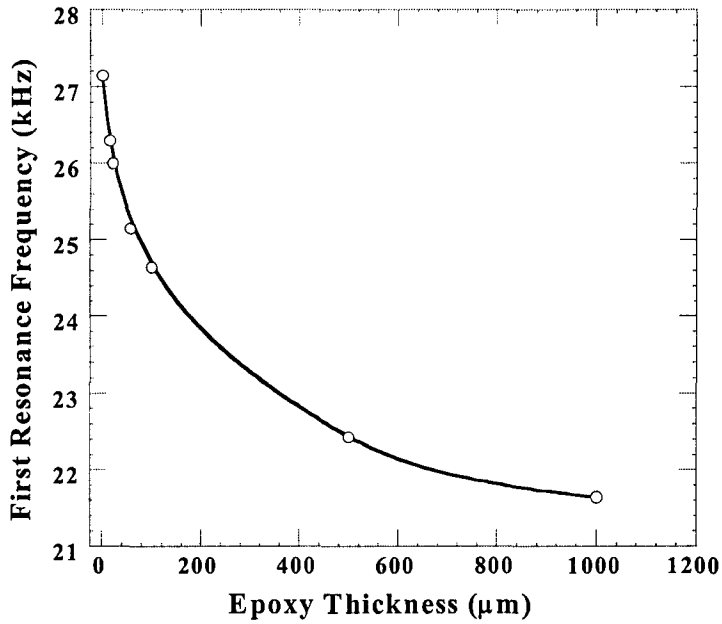

Figure 7. Effect of epoxy thickness on first resonance frequency for reference-size cymbals. PZT 5H disks, brass endcaps and Eccobond45/LV epoxy were used (in-air, calculated)

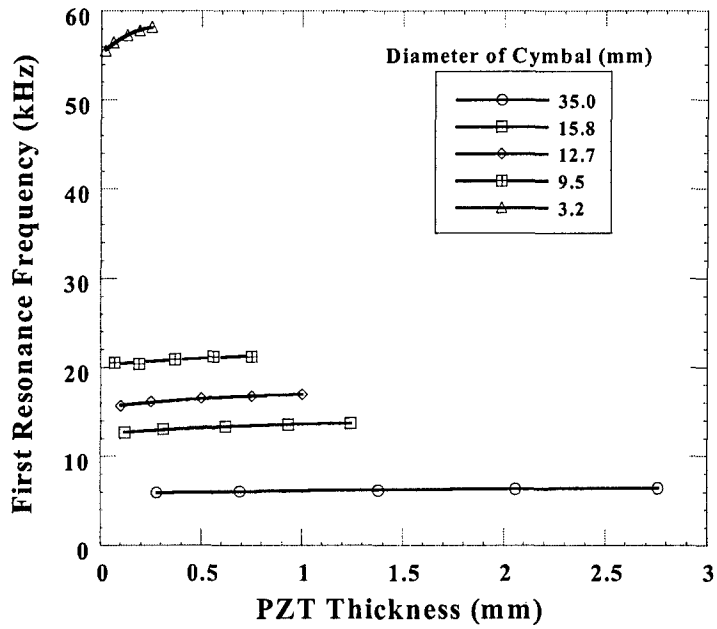

Figure 8. Effect of PZT thickness on the first resonance frequency for various sized transducers. All other dimensions are scaled (in-water, calculated)

a-)

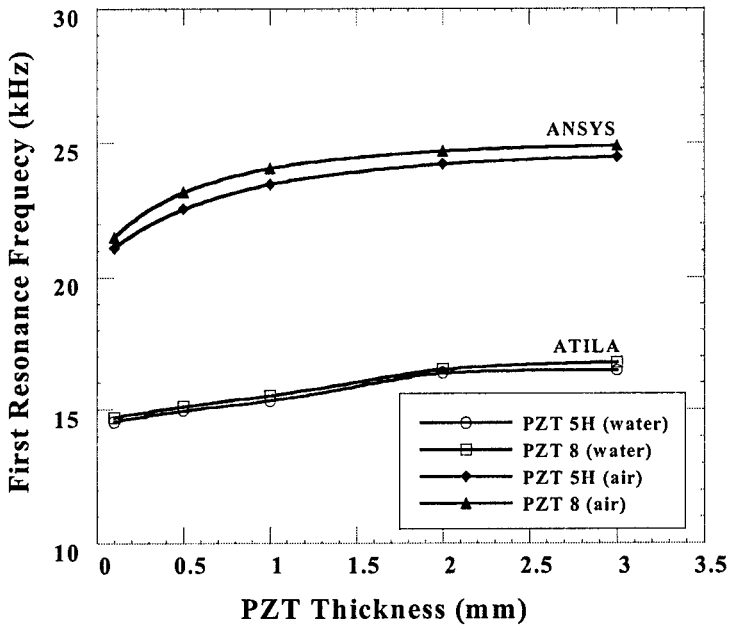

b-)

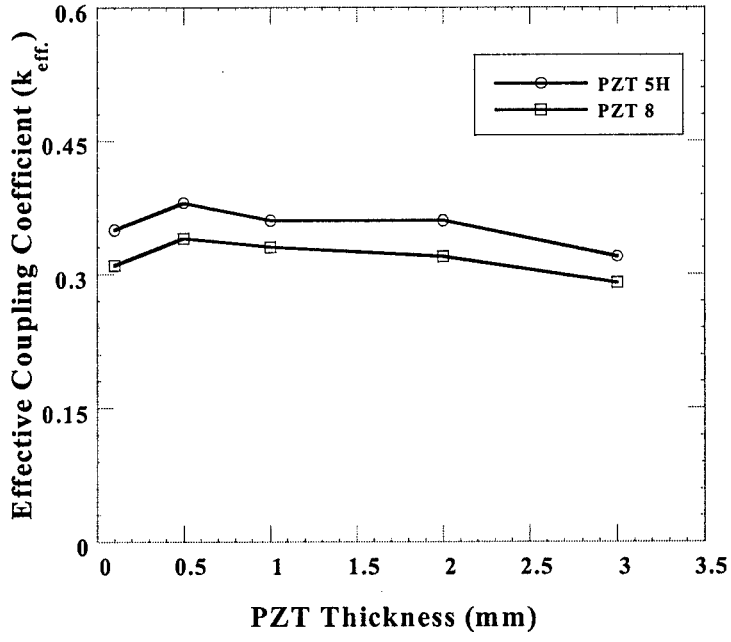

Figure 9. Calculated effect of PZT thickness and material a-) on the first resonance frequency for the reference size transducer. Because of their greater stiffness hard PZTs such as PZT 8 have slightly higher resonant frequencies than PZT 5H and other soft PZTs and, b-) on effective coupling coefficient in water.

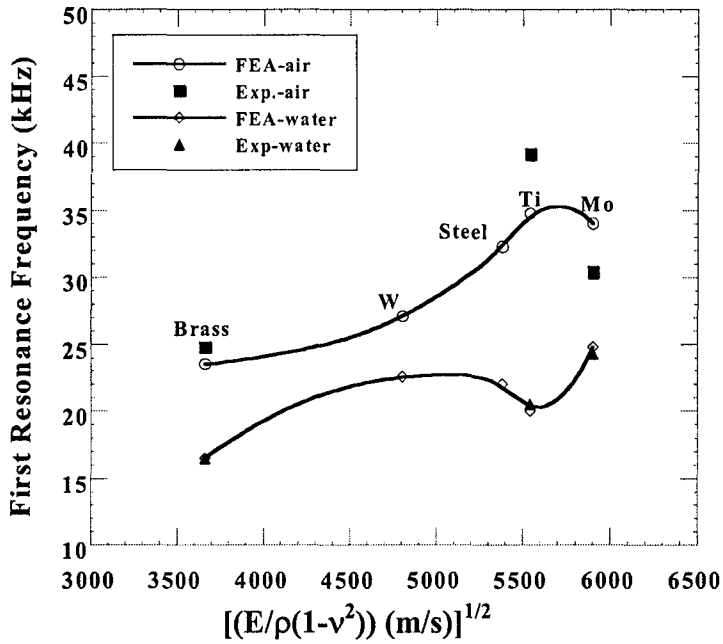

Figure 10. Measured and calculated effect of endcap material ultrasonic velocity on first resonance frequency of reference size transducers (PZT 5H ceramic)

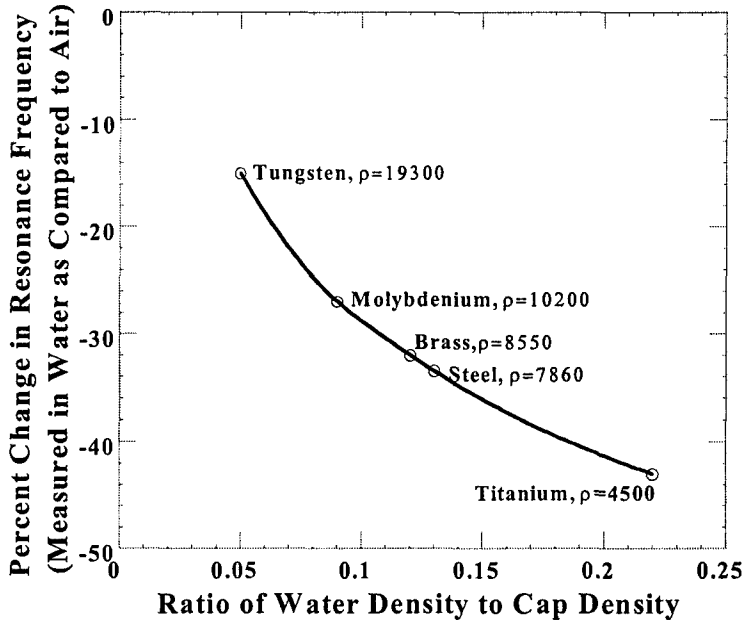

Figure 11. Percent change in resonance frequency from air to water as a function of the ratio of water density to endcap material density

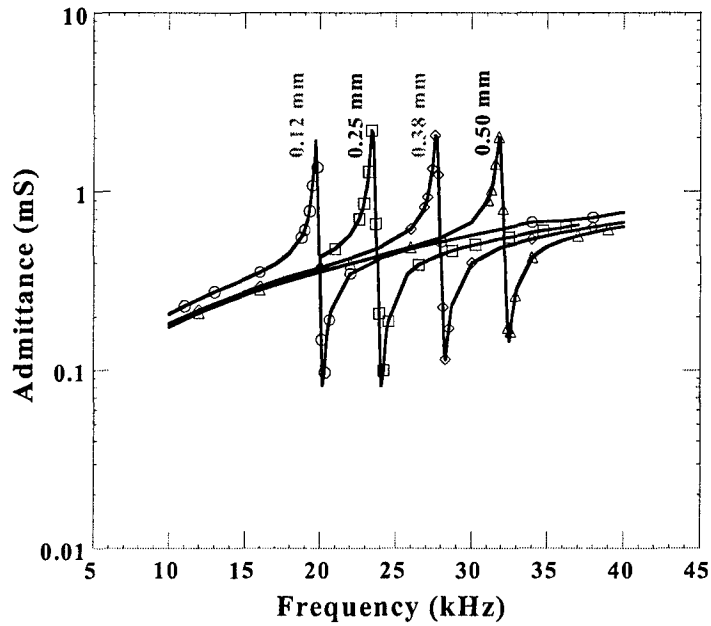

Figure 12. Admittance spectra of the reference cymbal transducer with varying endcap thickness (in-air, calculated)

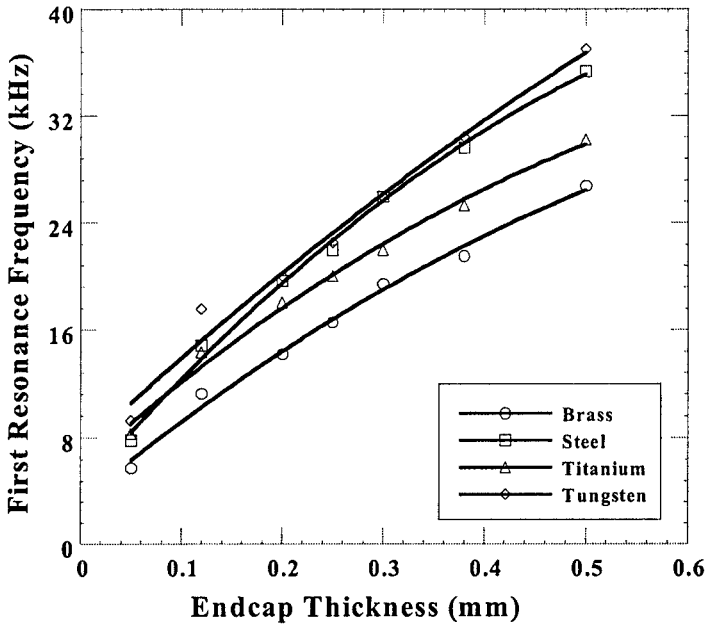

Figure 13. Effect of end-cap thickness on first resonance frequency for various endcap materials (in-water, calculated)

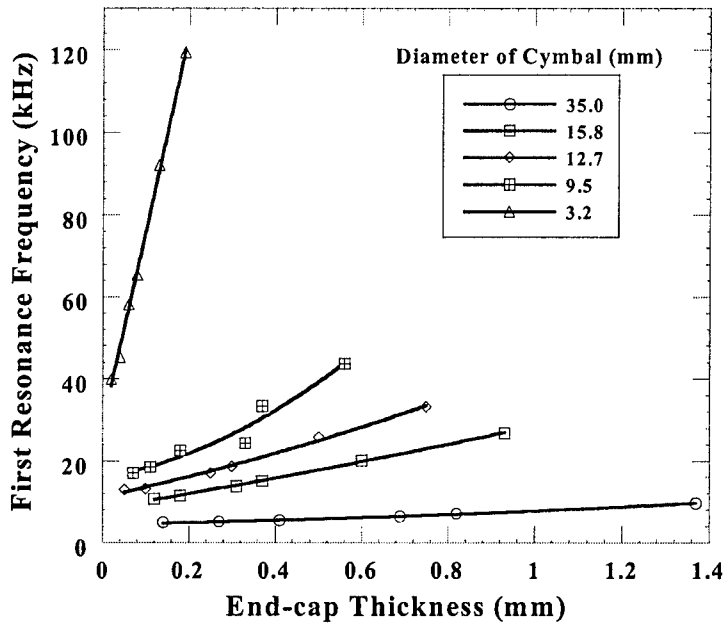

Figure 14. Effect of end-cap thickness on first resonance frequency for various transducer diameters. All other dimensions are scaled (in-water, calculated)

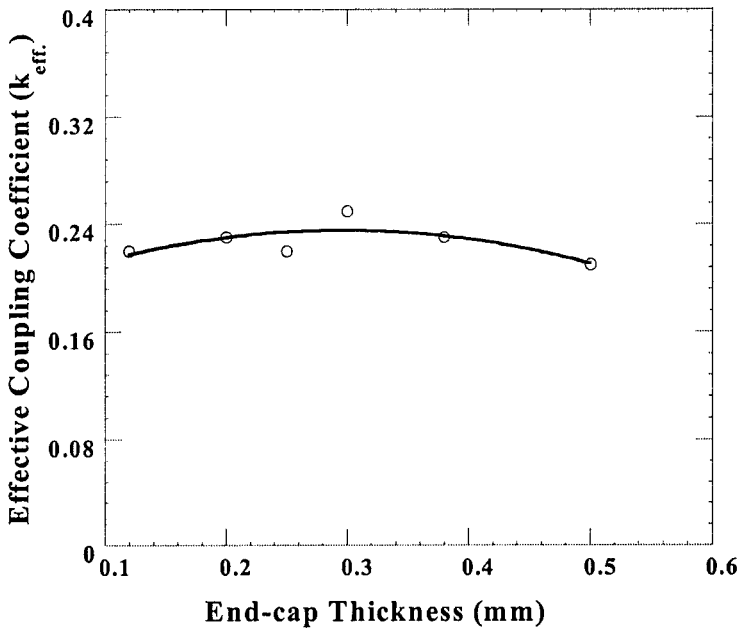

Figure 15. Effect of end-cap thickness on coupling coefficient for reference size cymbals with brass endcaps (in-water, calculated)

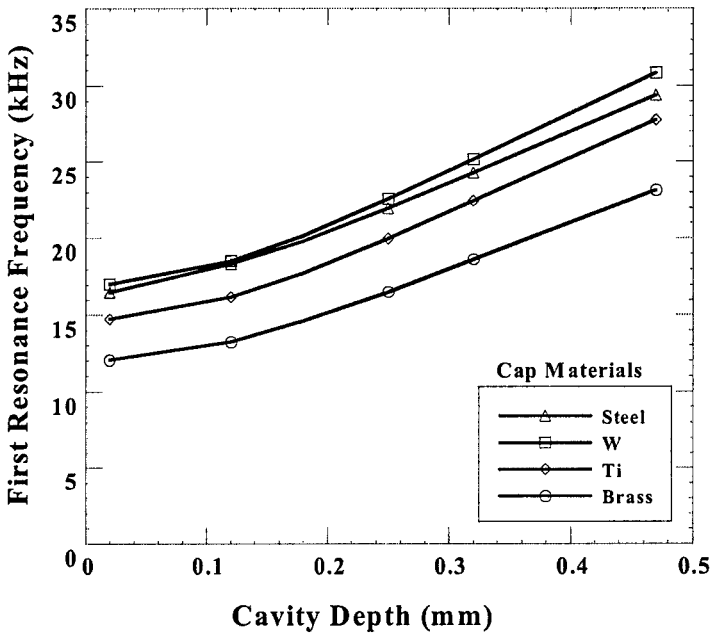

Figure 16. Effect of cavity depth on first resonance frequency for various end cap materials of the reference size transducer (in-water, calculated)

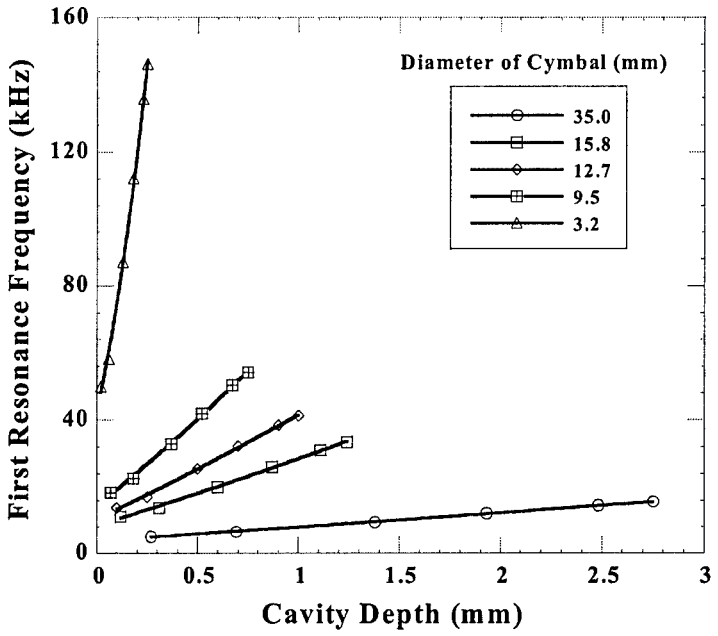

Figure 17. Effect of cavity depth on first resonance frequency for various transducer sizes. All other dimensions are scaled (in-water, calculated)

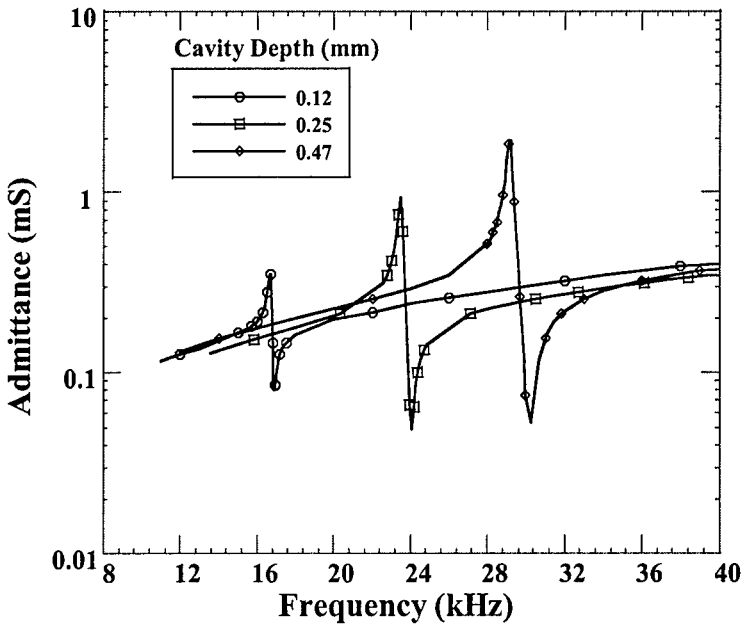

Figure 18. Admittance spectra of reference cymbal transducer with various cavity depths (in-air calculated)

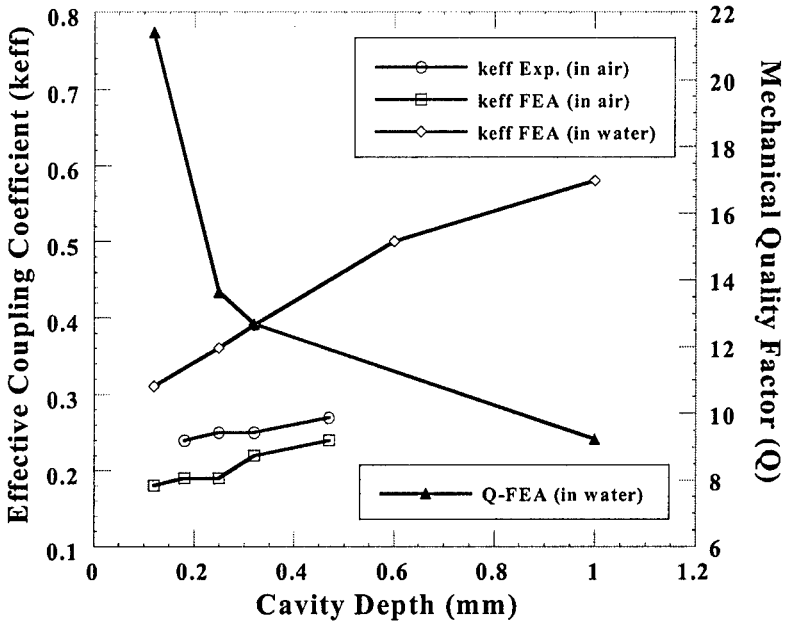

Figure 19. Effect of cavity depth on coupling coefficient and mechanical quality factor,for reference-sized cymbal with PZT 5H and brass endcaps

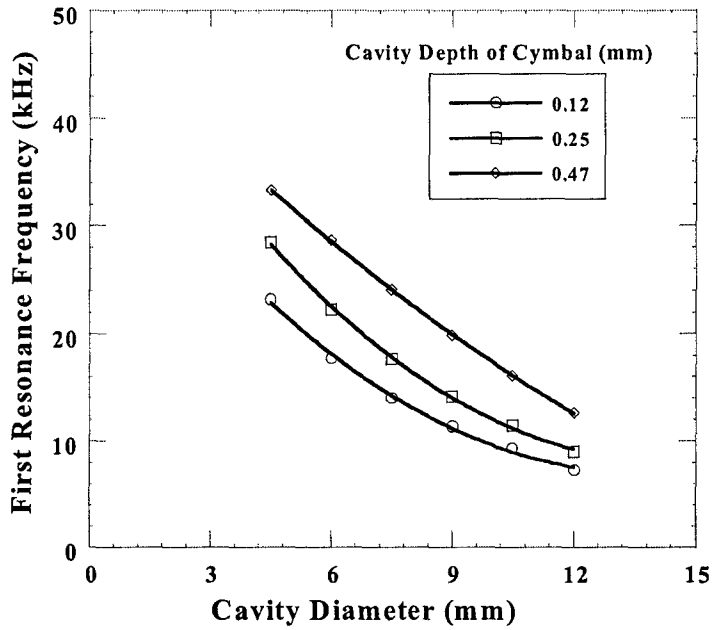

Figure 20. Effect of cavity diameter on first resonance frequency for various cavity depth of reference size transducer (in-water, calculated)

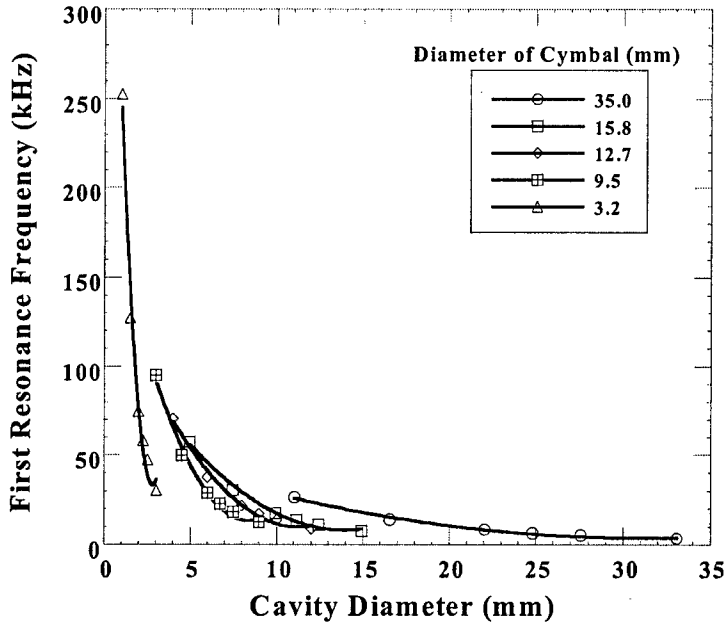

Figure 21. Effect of cavity diameter on first resonance frequency for various transducer sizes. All other dimensions are scaled (in-water, calculated)

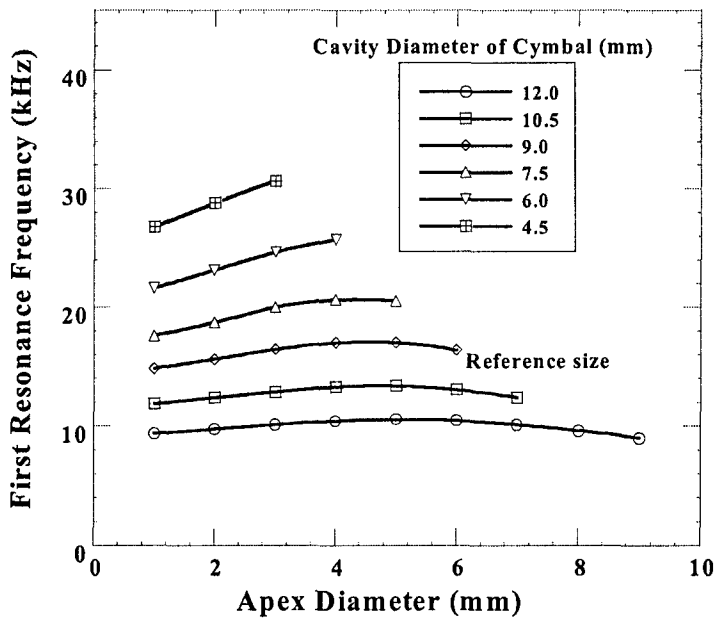

Figure 22. Effect of apex diameter on first resonance frequency for reference size cymbal with various cavity diameters (in-water calculated)

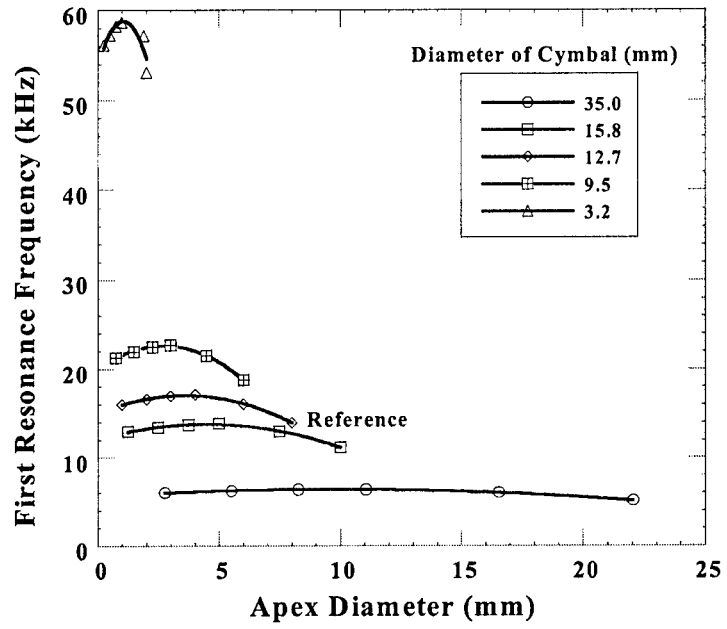

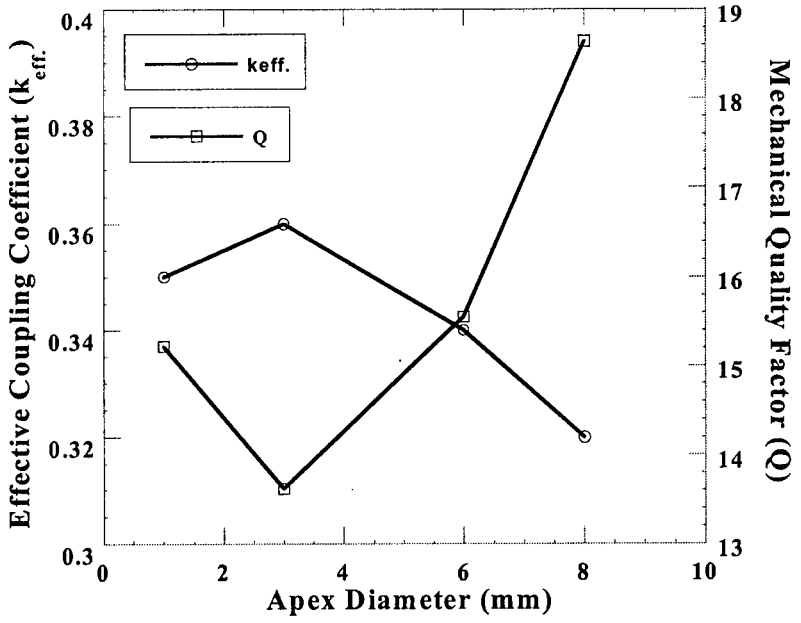

Figure 23. Effect of apex diameter a-) on first resonance frequency for various transducer sizes. All other dimensions are scaled b-) effective coupling coefficient ($k_{eff.}$) and mechanical quality factor (Qm) for reference sized cymbal; (in-water, calculated).

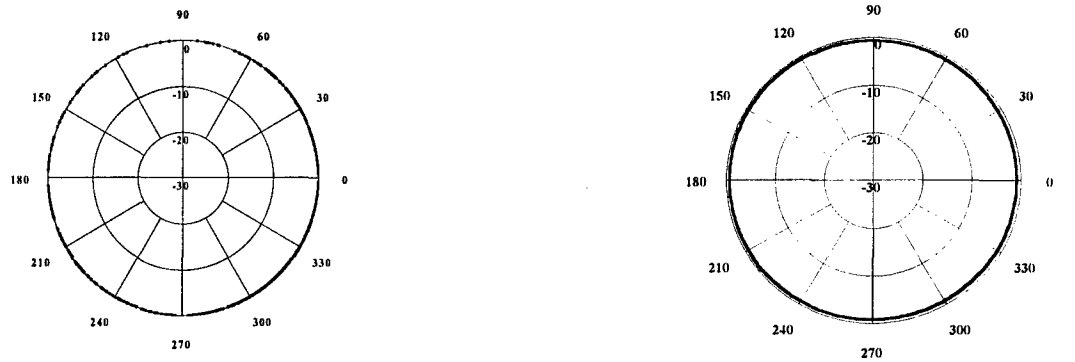

(a) 10 kHz

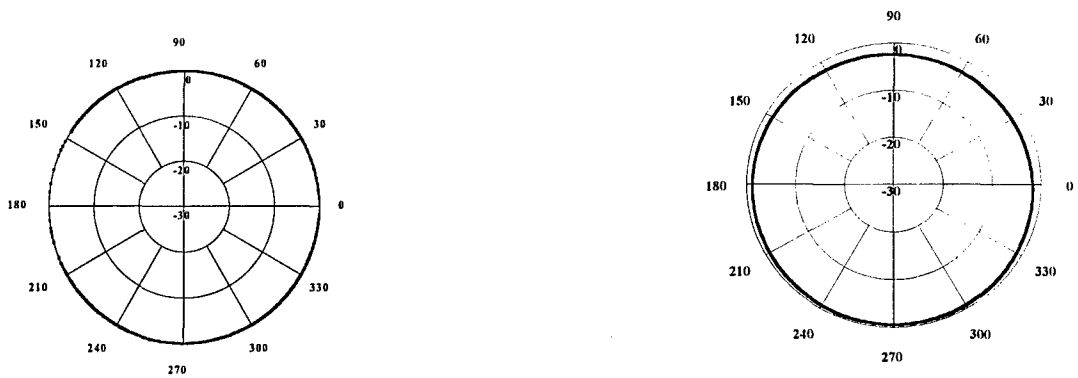

(b) 30kHz

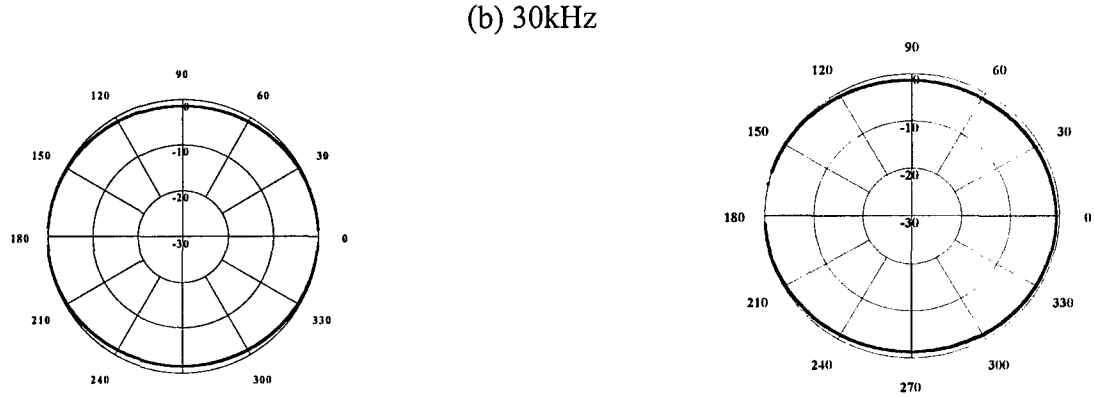

(c) 50kHz

Figure 24. Calculated (left column) and Measured (right column) beam patterns of the cymbal transducer by ATILA at (a) 10kHz, (b) 30kHz and (c) 50kHz). Values are reported for the plane normal to the disk.

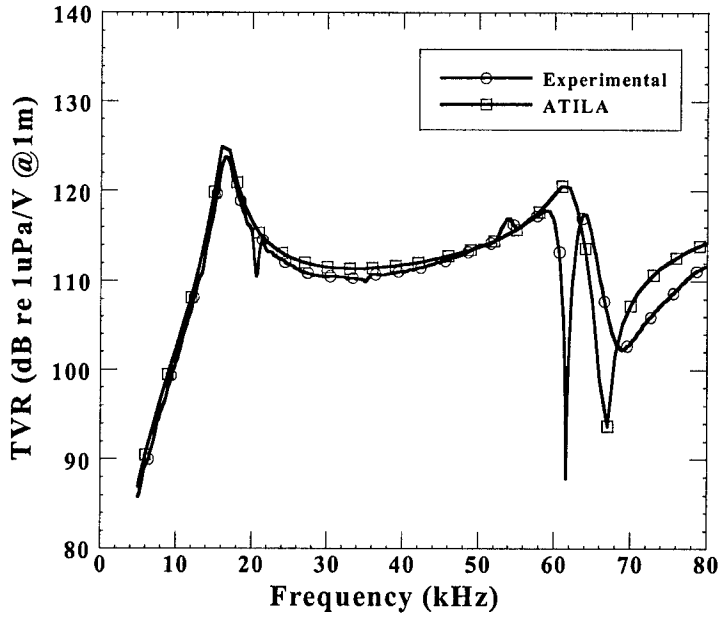

Figure 25. Calculated and measured TVR of a cymbal transducer (under free mechanical boundary conditions, reference size cymbal with 0.32 mm cavity depth, brass endcap and PZT 5H driving element) [30]

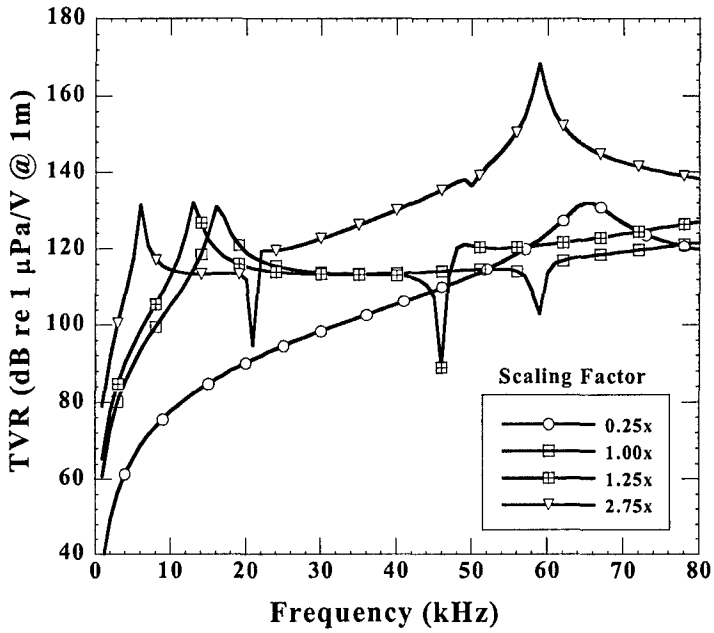

(a) TVR

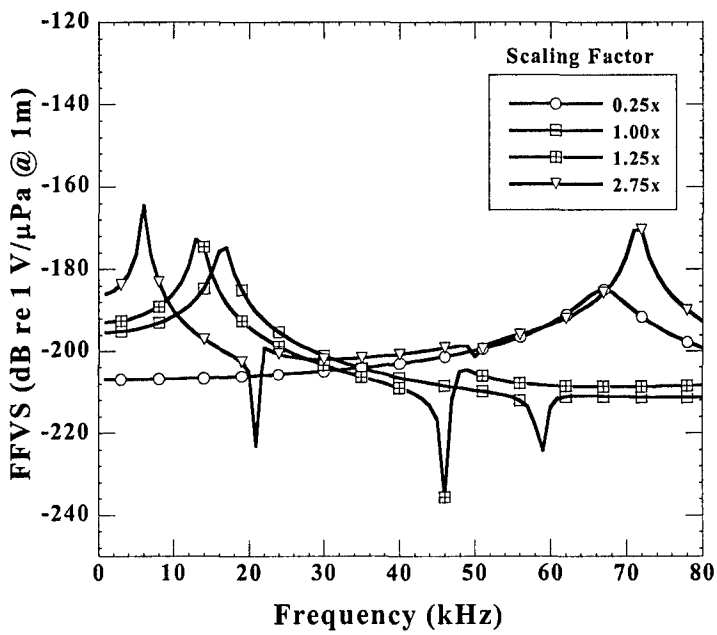

(b) FFVS

Figure 26. The calculated a-) TVR b-) FFVS of cymbal as a function of scaling factor

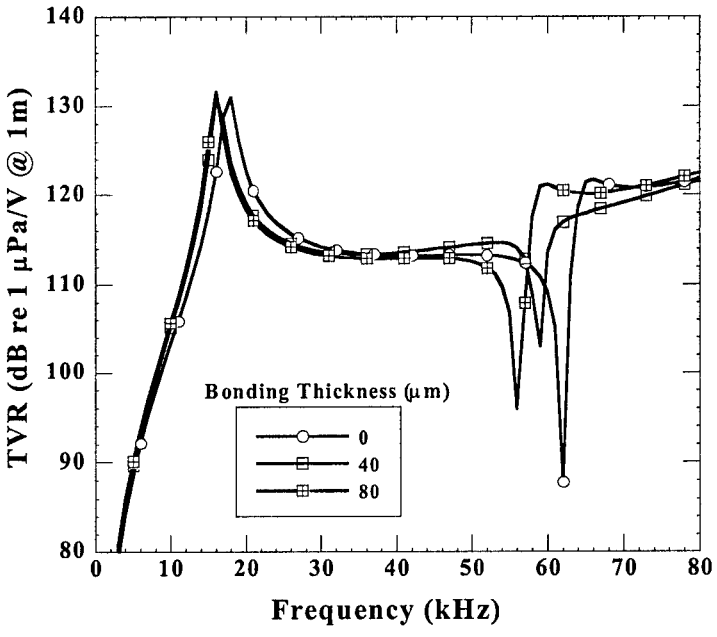

(a) TVR

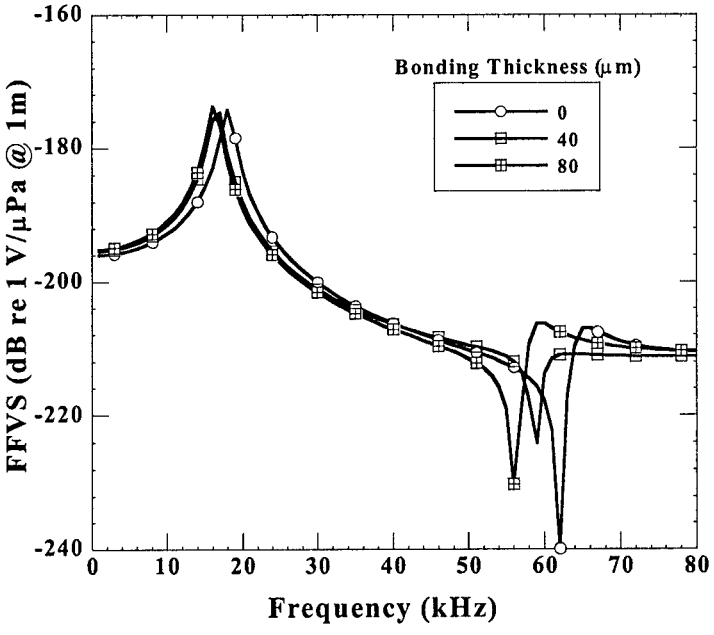

(b) FFVS

Figure 27. The in-water calculated a-) TVR b-) FFVS of reference cymbals with brass endcaps and PZT- 5H as a function of epoxy bonding layer thickness

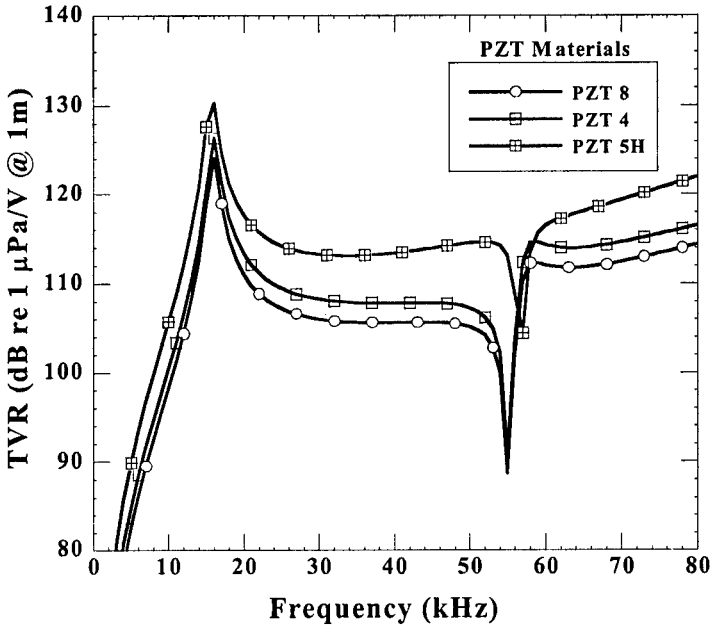

(a) TVR

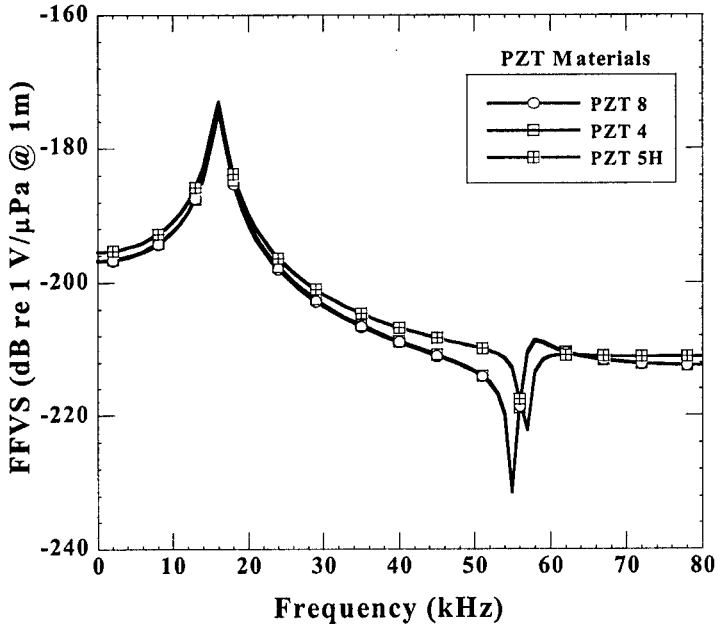

(b) FFVS

Figure 28. The calculated effect of different PZTs on the (a) TVR (b) FFVS of reference-size cymbals made with hard and soft PZT and brass endcaps.

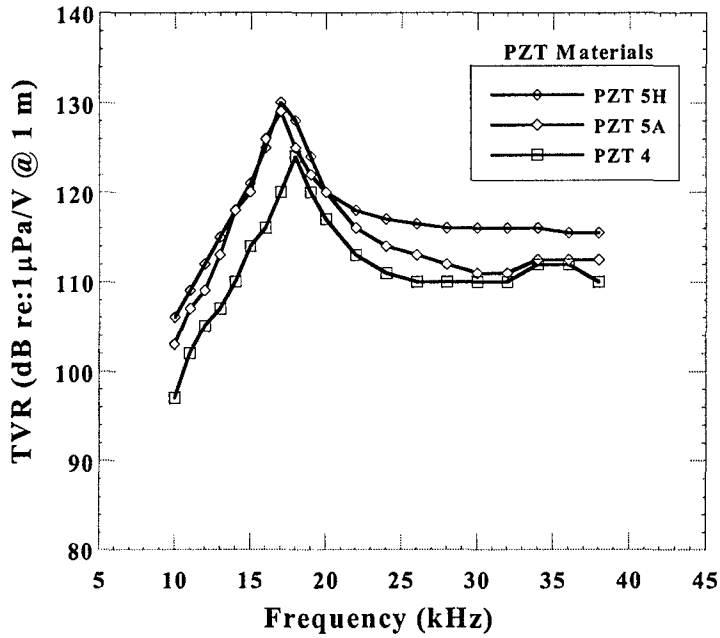

Figure 29. Measured TVR curves in the near the fundamental resonance for reference size brass capped cymbals using different PZT materials

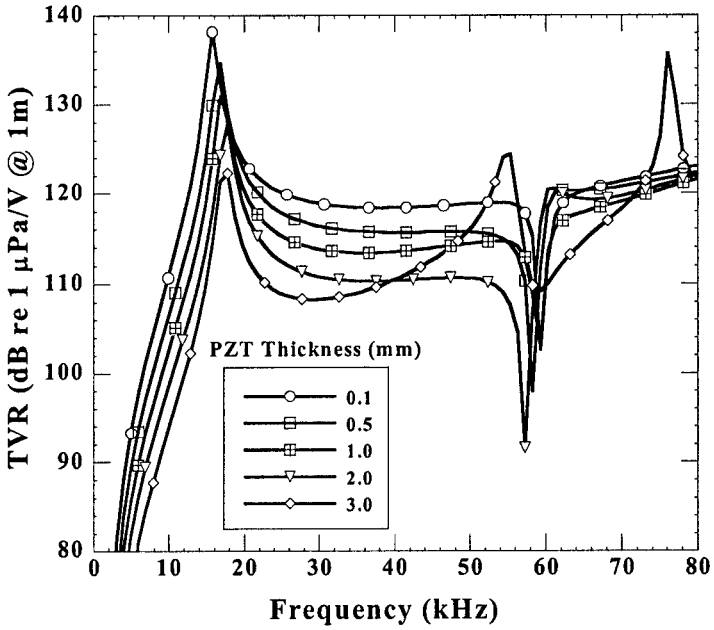

(a) TVR

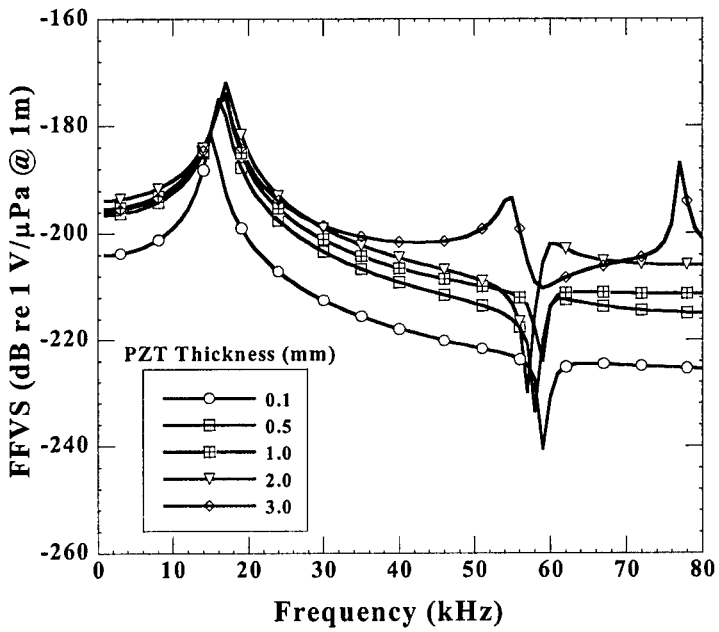

(b) FFVS

Figure 30. The calculated a-) TVR b-) FFVS of reference size cymbals with brass endcaps and PZT 5H as a function of PZT thickness

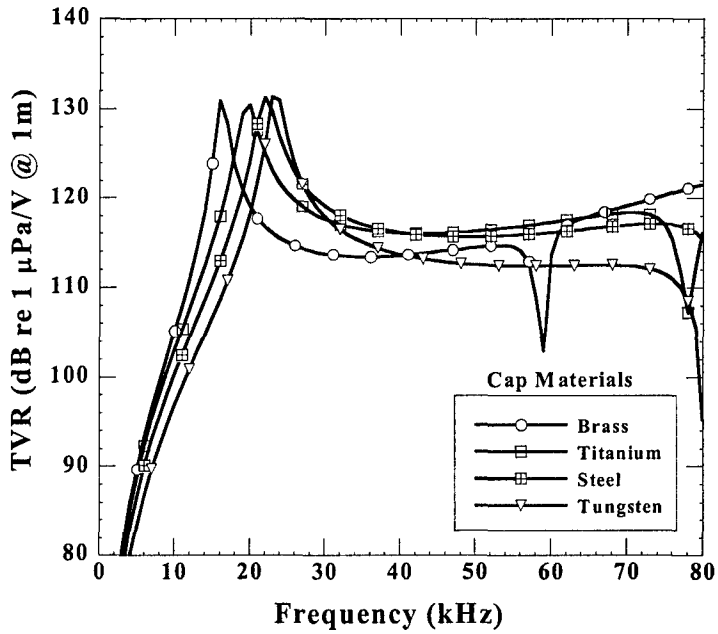

(a) TVR

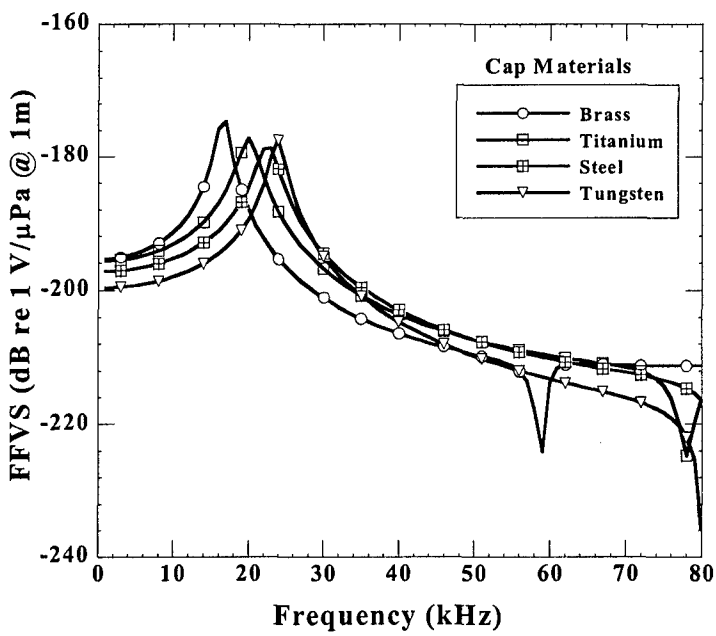

(b) FFVS

Figure 31. The calculated effect of endcap materials on the (a) TVR (b) FFVS of reference size cymbals with PZT 5H

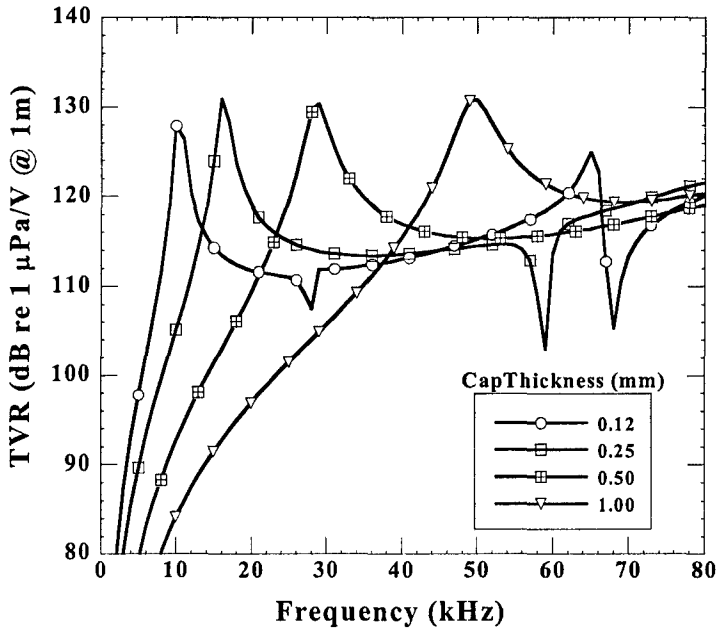

(a) TVR

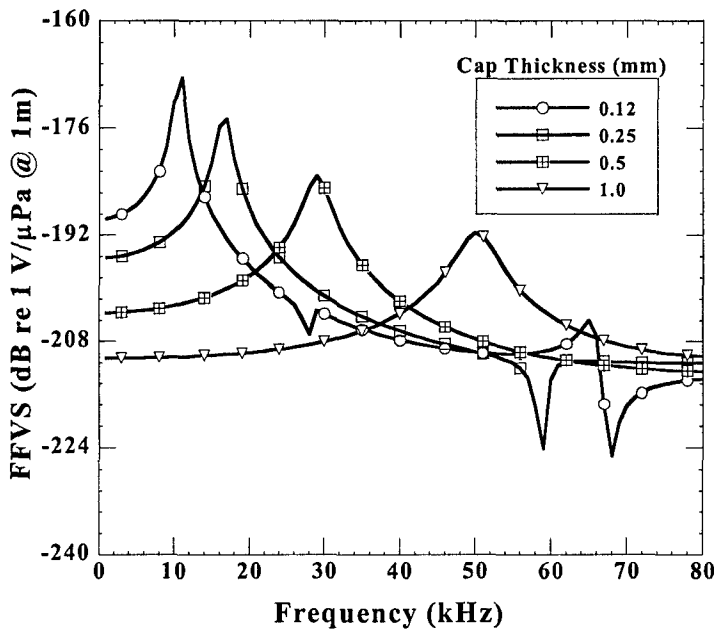

(b) FFVS

Figure 32. The calculated a-) TVR b-) FFVS of reference size cymbals with brass endcaps and PZT 5H as a function of endcap thickness

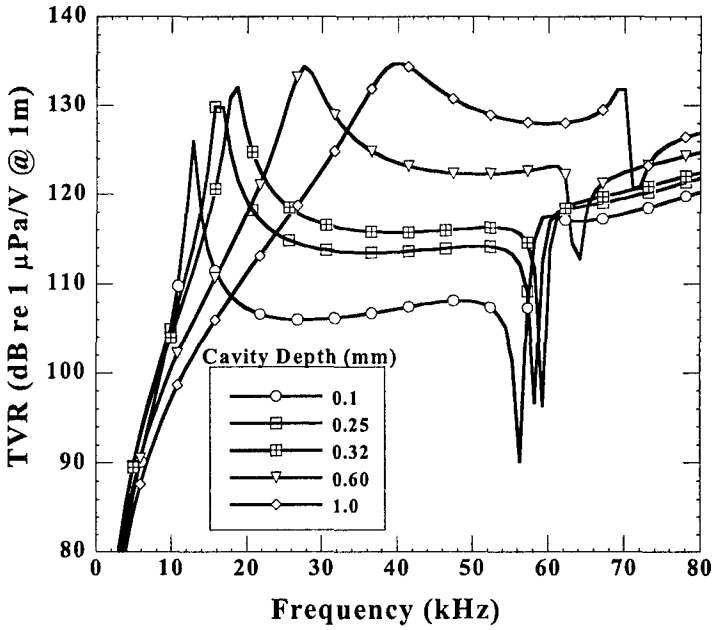

(a) TVR

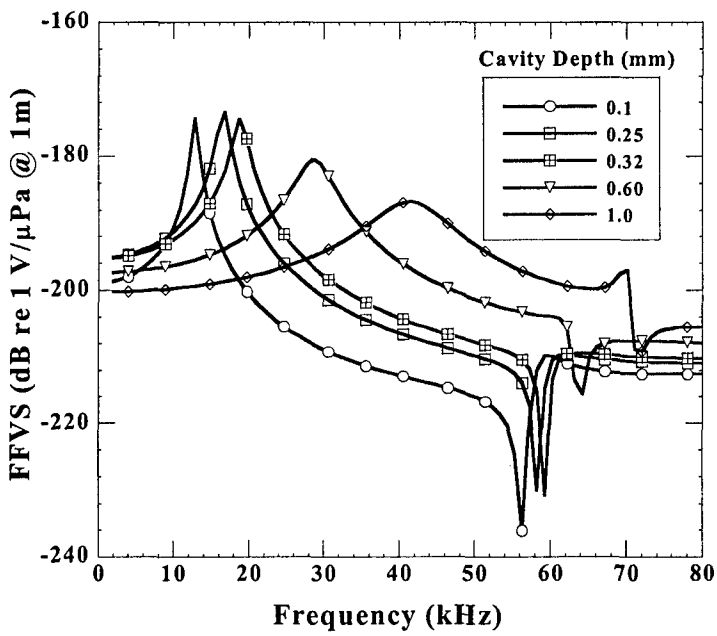

(b) FFVS

Figure 33. The calculated a-) TVR b-) FFVS of reference size cymbals with PZT 5H and brass endcaps as a function of cavity depth. The reference size cymbal has a 0.25 mm cavity depth.

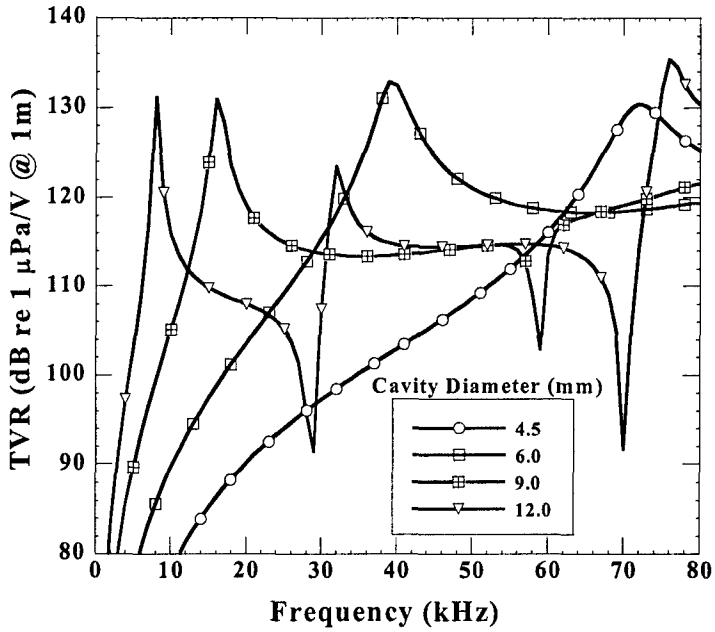

(a) TVR

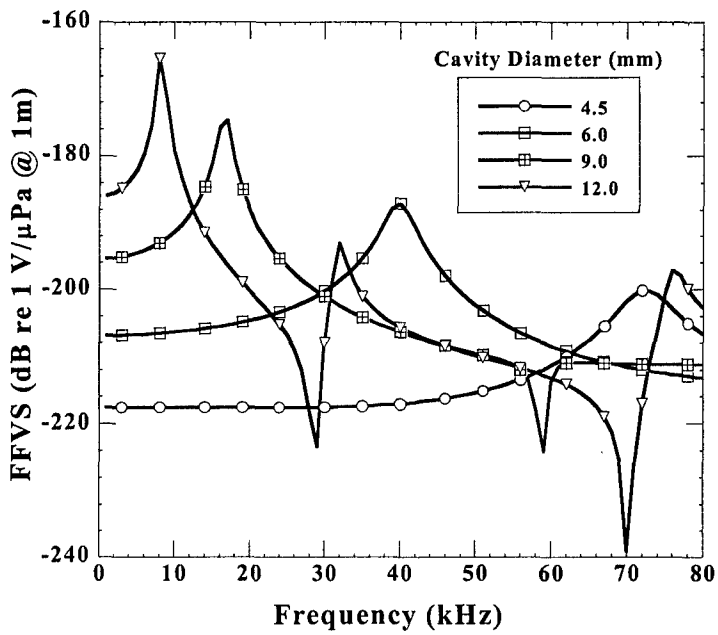

(b) FFVS

Figure 34. The calculated a-) TVR b-) FFVS of reference size cymbals with brass endcaps and PZT 5H as a function of cavity diameter

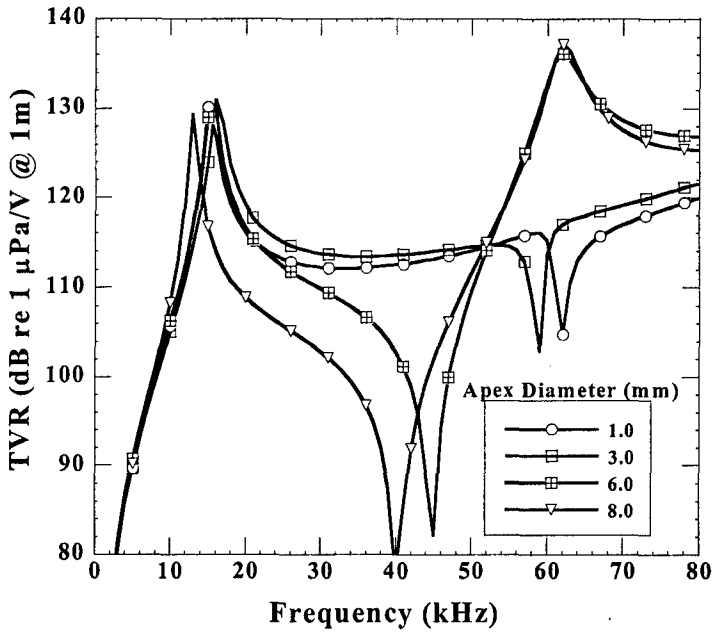

(a) TVR

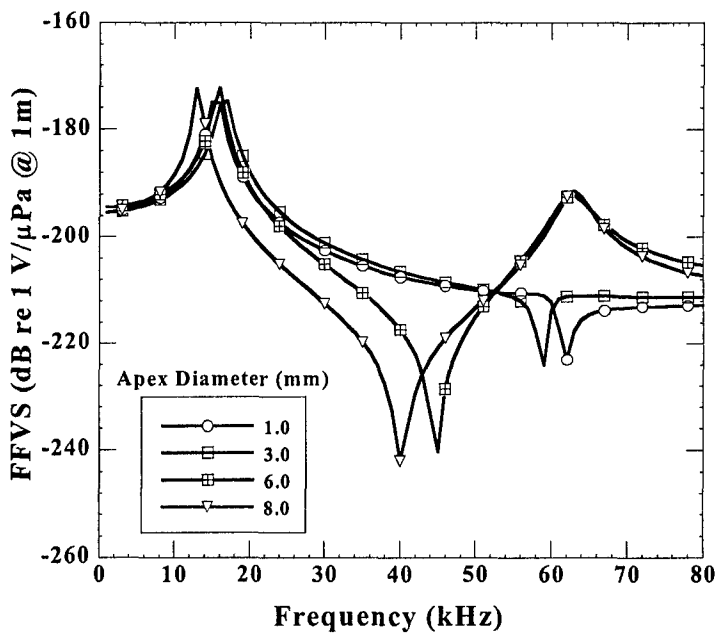

(b) FFVS

Figure 35. The calculated a-) TVR b-) FFVS of reference size cymbals with brass endcaps and PZT 5H as a function of apex diameter

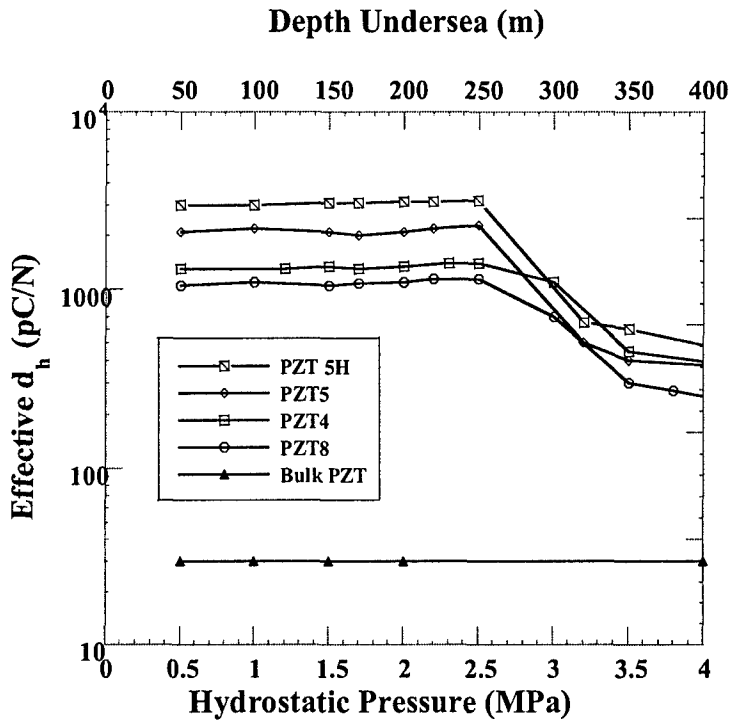

Figure 36. Measured pressure dependence of effective d_h for various types of PZT materials in reference size transducers with brass endcaps

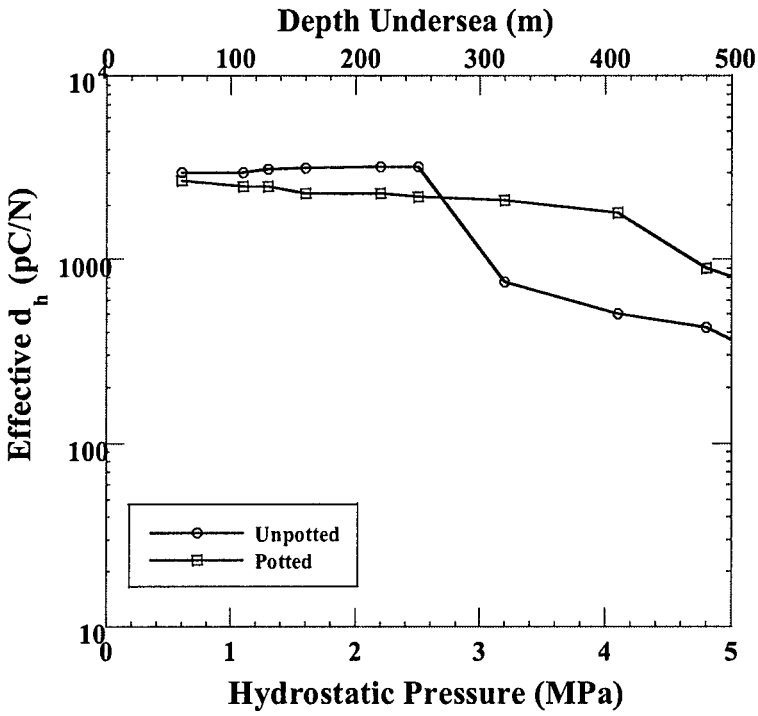

Figure 37. Comparison of the pressure dependence of the measured effective d_h coefficients for reference size transducers with PZT 5H ceramics and brass endcaps unpotted vs. potted in polyurethane

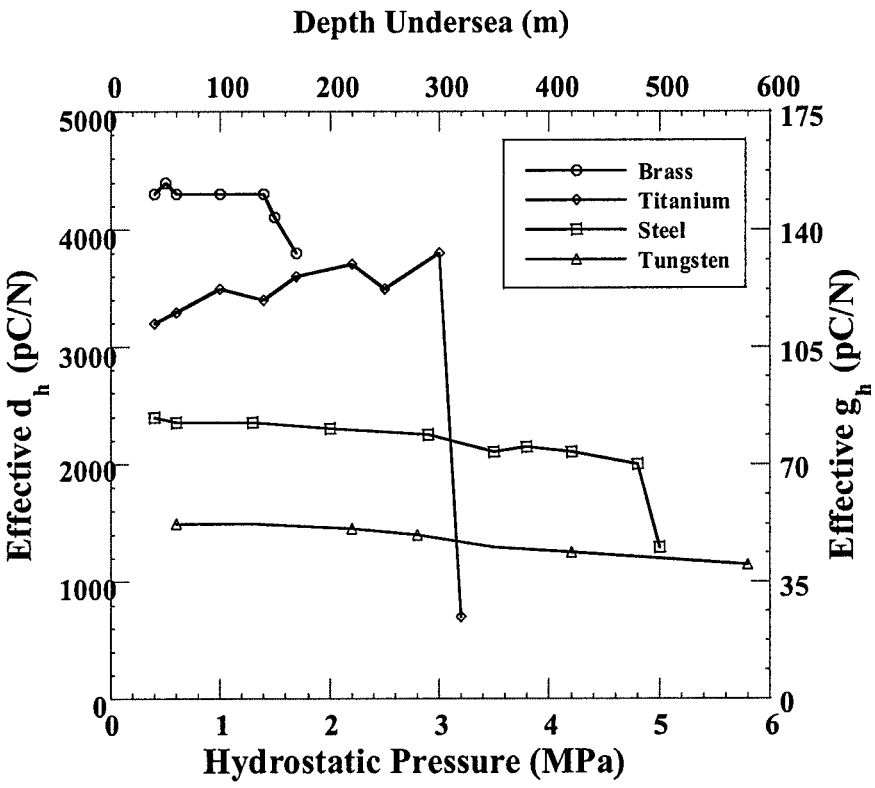

Figure 38. Measured pressure dependence of effective d_h and g_h coefficients for various types of endcap materials on reference size transducers with PZT 5H ceramics

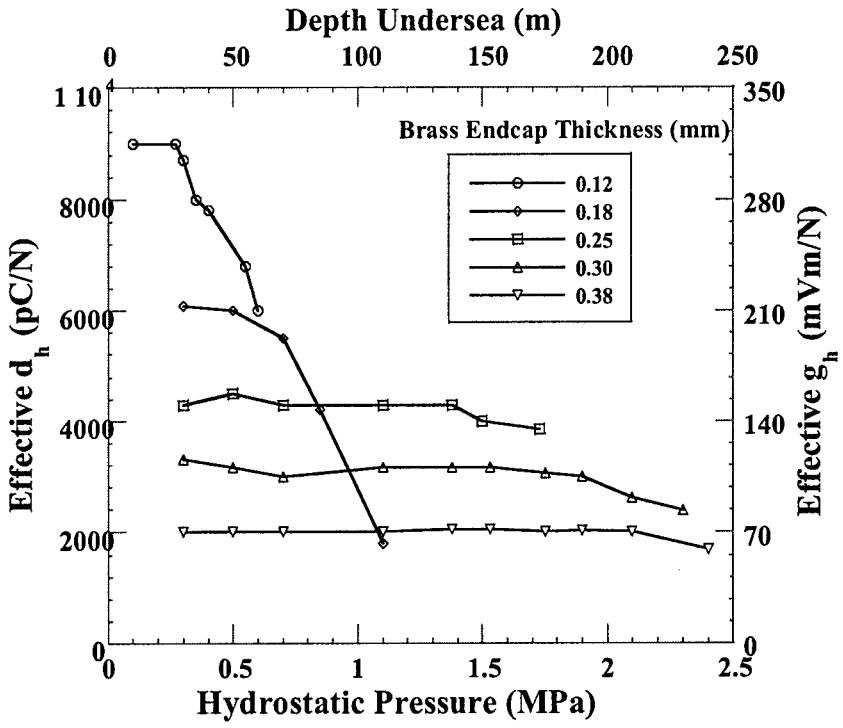

Figure 39. Measured pressure dependence of effective d_h and g_h coefficients of reference size transducers with varying endcap thicknesses (brass endcaps and PZT 5H ceramics)

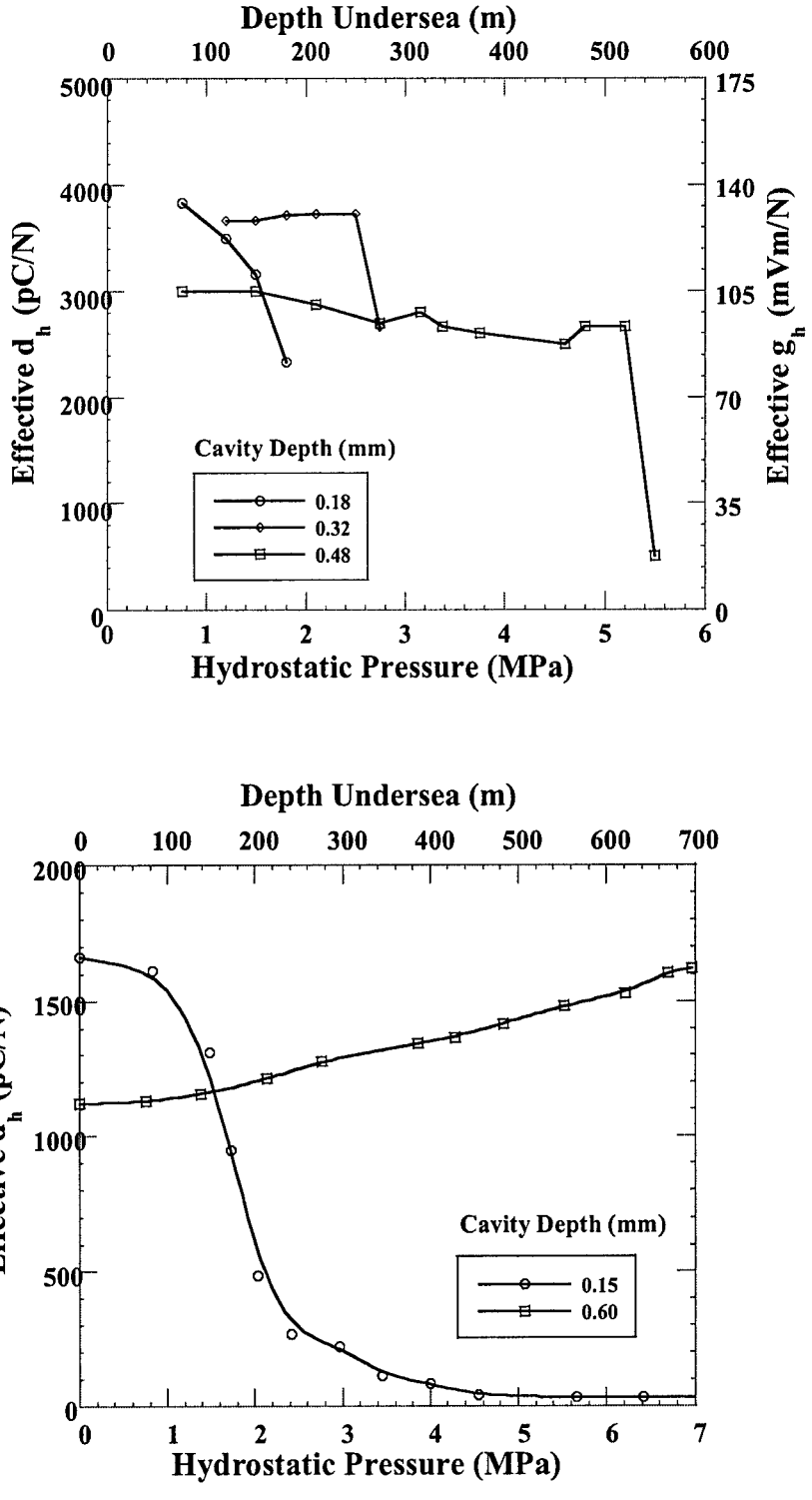

Figure 40. a) Measured pressure dependence of effective d_h and g_h coefficients of reference size unpotted transducers with PZT 5H ceramics and brass endcaps having varying cavity depths, b) Measured pressure dependence for potted reference size cymbals with titanium endcaps and different cavity depths

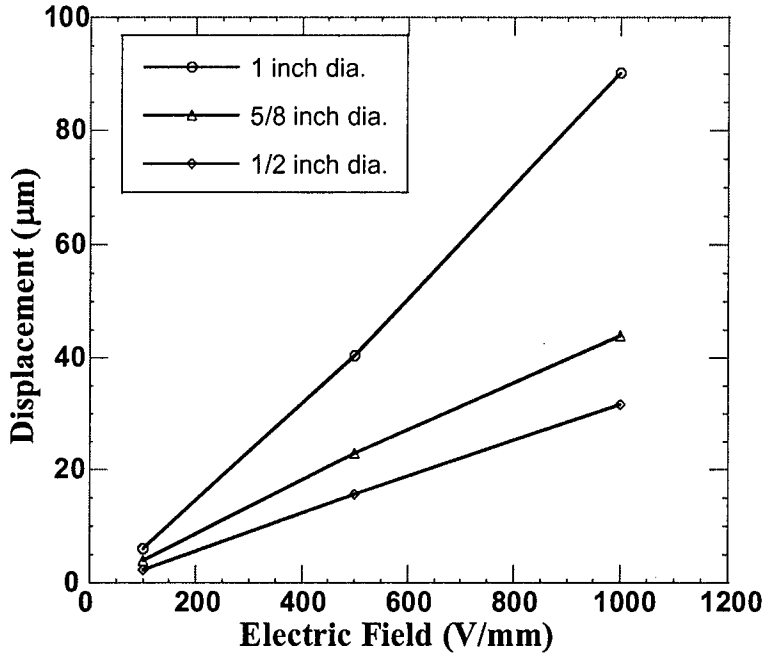

Figure 41 Measured displacements for three different brass-capped cymbals. The 1-inch cymbal has a 250 μm cavity depth, 17.4 mm cavity dia. and a 6 mm apex; the 5/8 –inch cymbal has a 310 μm cavity depth, 12 mm cavity diamter, and 2 mm apex; the ½ cymbal has a 320 μm cavity depth, 9 mm cavity dia. and 3 mm apex. All three use 0.2 mm cap thickness.

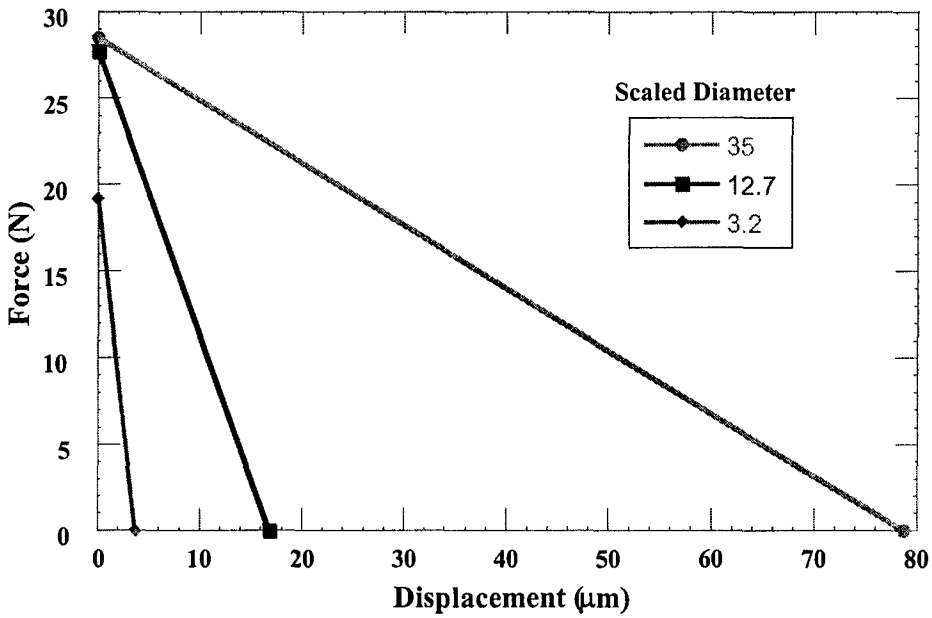

Figure 42 Calculated (ANSYS) Force vs. Displacement load-line for cymbals of different overall size, in which each parameter is multiplied by a scaling factor. PZT 5H disks and brass endcaps were used. The device diameter is given in millimeters in the legend. (1kHz, 1kV/mm).

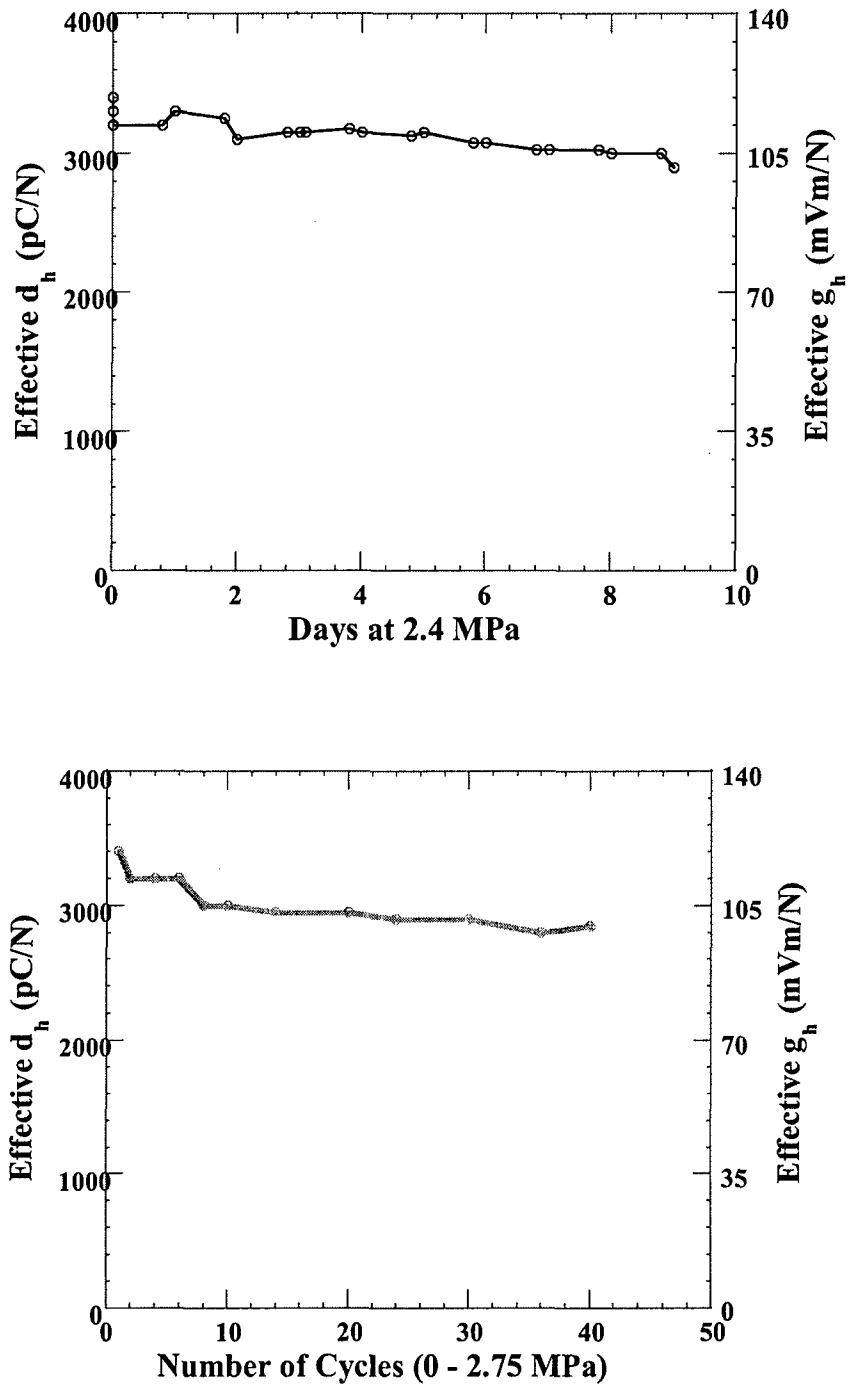

Figure 43. Measured effective d_h and calculated effective g_h coefficients of the reference size cymbal transducer with PZT 5H and brass endcaps, a-) through 8 days at 2.4 MPa, and b-) as a function of the number of times cycled between 0 and 2.75 MPa

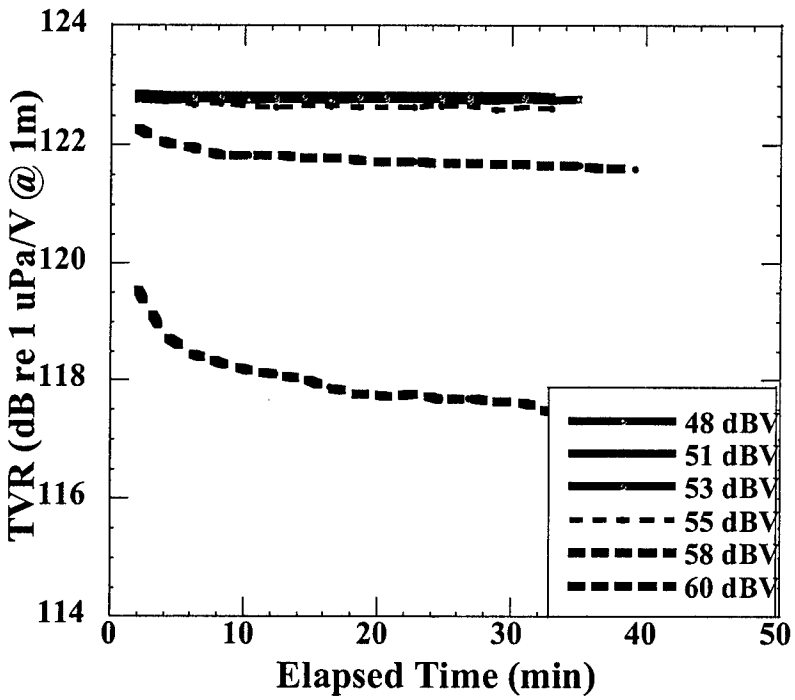

Figure 44. TVR vs. elapsed time results as drive level increases for a 3X3 cymbal array made from titanium caps with 150 μm cavity depth, using 1 mm thick PZT 4. The array was potted in EN-9 polyurethane prior to testing. The TVR was measured using 15 kHz pings 5 ms on; 67 ms off (7.5% duty cycle) sampled every two minutes with a 2 ms gated pulse. The TVR remains constant up to about 53 dBV.

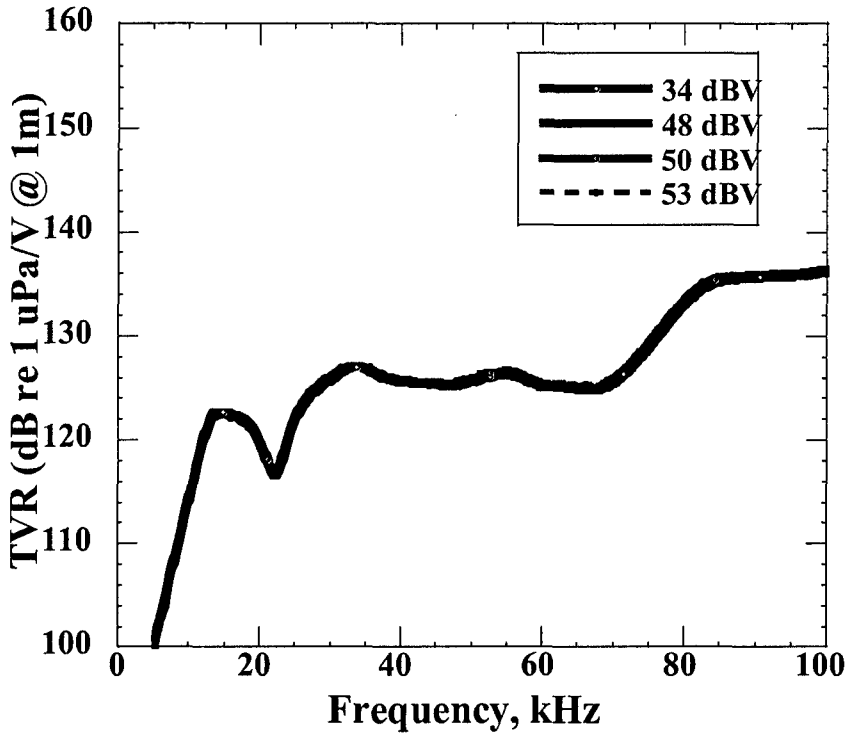

Figure 45. Frequency response of TVR vs. drive level increases for a 3X3 cymbal array made from titanium endcaps with 150 μm cavity depth, using 1 mm thick PZT 4. The array was potted in EN-9 polyurethane prior to testing. The frequency sweeps were performed using 2 ms pulses every 1 second at 200 Hz steps. Drive level in dBV is listed in the legend. The frequency and resonance behavior is essentially unchanged with increasing drive.

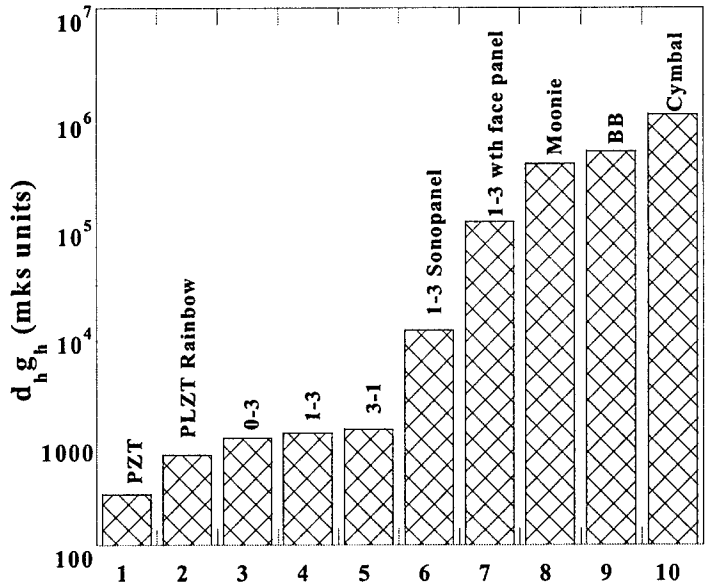

Figure 46. Hydrophone figures of merit ($d_h g_h$) of some of the widely used composites and single elements